Insights into membrane solubilization by styrene-maleic acid copolymers

Juan Julio Domínguez Pardo

Insights into membrane solubilization by styrene-maleic acid copolymers

Juan Julio Domínguez Pardo

PhD thesis, Utrecht University

In English with summaries in Spanish and in Dutch.

ISBN: 978-90-393-6945-6

The research described in this thesis was conducted in the Membrane Biochemistry & Biophysics group at the Bijvoet Center for Biomolecular Research at Utrecht University

Cover Design: Juan J. Domínguez Pardo

Layout and Print: Ridderprint | www.ridderprint.nl

Insights into membrane solubilization by styrene-maleic acid copolymers

Inzicht in membraan solubilisatie door styreen-maleïnezuur copolymeren

(Met een samenvatting in het Nederlands)

Información sobre la solubilización de membranas mediante polímeros de estireno y ácido maleico

(Con un resumen en español)

Proefschrift

ter verkrijging van de graad van doctor aan de Universiteit Utrecht op gezag van de rector magnificus, prof.dr.G.J. van der Zwaan, ingevolge het besluit van het college voor promoties in het openbaar te verdedigen op maandag 19 maart 2018 des middags te 4.15 uur

door

Juan Julio Domínguez Pardo

geboren op 20 november 1988 te València, Spanje

Promotor:

Prof. dr. J. A. Killian

The research described in this thesis is part of the research programme of ECHO-subsidies which is part of the Netherlands Organization for Scientific Research (NWO)

Para mi familia: para los que están y para los que no están.

A mi tío Enrique por apoyarme en mis decisiones

y a mi abuela Vicenta por dármelo todo.

"Las cosas tienen vida propia, todo es cuestión de despertarles el ánima"

"Things have a life on their own, it's simply a matter of waking up their souls"

Gabriel García Márquez

Table of contents

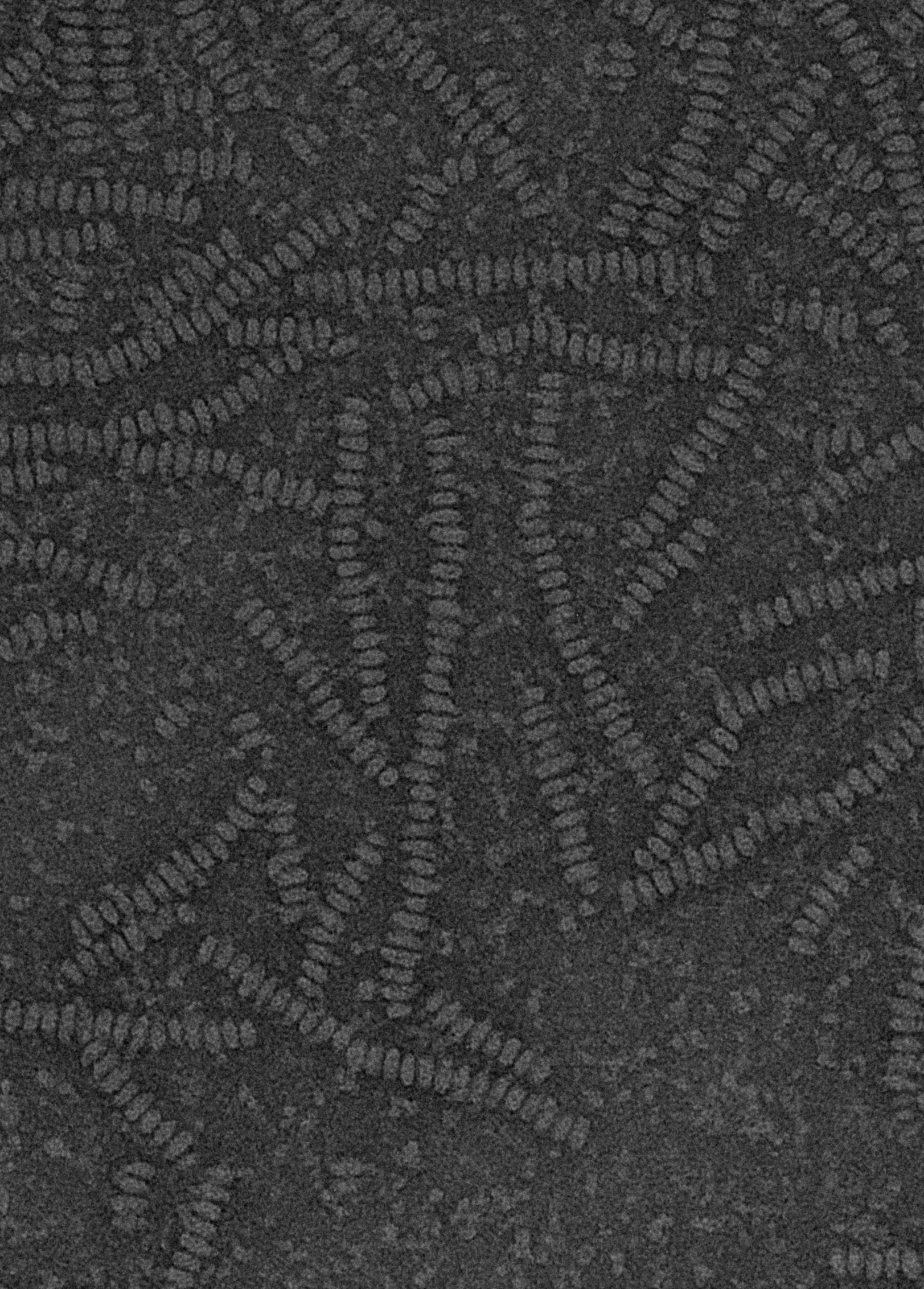

Chapter I

Introduction

The cellular membrane

Biological membranes consist of a semipermeable barrier mainly composed of lipids, carbohydrates and proteins, that separates the inside of the cell from the extracellular environment (Luckey 2008; Gennis 2013). Biological membranes are not exclusively found surrounding cells but are also found surrounding different cell organelles (e.g. mitochondria, endoplasmic reticulum, nucleus) where they play an essential role in the function of organelles. Vital processes take place through this semipermeable barrier (Nelson 2016). For example the uptake of nutrients in the cytoplasm or the release of harmful agents to the extracellular space is regulated through the membrane. Overall, each membrane is unique with respect to molecular composition, organization and functional properties.

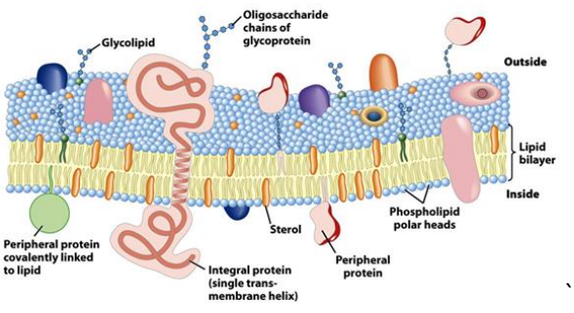

Figure 1. Representation of the cellular membrane. Biological membranes contain lipids (e.g. sterols,phospholipids, sphingolipids), proteins (e.g. integral, peripheral) and carbohydrates (e.g. glycolipids, glycoproteins).Figure is adapted from (Nelson 2016).

The first section below consists of an introduction to the molecular composition and to the biophysical properties of the major building block of biological membranes: lipids. Next, we will briefly go over the molecular composition of membrane spanning proteins and over the problems associated with their purification by conventional methods using detergents. The introduction will conclude with a detailed description of a detergent-free tool to achieve the solubilization of membrane proteins enabling their subsequent characterization: the styrene and maleic acid copolymers.

Lipids

Membranes are mainly composed of lipids that are spontaneously organized in a bilayer conformation. The main driving force for the system to adopt the bilayer conformation in an aqueous environment is the so-called hydrophobic effect. In brief, this force is entropically-driven and is based on the motional constraints of water molecules when solvating a non-polar substance. In a lipid

bilayer, the unfavorable interaction between non-polar hydrocarbon chains and water molecules is prevented by the hydrophilic polar headgroups which cover the hydrophobic core of the bilayer and by the close interaction between neighbor non-polar hydrocarbon chains (weak van der Waals forces), resulting in a closed bilayer conformation. Other forces found to play a role in the stabilization of the bilayer conformation consist of hydrogen bonds between polar lipid headgroups (exclusive of some lipid species). The lipid components that can be found in most biological membranes consist of sterols, sphingolipids and gylcerophospholipids.

Sterols

Sterols are lipids that consist of a main core structure composed of 17 C-atoms arranged in a fused 4-ring system (3 cyclohexane rings connected to a cyclopentane ring) connected to a hydroxyl group located at position 3 in cyclohexane A (Figure 2). The alkylated residue located at position 17 in cyclopentane D serves as a specific fingerprint that helps to distinguish the different types of sterols (Demel and De Kruijff 1976). The most abundant sterol found in mammalian eukaryotic cells is cholesterol, constituting approximately 30% of the total lipid found in the plasma membrane. Other eukaryotic organisms such as yeast and fungi do not contain cholesterol but ergosterol (Pasanen et al. 1999), while β-sitosterol and stigmasterol are found in plants (Griebel and Zeier 2010). Sterols play a key role in the formation of membrane microdomains termed lipid rafts or liquid-ordered domains as will be further discussed below.

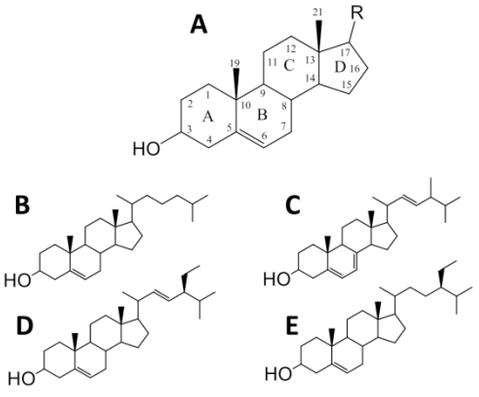

Figure 2. Schematic representation of the main structure of sterols (A) and of the structures of cholesterol (B), ergosterol (C), stigmasterol (D) and β-sitosterol (E).

Sphingolipids

Sphingolipids are located almost exclusively in the outer surface of the mammalian plasma membranes. Their low abundance may indicate that they are far away from playing a decisive role in cellular processes but eventually they are fundamental for cell recognition and signaling. Sphingolipids consist of a sphingosine backbone (Figure 3A) that is attached to an extra fatty acid via an amide-linkage, receiving the name of ceramide (Figure 3B). The extra fatty acid in mammalian cells is generally saturated and contains from 16 to 24 C-atoms (Luckey 2008; Gennis 2013). Different residues may be attached to the terminal hydroxyl such as i) phosphatidylcholine or phosphatidylethanolamine residues (i.e. sphingomyelin, Figure 3C), ii) monosaccharides (i.e. cerebrosides) or oligosaccharides (i.e. gangliosides) .The biological relevance of sphingomyelin will be discussed further on in terms of specific interactions with cholesterol.

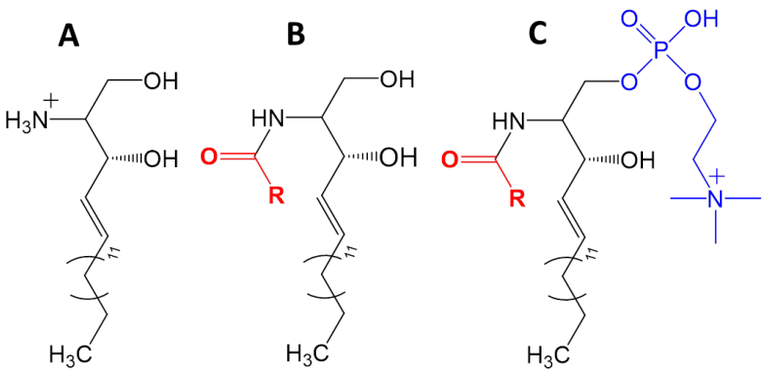

Figure 3. Schematic representation of the structure of sphingosine (A), ceramide (B) and sphingomyelin (C).

Phospholipids

Phospholipids (also known as glycerophospholipids) consist of a glycerol-3-phosphate backbone connected to two fatty acids via an ester-linkage in positions *sn1* (stereospecific numbering) and *sn2*. When the phosphate is not esterified the phospholipid is known as phosphatidic acid (PA). PA can be considered as the main building block of phospholipids, since the synthesis of all phospholipids depicted in Figure 4 can be accomplished by esterification of PA with different alcohols (Figure 4). As an example, esterification of PA with choline leads to the synthesis of phosphatidylcholine (PC) that is the most abundant phospholipid in mammalian eukaryotic cells. Other phospholipids, such as phosphatidylethanolamine (PE) or phosphatidylglycerol (PG) can be obtained after the esterification of PA with ethanolamine and glycerol respectively and are considered to be the major lipid constituents of bacterial membranes. PG can “dimerize” through its glycerol group to form

diphosphatidylglycerol (i.e. cardiolipin, CL), also abundant in bacterial membranes. Other phospholipids not depicted in the figure below, such as phosphatidylserine (PS) or phosphatidylinositol (PI) can be obtained from the esterification of PA with serine or inositol, respectively.

Hydrophobic acyl chains of phospholipids generally consist of a 16 C-atom or 18 C-atom saturated fatty acid chain at the *sn1* position and of an unsaturated hydrocarbon fatty acid chain at the *sn2* position (Gennis 2013). Figure 4 includes an illustration of the molecular structure and shape of each phospholipid together with an indication of their overall charge at physiological pH.

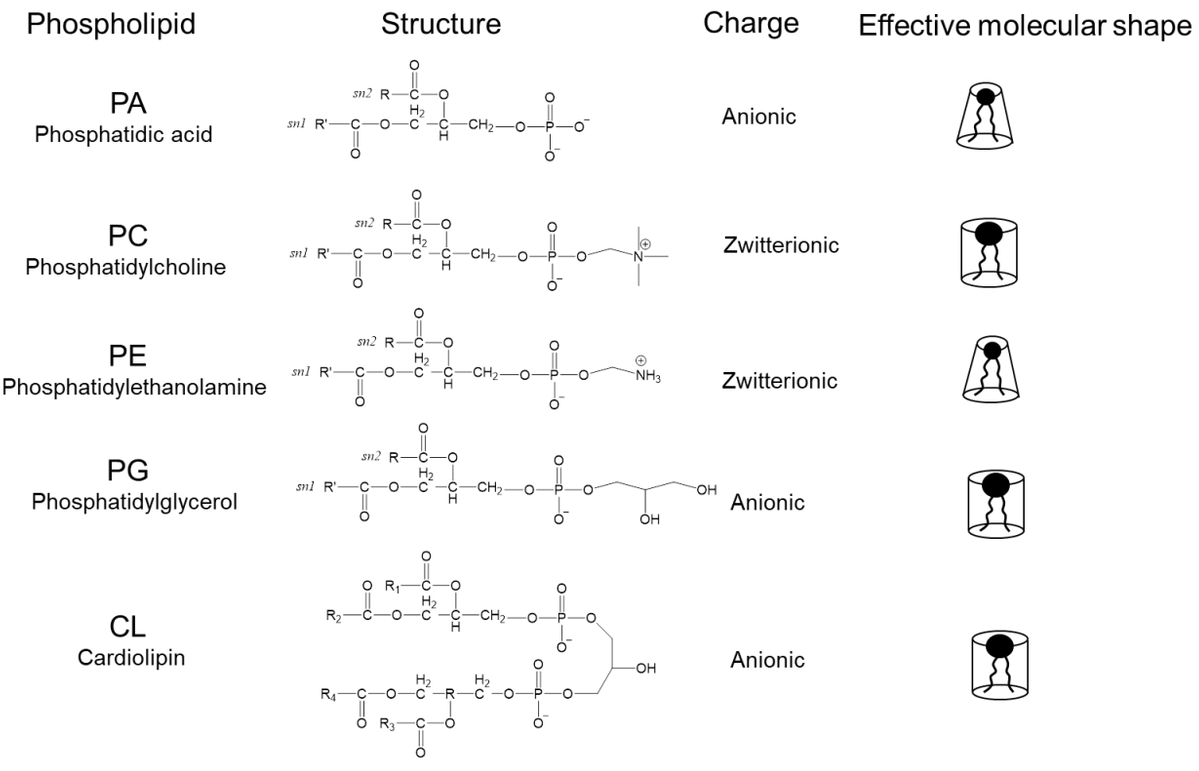

Figure 4. Schematic representation of the main phospholipids found in biological membranes. Molecular structure is shown at physiological pH.

Lipid polymorphism

The addition of water to a dried lipid film makes the lipids adopt one out of several structures also known as polymorphic (poly, many; morphus; shape) phases. Whether lipids organize in one phase or another will be determined by the effective molecular shape of the lipids (Cullis and Kruijff 1979;

Cullis et al. 1986; Jouhet 2013) (see Figure 4).The shape of a lipid is determined by the relation between the cross sectional area of the lipid headgroup (A_{HG}) and the cross sectional area of the hydrocarbon region (A_{HC}). As an example, when A_{HG}~A_{HC} lipids exhibit a so-called cylindrical shape (e.g. PC, PG) they will have a thermodynamic preference to form lamellar structures. By contrast when A_{HG}<A_H (e.g. PE), lipids exhibit an overall cone-shaped structure, this will favor the adoption of inverted phases. Hence these lipids are known as non-bilayer lipids. Phospholipids that only contain one acyl chain (lysolipids) exhibit A_{HG}>A_{HC} and are prone to form micelles in solution.

An approximation to predict the phase preference of the lipids as function of their effective molecular shape is illustrated in Figure 5. Here, the cross-sectional areas (A_{HG} and A_{HC}) are not taken into consideration but the volumes of the lipid headgroup and of the lipid acyl chain regions. The approximation can be summarized as follows: the adoption of one polymorphic phase or another is ascribed to a specific "*P*" value, that is defined as $P = v / al$ (Jouhet 2013), where *v* is the volume per lipid molecule, *a* is the cross sectional area of the headgroup and is the length of the fully extended acyl chain.

Finally, it is important to note that the lipid behavior and shape is not specific to each "headgroup family" but may be affected by several other parameters (e,g. temperature, presence of unsaturations, presence of divalent cations).

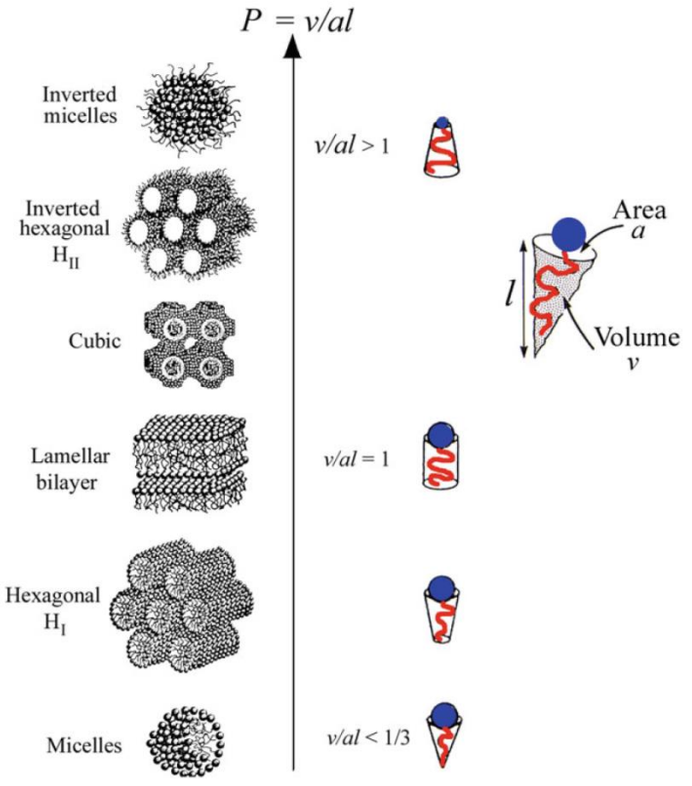

Figure 5. Polymorphic phases and molecular shapes of lipids. Figure is adapted from (Jouhet 2013).

Lamellar phase

Biological membranes (and lipid bilayers in general) are mainly lamellar. Within lamellar phases several options can be found, being the two most common the liquid crystalline phase (L_α or L_D) and the gel phase (L_β). Additionally, some phospholipids exhibit the so-called ripple phase (P_β), that takes place between L_β and L_α and consist of membrane ripples with periods up to several hundreds of nanometers (Czajkowsky et al. 1995; Heimburg 2000). To conclude, the association between sphingolipids or saturated phospholipids with cholesterol leads to the so-called lamellar liquid-ordered phase (L_o), with intermediate properties between L_β and L_α phases.

Lamellar lipid phase transitions

Lipids undergo a sharp lamellar gel-to-lamellar liquid crystalline phase transition as temperature is increased. The exact temperature at which the main phase transition takes place (T_m) is specific for every lipid and is affected by i) the acyl chain length (Lewis et al. 1987; Lewis et al. 1989) ii) the lipid headgroup (Koynova and Caffrey 1998) and iii) the presence of unsaturations (Koynova and Caffrey 1998). First we will discuss the phase transitions of lipids with saturated acyl chains. Each Csp^3—Csp^3

bond along the acyl chain exhibits free rotation and therefore is able to adopt a wide variety of configurations. As illustrated in Figure 6, the *anti* or *trans* configuration is the most stable, followed by the *gauche* and the *eclipsed* configurations, showing respectively energetic barriers of 0.9 kcal/mol and 3.6 kcal/mol. It must be noted that all the enthalpy values reported here correspond to those obtained from n-butane molecules under vacuum conditions, thus may fluctuate from those of methylene units constituting the acyl chain of phospholipids. In the gel-phase, the acyl chains of the lipids are tightly packed holding exclusively an *anti* or *trans* configuration. Furthermore, acyl chains in the gel-phase are found to be fully extended, leading to an increase in the hydrophobic thickness of the bilayer (Marrink et al. 2005).

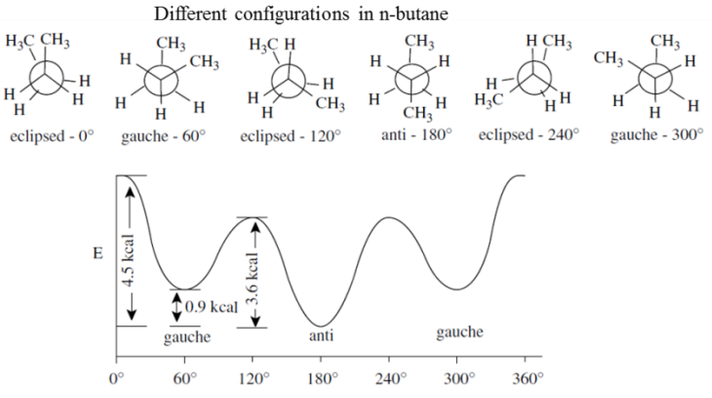

Figure 6. Energy changes during the rotation of n-butane around C_2-C_3. Different configurations are shown in a Newman projection. Figure is adapted from (Hoffman 2004).

As temperature is increased, Csp^3—Csp^3 bonds rotate resulting in *anti*-to-*gauche* conformer interconversion. A sequence of *gauche-anti-gauche* conformers for three consecutive Csp^3—Csp^3 bonds will result in the formation of a kink that will displace the rest of the acyl chain and force the lipid to adopt a liquid crystalline phase.

The kink present in the acyl chains as a result of *anti*-to-*gauche* interconversion is rather similar to that observed by the presence of *cis* double bonds, explaining why T_m values reported for *cis* di-unsaturated phospholipids are generally below 0 °C (Koynova and Caffrey 1998). After gel-to-liquid crystalline phase interconversion has taken place the lipids show an increase in their hydrophobic cross sectional area and this affects the organization of the lipid bilayer. As a consequence, liquid crystalline membranes show bigger headgroup—headgroup spacings than gel-membranes, thus leaving small voids at the headgroup—water interface between neighbor lipids.

Tools to detect lipid phase transitions

Several techniques are available to monitor phase transitions, the two most common being differential scanning calorimetry (DSC) and fluorescence by membrane-inserted fluorophores. While DSC is based on the heat exchanged whenever a thermotropic event occurs within the membrane, fluorescence properties of fluorophores reflect the differences in fluidity of gel and fluid membranes.

Differential scanning calorimetry

Differential scanning calorimetry (DSC) consists of a non-perturbing technique that allows the detection and characterization of thermotropic phase transitions in lipid membranes. In brief, the technique measures the difference in heat exchange between sample and reference as temperature is constantly increased. This will result in an endothermic or exothermic contribution of the phospholipids whenever a thermotropic event takes place. As shown in Figure 5, phospholipids organized in vesicles undergo a highly cooperative gel-to-fluid transition as indicated by the small width at half height ($\Delta T_{1/2}$).The value of $\Delta T_{1/2}$ increases with the complexity of the lipid membrane. As an example, DSC analyses on biological membranes result in extremely broad thermograms In this way, DSC is a useful tool to help to characterize and understand the effects of sterols in model membranes or other intrinsic perturbing molecules (i.e. proteins, peptides, small alcohols), based on to what extent the lipid phase transitions are perturbed. Another parameter that can be investigated by calorimetry is the calorimetric enthalpy (ΔH_{cal}) of the main gel-to-fluid phase transition that provides insight into the heat exchanged per lipid during the melting process. The values of ΔH_{cal} are obtained from the integral of the thermogram and increase with the length of the fatty acid chains of the lipids. The presence of sterols or membrane-spanning molecules in a lipid bilayer generally results in a loss of ΔH_{cal} of the main lipid phase transition. This is ascribed to the fact that lipids are so perturbed by the presence of membrane spanning molecules that they are withdrawn from the transition.

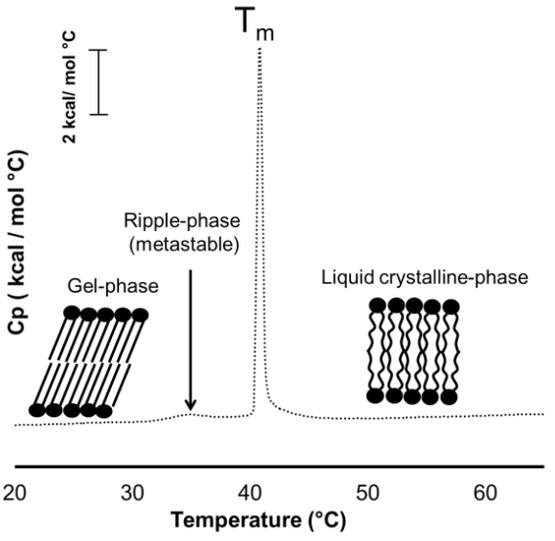

Figure 7. DSC thermogram of di-16:0 PC vesicles (T_m~41°C (Lewis et al. 1987)). Scale bar corresponds to 2 kcal/mol.

Membrane-spanning fluorophores

The study of lipid phase transitions is not exclusively assigned to calorimetric techniques but fluorescent probes also provide accurate insight into the thermotropic properties of lipids. As an example, laurdan consists of a two naphthalene-derivative molecule that was first synthesized by Gregorio Weber in 1979 (Weber and Farris 1979; Macgregor and Weber 1981) and is extremely sensitive to changes in both the polarity of the solvent and the relaxation rate of the solvent molecules. Due to partial phase separation between the 2-dimethylamino and the 6-carbonyl residues the probe exhibits a dipole moment that will increase upon excitation and therefore affect the orientation of the polar solvent molecules surrounding it. The energy required for the solvent molecules to reorient will decrease the energy of the probe's excited state, resulting in a blue shift of the emission spectra (Krasnowska et al. 1998; Parasassi et al. 1998). As illustrated in Figure 6, in liquid crystalline membranes the laurdan probes locate near the phosphate—headgroup interface and will be solvated by a higher number of polar solvent molecules (water) than when embedded in gel-phase membranes. Thus a bathochromic shift is expected in the fluorescence spectra of laurdan upon melting. This property turns the laurdan probes into excellent tools to study phase transitions and fluidity in lipid membranes (Parasassi et al. 1991; Denisov et al. 2005).

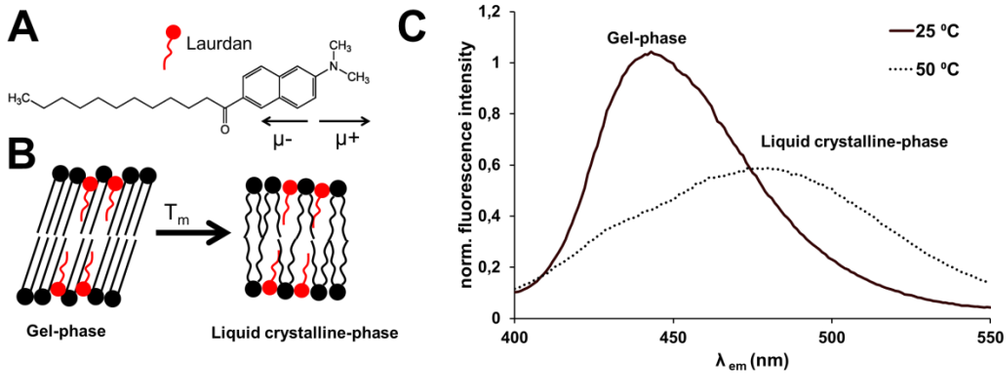

Figure 8. A) Molecular structure of laurdan. B) Schematic representation of laurdan molecules partitioned in either gel or liquid crystalline membranes. C) Fluorescence spectra of laurdan molecules embedded in di-16:0 PC vesicles (T_m~41ºC(Lewis et al. 1987)). Spectral shift indicates gel (440 nm)-to-liquid crystalline (490 nm) phase transition.

Liquid ordered domains

The specific interaction between cholesterol and shingolipids or saturated phospholipids results in the formation of the so-called liquid ordered domains (L_o) (Sankaram and Thompson 1990; Sot et al. 2002; Veatch and Keller 2003; Marsh 2013). Lipids in a liquid ordered phase show intermediate phase properties between the gel and the liquid crystalline phase. As an example, liquid ordered lipids show similar packing properties as lipids in a gel phase but show the lateral diffusion rate of lipids in a liquid crystalline phase (Vist and Davis 1990; McMullen et al. 2004). The resistance of the liquid ordered domains to be solubilized by detergents has been extensively analyzed in model membranes of different lipid composition (London and Brown 2000; Heerklotz 2002; Sot et al. 2002). It is logical to think that the poor solubilization rates observed for liquid ordered domains against detergents is ascribed to the tight interaction between the lipids components. Several models have been proposed providing insight into the nature of this interaction, such as the condensed complex model (Radhakrishnan and McConnell 1999), the superlattice model (Somerharju et al. 2009) or the umbrella model (Huang and Feigenson 1999). Interestingly, the three models consider the direct coalescence between cholesterol molecules as an energetically unfavorable interaction (Dai et al. 2010). Briefly, the condensed-complex model defends the existence of a “chemical interaction” between cholesterol and phospholipids occupying smaller areas as they would occupy by separate (Radhakrishnan and McConnell 1999). The superlattice model defends that the interaction between cholesterol and phospholipids exists as a superlattice, with local minima in the membrane free energy (Somerharju et al. 2009). The umbrella model suggests that phospholipids cover cholesterol molecules in order to prevent the direct exposure of their hydrophobic moiety to the aqueous

environment (Huang and Feigenson 1999). Overall, the nature of this specific interaction is not fully known yet but it has been demonstrated that is extremely affected by i) the chemical modification of cholesterol ii) the presence of different sterol molecules (Bernsdorff and Winter 2003) and iii) the presence of unsaturated phospholipids (Veatch and Keller 2003; Aittoniemi et al. 2006; Bakht et al. 2007).

Lipid raft domains

Lipid rafts were firstly introduced by Simons and Ikonen (Simons and Ikonen 1997) and were described as highly ordered lipid domains obtained as a result of the interaction between cholesterol and sphingolipids onto which specific proteins may attach. Some of these proteins may consist of GPI-anchored proteins (Sargiacomo 1993; Danielsen 1995) or doubly acylated tyrosine kinases of the Src family (Casey 1995). During the last decade it has been suggested that the biological relevance of these domains is huge, playing a key role in membrane trafficking and signal transduction (Simons and Ikonen 1997b; Brown and London 1998). As an example, several cell signaling pathways have been found to be concentrated in caveolae that consist of invaginations of the plasma membrane enriched in cholesterol, sphingolipids and integral caveolin proteins (Anderson 1998; Nabi and Le 2003). However, the existence of lipid rafts is still under dispute since most of the evidence compiled proving their existence is based on indirect methods such as extraction by detergent. Direct methods such as raft visualization from living cells are far away from providing reliable and decisive information regarding their size and furthermore their existence (Anderson and Jacobson 2002; Munro 2003). Recent studies have provided direct evidence for the existence of sphingolipid microdomains in the plasma membrane of fibroblasts but depleted in cholesterol and therefore questioning the existence of lipid rafts (Frisz et al. 2013a; Frisz et al. 2013b). The existence of lipid rafts will still be under dispute until a direct technique permits their visualization at a (sub)nanometer scale.

Detergent resistant membranes

The direct comparison of lipid raft domains with detergent resistant membranes (DRMs) still generates great controversy in the field of membrane biophysics. DRMs consist of the insoluble lipid fraction obtained after addition of detergents at 4 °C to eukaryotic cells. These insoluble fractions are found to be enriched in cholesterol and sphingolipids (Hanada et al. 1995; London and Brown 2000) and may suggest the existence of lipid rafts in biological membranes. However, this suggestion is rather weak, since assumes that raft domains isolated at 4 °C are already present in biological

membranes at 37 °C and in the absence of detergent (Lichtenberg et al. 2005). Furthermore, direct evidence has been provided showing that detergents (i.e. Tx-100) can promote domain formation in ternary model membranes constituted by sphingomyelin, cholesterol and unsaturated phosphatidylcholines (Heerklotz 2002; Marsh 2013). In brief, DRMs should not be identified as lipid rafts (Lichtenberg et al. 2005).

Membrane Proteins

Analysis of genomic sequence data predicts that approximately ~30% of the proteins produced by humans consist of membrane proteins (Wallin and Heijne 1998). Membrane proteins are found in cellular membranes either attached to their surface (i.e. peripheral protein) or directly embedded in them (i.e. integral protein). The focus in this thesis will be exclusively on the membrane spanning proteins. Membrane spanning proteins are defined as proteins that interact with a biological membrane either by spanning completely the lipid bilayer with a single transmembrane peptide chain (i.e. transmembrane domain) or multiple times with several transmembrane domains (Blobel 1980; Nørholm et al. 2011).

Solubilization of membrane proteins

The complexity and heterogeneity of biological membranes limits the study of membrane proteins by most biophysical approaches. This turns the purification of membrane proteins in a fundamental requisite for their later study. However, many problems rise from the purification of integral proteins from biological membranes. Most importantly, membrane proteins are generally insoluble in water, and need to be surrounded by detergent molecules to shield their hydrophobic parts when extracted from the membrane (Seddon et al. 2004) (Figure 9). Unfortunately, the use of detergents shows many disadvantages. First, detergents have been shown to affect the functionality of proteins, that tend to aggregate or misfold when extracted from their native lipid environment (Carruthers and Melchior 1986). Second, detergent micelles are considered a very poor mimic of a lipid bilayer and are far away of satisfying the native membrane biophysical properties that often are important for structure and functionality of membrane proteins (Zhou and Cross 2013). Third, trials to find most suitable detergent can be cumbersome. Despite the negative implications of detergents in the purification of membrane proteins, they are still extensively used by the scientific community as a tool for membrane protein research.

Nanodiscs bounded by membrane scaffold proteins

Sligar and coworkers have been developing over the last 20 years a new approach to reconstitute membrane proteins from biological membranes into nanodiscs (Bayburt et al. 2002; Denisov et al. 2004; Shaw et al. 2004; Denisov et al. 2005; Bayburt and Sligar 2010). Membrane proteins are first solubilized in micelles (usually cholate-micelles) and later are reconstituted into nanodiscs. Nanodiscs consist of approximately ~150 lipid molecules organized in a circular lipid bilayer of d~10 nm diameter (Figure 9). The structure is illustrated in Figure 9. The overall structure is stabilized by so-called membrane scaffold proteins (MSPs) that are derived from the human apolipoprotein A-1(Bayburt and Sligar 2010). Calorimetric studies have shown that MSPs are exclusively interacting with the boundary lipids of the nanodiscs, as estimated by the loss in calorimetric enthalpy of the gel-to-fluid phase transition of the lipids constituting the nanodisc(Shaw et al. 2004; Denisov et al. 2005). MSP-nanodiscs present many advantages over detergent micelles. For example, nanodiscs confer membrane proteins a lipid environment that resembles the architecture of membranes. Furthermore, it was found that the native thermotropic properties of lipids in nanodiscs are highly retained, which further supports their use of a convenient mimic of the native membranes (Shaw et al. 2004). An additional advantage of using nanodiscs is the ability of modulating the lipid composition and size of the nanodiscs more or less at will (Bayburt et al. 2002). The use of one MSP variant or another will determine the diameter of the nanodisc (Denisov et al. 2004). For example, nanodiscs bound by long MSPs will yield bigger nanodiscs than those bound by shorter variants. The most commonly used MSP variant (MSP1) consist of 200 aminoacids. A shorter MSP variant has been found to yield small nanodiscs suitable for NMR studies (Raschle et al. 2009). Extended scaffold proteins have been designed with one, two or three additional 22-mer amphipathic helices inserted in the center of the MSP1 (Denisov et al. 2004). Overall, nanodiscs are a promising and useful tool for membrane protein research besides its main disadvantage of requiring detergent.

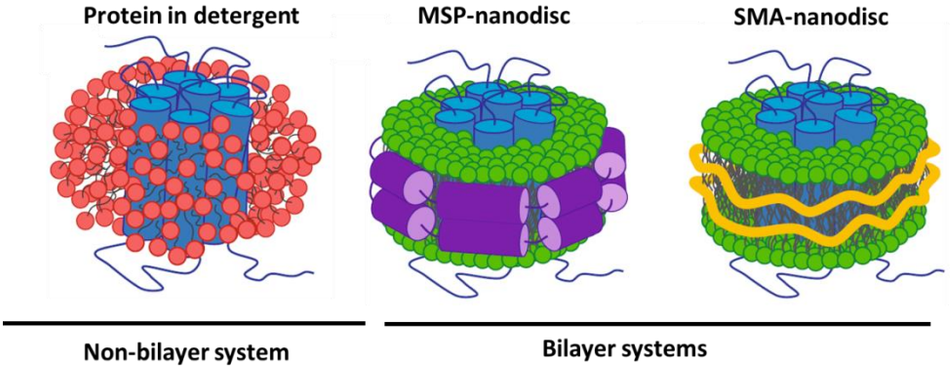

Figure 9. Models proposed for membrane protein stabilization in aqueous media. Figure is adapted from (Dörr et al. 2016).

The SMA copolymer

Styrene and maleic acid copolymers are extensively used in industry in both the anhydride form (SMAnh) and the hydrolyzed form (SMA). Hydrolyzed SMA copolymers are used as dispersing agents for ink formulations and coatings while anhydride SMAnh copolymers are used as thermal stabilizers in plastic blends(Dörr et al. 2016). In the early 2000's, it was found that the addition of SMA to a lipid membrane resulted in the formation of discoidal particles (Tonge, SR and Tighe 2001). This application was further patented by Malvern Cosmeceutics™ (Worchester, UK) for its commercial use(Tonge and Tighe 2002).The SMA copolymers used in this thesis were kindly provided by Polyscope™ (Geleen, The Netherlands), but other companies also supply SMA copolymers worldwide such as TOTAL Cray Valley™ (PA, USA). Here, we will focus only on the polymers obtained by Polyscope™. Polyscope™ name their polymers with a five digit number, where the two first numbers provide information regarding the maleic acid/maleic anhydride content (mol%) and the three last numbers are used to define the size of the polymer (kDa). As an example, the three SMA variants used in this thesis are named as Xiran 20010, Xiran 25010 and Xiran 30010, with a maleic acid/maleic anhydride content of 20%, 25%, and 30% mol respectively and with an average size of 10 kDa.

Synthesis of the SMA copolymer

Styrene and maleic anhydride copolymers (SMAnh) are synthesized by a radical chain reaction of the styrene and maleic anhydride monomers. This reaction is illustrated in Figure 10 and leads to the formation of a wide variety of SMAnh copolymers of different length and styrene-to-maleic anhydride ratios.

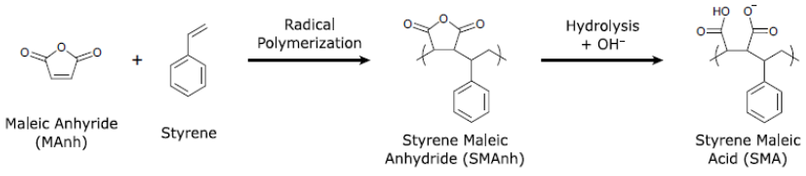

Figure 10. Schematic representation of the copolymerization reaction of styrene and maleic anhydride and further hydrolysis in alkaline medium. Figure is adapted from (Dörr et al. 2016).

The polydispersity of the mixtures of SMAnh polymers is characterized by the polydispersity index (PDI) which for SMAnh polymers is usually in the range of PDI: 2.0—2.5. The PDI is defined as the relation between the average number molecular weight (M_n) and the average mass molecular weight (M_w) where N_i is the number of polymer molecules with a M_i molecular weight.

$$\text{PDI}=\frac{M_w}{M_n};\ M_n=\frac{\sum N_i M_i}{\sum N_i} \text{ and } M_w=\frac{\sum N_i M_i^2}{\sum N_i M_i}$$

The overall styrene-to-maleic anhydride ratio may be modified by changing the feed monomer ratio during the copolymerization reaction (Klumperman 2010). The monomer sequence of SMA polymers is determined by the copolymerization kinetics and by the initial amount of reactants (Klumperman 2010). As a remak, despite the strong alternative character of SMA copolymers (Deb and Meyerhoff 1985; Sanayei et al. 1994), increasing amounts of styrene lead to the repetition of styrene monomers in the growing polymer chain (Scheidelaar et al. 2016).

Hydrolysis of the SMA copolymer

The solubilization power of SMAnh polymers is not based on their anhydride form but on their hydrolyzed form (SMA). The hydrolysis of SMAnh polymers have been well described in several studies(Scheidelaar et al. 2015; Dörr et al. 2016; Scheidelaar et al. 2016; Pardo et al. 2017) and is represented in Figure 10. In brief, 10% (w/v) SMAnh in alkaline solution (NaOH or KOH 1-M) is heated to reflux overnight. Next, SMA is precipitated by addition of excess HCl and washed extensively with NaOH 0.1-M solutions. The resulting humid precipitate is stored unsealed at room temperature for complete dryness. Once dried, SMA powder can be dissolved in water..

Nanodiscs bounded by styrene and maleic acid (SMA) copolymers

The addition of water-soluble SMA to a lipid membrane results in the spontaneous formation of nanodiscs illustrated in Figure 9 (Scheidelaar et al. 2015). The solubilization process can be followed by biophysical techniques (i.e. turbidimetry) as illustrated in Figure 11. Here the formation of nanodiscs is indicated by a decrease in the total amount of scattered light. Furthermore, SMA enables the retention of the native lipid annular shell of the membrane protein (Swainsbury et al. 2014; Prabudiansyah et al. 2015; Dörr et al. 2016) and hence, assuring their stability and helping preserve their biological function. Special attention has been paid on SMA during the last five years resulting in a great number of biophysical studies in both model membranes (Knowles et al. 2009; Scheidelaar et al. 2015; Vargas et al. 2015; Arenas et al. 2016; Scheidelaar et al. 2016, Pardo et al.

2017) and biological membranes (Long et al. 2013; Gulati et al. 2014; Swainsbury et al. 2014; Jamshad et al. 2015; Prabudiansyah et al. 2015; Dörr et al. 2016). Most of these studies are recollected in an extensive review (Dörr et al. 2016). It was found that the solubilizing properties of SMA copolymers are modulated by i) pH (Scheidelaar et al. 2016), ii) surface pressure (Scheidelaar et al. 2015), iii) lipid packing (Scheidelaar et al. 2015) and iv) lipid acyl chain length (Scheidelaar et al. 2015). Furthermore, membranes with low lipid-to-protein density ratios were found to be rather difficult to solubilize by SMA (Bell et al. 2015). A similar resistance against SMA was exhibited by ternary model membranes consisting of liquid ordered domains in a liquid crystalline matrix. Similarly to DRMS, the insoluble fraction was found to be enriched in liquid ordered-forming lipids while the solubilized fraction was enriched in lipids in the liquid crystalline. These results pave the way for the utilization of SMA as a tool to isolate highly ordered domains from membranes without the use of detergents.

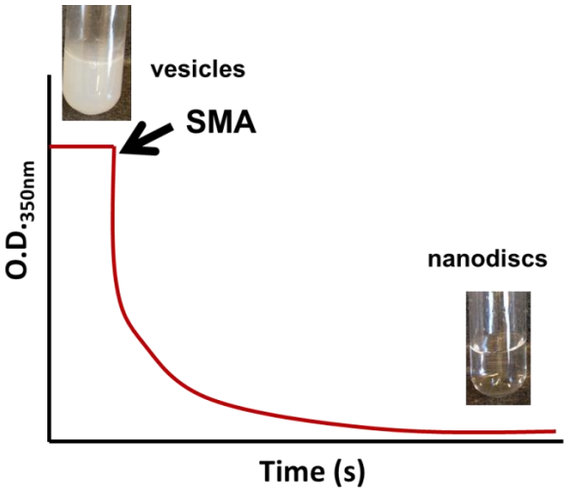

Figure 11. Schematic representation of a turbidimetry experiment. Arrow indicates the moment when SMA is added to the vesicle dispersion resulting in its immediate solubilization.

Structure of SMA nanodiscs

Small angle neutron scattering analyses on di-14:0 PC nanodiscs revealed that the particles have a disc-like conformation where the overall structure is encircled by a belt of SMA. This model is illustrated in Figure 12. Nanodiscs consisting of di-14:0 PC were found to have an average diameter of approximately ~10 nm and a thickness of ~4.6 nm (Jamshad et al. 2015) in line with the full bilayer thickness values reported for di-14:0 PC bilayers (Nagle and Tristram-Nagle 2000). It has been found

that SMA molecules act as belt encircling the edge of the nanodiscs whereby the hydrophobic styrene units insert in between the lipid acyl chains (Orwick et al. 2012; Jamshad et al. 2015). Due to this interaction the packing properties of the lipids are somewhat affected, leading to a downshift in T_m values and in a loss of cooperativity of the gel-to-liquid crystalline transition (Orwick et al. 2012; Jamshad et al. 2015; Tanaka et al. 2015; Oluwole et al. 2017). On the other hand, EPR studies using spin-labeled stearic acid (C11) on di-14:0 PC nanodiscs reported an increase in the order of lipids located in the center of the nanodiscs between C8-C12 (Orwick et al. 2012). Overall, lipids enclosed in nanodiscs thus show broad thermotropic transitions while apparently being more ordered in the center of their hydrophobic acyl chains.

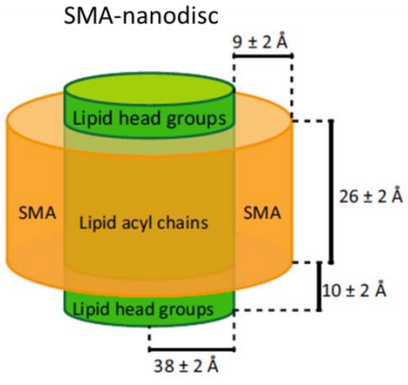

Figure 12. Dimensions of SMA-bounded nanodiscs consisting of di-14:0 PC as determined from small-angle neutron scattering (Jamshad et al. 2015). Figure is adapted from (Dörr et al. 2016).

Scope of the thesis

Chapter II investigates whether SMA has a preference to solubilize specific lipids or lipid phases. This is addressed by partly solubilizing lipid vesicles of different lipid composition and analyzing the composition of the part that becomes solubilized. This study is divided in two main sections: the first one focused on homogeneously fluid membranes and the second one on membranes with phase coexistence. It was found that SMA behaves as a fully promiscuous solubilizer when added to fluid membranes but shows particularly low solubilization efficiency against gel or liquid-ordered domains. This last result is rather similar to that shown by conventional detergents, paving the way for a new method for purifying condensed lipid complexes (SMA-resistant membranes, SRMS).

Chapter III consists of a systematic study of the thermotropic properties of saturated phosphatidylcholines organized in nanodiscs bounded by different SMA variants. This study investigates the extent to which the thermotropic properties of lipids in nanodiscs are affected

(compared to those in vesicular self-assemblies) when bounded by different commercially available SMA blends. It was found that SMA 2:1 retained to a higher extent the T_m than its other polymer analogues. In addition, it was found that the morphological integrity of nanodiscs is somewhat lost when a high concentration of SMA is present in solution. This is particularly pronounced in nanodiscs bounded by SMA 4:1 polymers that seem to be unable to form well-defined circular nanodiscs but aggregates. To conclude, this study provides evidence for reorganization of the SMA polymers in the gel phase and in the fluid phase.

Chapter IV investigates whether the SMA belt encircling the nanodiscs behaves in a rather flexible way or the opposite, if it consists of a stiff polymer rim. This was addressed by the synthesis of photoisomerizable azobenzene-labeled phospholipids. These lipids were incorporated in phosphatidylcholine self-assemblies of both vesicles and nanodiscs. The rates of isomerization and the isomerization extent of the azolipids were investigated. The results show that azolipids are able to isomerize fast and efficiently in nanodiscs, and hence the SMA belt is able to accommodate an increase in the geometric volume of the enclosed lipid material. By applying molecular mechanics we estimate an increase in nanodiscs diameter of approximately ~0.5—2.5, evidencing the flexibility of the SMA polymer.

In **Chapter V** we describe a method to purify commercially available SMAnh blends into SMAnh fractions of better-defined length based on their differential solubility in acetone/hexane mixtures. We obtained 4 different pools of polymers of different number average molecular weight (M_n) of 1.1—6.5 kDa and next we hydrolyzed them and tested their interaction with lipid membranes. Results showed that SMA fractions containing low M_n polymers solubilize simple PC membranes very fast and insert into a much higher extent into PC monolayers than those consisting of high M_n polymers. In addition, fractions containing low M_n polymers were found to affect the most the thermotropic properties of the enclosed lipids and lead to faster lipid exchange rates between nanodiscs. This study provides solid insight into the role of polymer length into membrane solubilization and into the biophysical properties of the enclosed lipids.

A summarizing discussion is provided in **Chapter VI**. A brief review of all the literature to our current knowledge is provided in combination with the experimental results showed in this thesis.

References

Aittoniemi J, Róg T, Niemelä P, Pasenkiewicz-Gierula M, Karttunen M, Vattulainen I (2006) Tilt: major factor in sterols' ordering capability in membranes. J Phys Chem B 110:25562–25564.

Anderson RG (1998) The caveolae membrane system. Annu Rev Biochem 67:199–225.

Anderson RGW, Jacobson K (2002) A Role for Lipid Shells in Targeting Proteins to Caveolae, Rafts, and Other Lipid Domains. Science 296:1821–1825

Arenas RC, Klingler J, Vargas C, Keller S (2016) Influence of lipid bilayer properties on nanodisc formation mediated by styrene/maleic acid copolymers. Nanoscale 8:15016–15026

Bakht O, Pathak P, London E (2007) Effect of the structure of lipids favoring disordered domain formation on the stability of cholesterol-containing ordered domains (lipid rafts): identification of multiple raft-stabilization mechanisms. Biophysical Journal 93:4307–4318.

Bayburt TH, Sligar SG (2010) Membrane protein assembly into Nanodiscs. FEBS Letters 584:1721–1727.

Bayburt TH, Grinkova YV, Sligar SG (2002) Self-Assembly of Discoidal Phospholipid Bilayer Nanoparticles with Membrane Scaffold Proteins. Nano Lett. 2:853–856.

Bell AJ, Frankel LK, Bricker TM (2015) High Yield Non-detergent Isolation of Photosystem I-Light-harvesting Chlorophyll II Membranes from Spinach Thylakoids: implications for the organization of the ps i atennae in higher plants. J Biol Chem 290:18429–18437.

Bernsdorff C, Winter R (2003) Differential Properties of the Sterols Cholesterol, Ergosterol, β-Sitosterol, trans -7-Dehydrocholesterol, Stigmasterol and Lanosterol on DPPC Bilayer Order. J Phys Chem B 107:10658–10664.

Blobel G (1980) Intracellular protein topogenesis. Proceedings of the National Academy of Sciences 77:1496–1500

Brown DA, London E (1998) Functions of lipid rafts in biological membranes. Annu Rev Cell Dev Biol 14:111–136.

Carruthers A, Melchior DL (1986) How bilayer lipids affect membrane protein activity. Trends in Biochemical Sciences 11:331–335.

Casey PJ (1995) Protein lipidation in cell signaling. Science 268:221–225

Cullis PR, Kruijff B de (1979) Lipid polymorphism and the functional roles of lipids in biological membranes. Biochimica et Biophysica Acta (BBA) - Reviews on Biomembranes 559:399–420.

Cullis PR, Hope MJ, Tilcock CP (1986) Lipid polymorphism and the roles of lipids in membranes. Chem Phys Lipids 40:127–144.

Czajkowsky DM, Huang C, Shao Z (1995) Ripple phase in asymmetric unilamellar bilayers with saturated and unsaturated phospholipids. Biochemistry 34:12501–12505

Dai J, Alwarawrah M, Huang J (2010) Instability of cholesterol clusters in lipid bilayers and the cholesterol's Umbrella effect. J Phys Chem B 114:840–848.

Danielsen EM (1995) A transferrin-like GPI-linked iron-binding protein in detergent- insoluble noncaveolar microdomains at the apical surface of fetal intestinal epithelial cells. The Journal of Cell Biology 131:939–950.

Deb PC, Meyerhoff G (1985) Study on kinetics of copolymerization of styrene and maleic anhydride in methyl ethyl ketone. Polymer 26:629–635

Demel RA, Kruyff B de (1976) The function of sterols in membranes. Biochimica et Biophysica Acta (BBA) - Reviews on Biomembranes 457:109–132.

Denisov IG, Grinkova YV, Lazarides AA, Sligar SG (2004) Directed self-assembly of monodisperse phospholipid bilayer Nanodiscs with controlled size. J Am Chem Soc 126:3477–3487.

Denisov IG, McLean MA, Shaw AW, Grinkova YV, Sligar SG (2005) Thermotropic phase transition in soluble nanoscale lipid bilayers. J Phys Chem B 109:15580–15588.

Dörr JM, Schäfer M, Koorengevel MC, Killian JA (2016a) Detergent-Free Isolation, Characterization and Functional Reconstitution of a K+ Channel: The Power of Native Nanodiscs. Biophysical Journal 110:421a

Dörr JM, Scheidelaar S, Koorengevel MC, Dominguez JJ, Schäfer M, van Walree CA, Killian JA (2016b) The styrene–maleic acid copolymer: A versatile tool in membrane research. European Biophysics Journal 45:3

Frisz JF, Lou K, Klitzing HA, Hanafin WP, Lizunov V, Wilson RL, Carpenter KJ, Kim R, Hutcheon ID, Zimmerberg J (2013a) Direct chemical evidence for sphingolipid domains in the plasma membranes of fibroblasts. Proceedings of the National Academy of Sciences 110:E613-E622

Frisz JF, Klitzing HA, Lou K, Hutcheon ID, Weber PK, Zimmerberg J, Kraft ML (2013b) Sphingolipid domains in the plasma membranes of fibroblasts are not enriched with cholesterol. Journal of Biological Chemistry 288:16855–16861

Gennis RB (2013) Biomembranes: Molecular structure and function. Springer Science & Business Media

Griebel T, Zeier J (2010) A role for beta-sitosterol to stigmasterol conversion in plant-pathogen interactions. Plant J 63:254–268.

Gulati S, Jamshad M, Knowles TJ, Morrison KA, Downing R, Cant N, Collins R, Koenderink JB, Ford RC, Overduin M (2014) Detergent-free purification of ABC (ATP-binding-cassette) transporters. Biochemical Journal 461:269–278

Hanada K, Nishijima M, Akamatsu Y, Pagano RE (1995) Both sphingolipids and cholesterol participate in the detergent insolubility of alkaline phosphatase, a glycosylphosphatidylinositol-anchored protein, in mammalian membranes. Journal of Biological Chemistry 270:6254–6260

Heerklotz H (2002) Triton Promotes Domain Formation in Lipid Raft Mixtures. Biophysical Journal 83:2693–2701.

Heimburg T (2000) A Model for the Lipid Pretransition: Coupling of Ripple Formation with the Chain-Melting Transition. Biophysical Journal 78:1154–1165.

Hoffman RV (2004) Organic chemistry: An intermediate text, 2nd ed. Wiley-Interscience, Hoboken N.J.

Huang J, Feigenson GW (1999) A Microscopic Interaction Model of Maximum Solubility of Cholesterol in Lipid Bilayers. Biophysical Journal 76:2142–2157.

Jamshad M, Charlton J, Lin Y-P, Routledge SJ, Bawa Z, Knowles TJ, Overduin M, Dekker N, Dafforn TR, Bill RM (2015a) G-protein coupled receptor solubilization and purification for biophysical analysis and functional studies, in the total absence of detergent. Bioscience reports 35:e00188

Jamshad M, Grimard V, Idini I, Knowles TJ, Dowle MR, Schofield N, Sridhar P, Lin Y, Finka R, Wheatley M, Thomas ORT, Palmer RE, Overduin M, Govaerts C, Ruysschaert J-M, Edler KJ, Dafforn TR (2015b) Structural analysis of a nanoparticle containing a lipid bilayer used for detergent-free extraction of membrane proteins. Nano Res. 8:774–789.

Jouhet J (2013) Importance of the hexagonal lipid phase in biological membrane organization. Front Plant Sci 4:494.

Klumperman B (2010) Mechanistic considerations on styrene–maleic anhydride copolymerization reactions. Polymer Chemistry 1:558–562

Knowles TJ, Finka R, Smith C, Lin Y-P, Dafforn T, Overduin M (2009) Membrane proteins solubilized intact in lipid containing nanoparticles bounded by styrene maleic acid copolymer. J Am Chem Soc 131:7484–7485.

Koynova R, Caffrey M (1998) Phases and phase transitions of the phosphatidylcholines. Biochimica et Biophysica Acta (BBA) - Reviews on Biomembranes 1376:91–145.

Krasnowska EK, Gratton E, Parasassi T (1998) Prodan as a Membrane Surface Fluorescence Probe: Partitioning between Water and Phospholipid Phases. Biophysical Journal 74:1984–1993.

Lewis RN, Mak N, McElhaney RN (1987) A differential scanning calorimetric study of the thermotropic phase behavior of model membranes composed of phosphatidylcholines containing linear saturated fatty acyl chains. Biochemistry 26:6118–6126

Lewis RN, Mannock DA, McElhaney RN, Turner DC, Gruner SM (1989) Effect of fatty acyl chain length and structure on the lamellar gel to liquid-crystalline and lamellar to reversed hexagonal phase transitions of aqueous phosphatidylethanolamine dispersions. Biochemistry 28:541–548

Lichtenberg D, Goñi FM, Heerklotz H (2005) Detergent-resistant membranes should not be identified with membrane rafts. Trends in Biochemical Sciences 30:430–436.

London E, Brown DA (2000) Insolubility of lipids in Triton X-100: Physical origin and relationship to sphingolipid/cholesterol membrane domains (rafts). Biochimica et Biophysica Acta (BBA) - Biomembranes 1508:182–195.

Long AR, O'Brien CC, Malhotra K, Schwall CT, Albert AD, Watts A, Alder NN (2013) A detergent-free strategy for the reconstitution of active enzyme complexes from native biological membranes into nanoscale discs. BMC biotechnology 13:41

Luckey M (2008) Membrane structural biology: With biochemical and biophysical foundations. Cambridge University Press, Cambridge, New York

Macgregor RB, Weber G (1981) Fluorophores in polar media: Spectral effects of the Langevin distribution of electrostatic interactions. Annals of the New York Academy of Sciences 366:140–154

Marrink SJ, Risselada J, Mark AE (2005) Simulation of gel phase formation and melting in lipid bilayers using a coarse grained model. Chem Phys Lipids 135:223–244.

Marsh D (2013) Handbook of lipid bilayers. CRC Press

McMullen TP, Lewis RN, McElhaney RN (2004) Cholesterol–phospholipid interactions, the liquid-ordered phase and lipid rafts in model and biological membranes. Current Opinion in Colloid & Interface Science 8:459–468.

Munro S (2003) Lipid Rafts. Cell 115:377–388.

Nabi IR, Le PU (2003) Caveolae/raft-dependent endocytosis. The Journal of Cell Biology 161:673–677.

Nagle JF, Tristram-Nagle S (2000) Structure of lipid bilayers. Biochim Biophys Acta 1469:159–195

Nelson DL (2016) Lehninger principles of biochemistry, 7th edition. W. H. Freeman, New York NY

Nørholm MHH, Shulga YV, Aoki S, Epand RM, Heijne G von (2011) Flanking residues help determine whether a hydrophobic segment adopts a monotopic or bitopic topology in the endoplasmic reticulum membrane. J Biol Chem 286:25284–25290.

Oluwole AO, Danielczak B, Meister A, Babalola JO, Vargas C, Keller S (2017) Solubilization of Membrane Proteins into Functional Lipid-Bilayer Nanodiscs Using a Diisobutylene/Maleic Acid Copolymer. Angewandte Chemie International Edition 56:1919–1924.

Orwick MC, Judge PJ, Procek J, Lindholm L, Graziadei A, Engel A, Gröbner G, Watts A (2012) Detergent-free formation and physicochemical characterization of nanosized lipid-polymer complexes: Lipodisq. Angewandte Chemie International Edition 51:4653–4657.

Parasassi T, Stasio G de, Ravagnan G, Rusch RM, Gratton E (1991) Quantitation of lipid phases in phospholipid vesicles by the generalized polarization of Laurdan fluorescence. Biophysical Journal 60:179–189

Parasassi T, Krasnowska EK, Bagatolli L, Gratton E (1998) Laurdan and Prodan as polarity-sensitive fluorescent membrane probes. Journal of Fluorescence 8:365–373

Pardo JJD, Dörr JM, Iyer A, Cox RC, Scheidelaar S, Koorengevel MC, Subramaniam V, Killian JA (2017) Solubilization of lipids and lipid phases by the styrene–maleic acid copolymer. European Biophysics Journal 46:91

Pasanen A-L, Yli-Pietilä K, Pasanen P, Kalliokoski P, Tarhanen J (1999) Ergosterol Content in Various Fungal Species and Biocontaminated Building Materials. Appl Environ Microbiol 65:138–142

Prabudiansyah I, Kusters I, Caforio A, Driessen AJM (2015) Characterization of the annular lipid shell of the Sec translocon. Biochimica et Biophysica Acta (BBA) - Biomembranes 1848:2050–2056

Radhakrishnan A, McConnell HM (1999) Condensed Complexes of Cholesterol and Phospholipids. Biophysical Journal 77:1507–1517.

Sanayei RA, O'Driscoll KF, Klumperman B (1994) Pulsed laser copolymerization of styrene and maleic anhydride. Macromolecules 27:5577–5582

Sankaram MB, Thompson TE (1990) Interaction of cholesterol with various glycerophospholipids and sphingomyelin. Biochemistry 29:10670–10675

Sargiacomo M (1993) Signal transducing molecules and glycosyl-phosphatidylinositol-linked proteins form a caveolin-rich insoluble complex in MDCK cells. The Journal of Cell Biology 122:789–807.

Scheidelaar S, Koorengevel MC, Pardo JD, Meeldijk JD, Breukink E, Killian JA (2015) Molecular model for the solubilization of membranes into nanodisks by styrene maleic acid copolymers. Biophysical Journal 108:279–290

Scheidelaar S, Koorengevel MC, van Walree CA, Dominguez JJ, Dörr JM, Killian JA (2016) Effect of Polymer Composition and pH on Membrane Solubilization by Styrene-Maleic Acid Copolymers. Biophysical Journal 111:1974–1986

Seddon AM, Curnow P, Booth PJ (2004) Membrane proteins, lipids and detergents: not just a soap opera. Biochim Biophys Acta 1666:105–117.

Shaw AW, McLean MA, Sligar SG (2004) Phospholipid phase transitions in homogeneous nanometer scale bilayer discs. FEBS Letters 556:260–264.

Simons K, Ikonen E (1997) Functional rafts in cell membranes. Nature 387:569

Somerharju P, Virtanen JA, Cheng KH, Hermansson M (2009) The superlattice model of lateral organization of membranes and its implications on membrane lipid homeostasis. Biochim Biophys Acta 1788:12–23. doi: 10.1016/j.bbamem.2008.10.004

Sot J, Collado MI, Arrondo JLR, Alonso A, Goñi FM (2002) Triton X-100-Resistant Bilayers: Effect of Lipid Composition and Relevance to the Raft Phenomenon. Langmuir 18:2828–2835.

Swainsbury DJK, Scheidelaar S, van Grondelle R, Killian JA, Jones MR (2014) Bacterial reaction centers purified with styrene maleic acid copolymer retain native membrane functional properties and display enhanced stability. Angewandte Chemie International Edition 53:11803–11807

Tanaka M, Hosotani A, Tachibana Y, Nakano M, Iwasaki K, Kawakami T, Mukai T (2015) Preparation and Characterization of Reconstituted Lipid-Synthetic Polymer Discoidal Particles. Langmuir 31:12719–12726.

Tonge, SR, Tighe BJ (2001) Responsive hydrophobically associating polymers: A review of structure and properties. Advanced drug delivery reviews 53:109–122

Tonge SR, Tighe BJ (2002) Lipid-containing compositions and uses thereof

Vargas C, Arenas RC, Frotscher E, Keller S (2015) Nanoparticle self-assembly in mixtures of phospholipids with styrene/maleic acid copolymers or fluorinated surfactants. Nanoscale 7:20685–20696

Veatch SL, Keller SL (2003) Separation of Liquid Phases in Giant Vesicles of Ternary Mixtures of Phospholipids and Cholesterol. Biophysical Journal 85:3074–3083.

Vist MR, Davis JH (1990) Phase equilibria of cholesterol/dipalmitoylphosphatidylcholine mixtures: Deuterium nuclear magnetic resonance and differential scanning calorimetry. Biochemistry 29:451–464

Wallin E, Heijne G von (1998) Genome-wide analysis of integral membrane proteins from eubacterial, archaean, and eukaryotic organisms. Protein Sci 7:1029–1038.

Weber G, Farris FJ (1979) Synthesis and spectral properties of a hydrophobic fluorescent probe: 6-propionyl-2-(dimethylamino)naphthalene. Biochemistry 18:3075–3078

Zhou H-X, Cross TA (2013) Influences of membrane mimetic environments on membrane protein structures. Annu Rev Biophys 42:361–392.

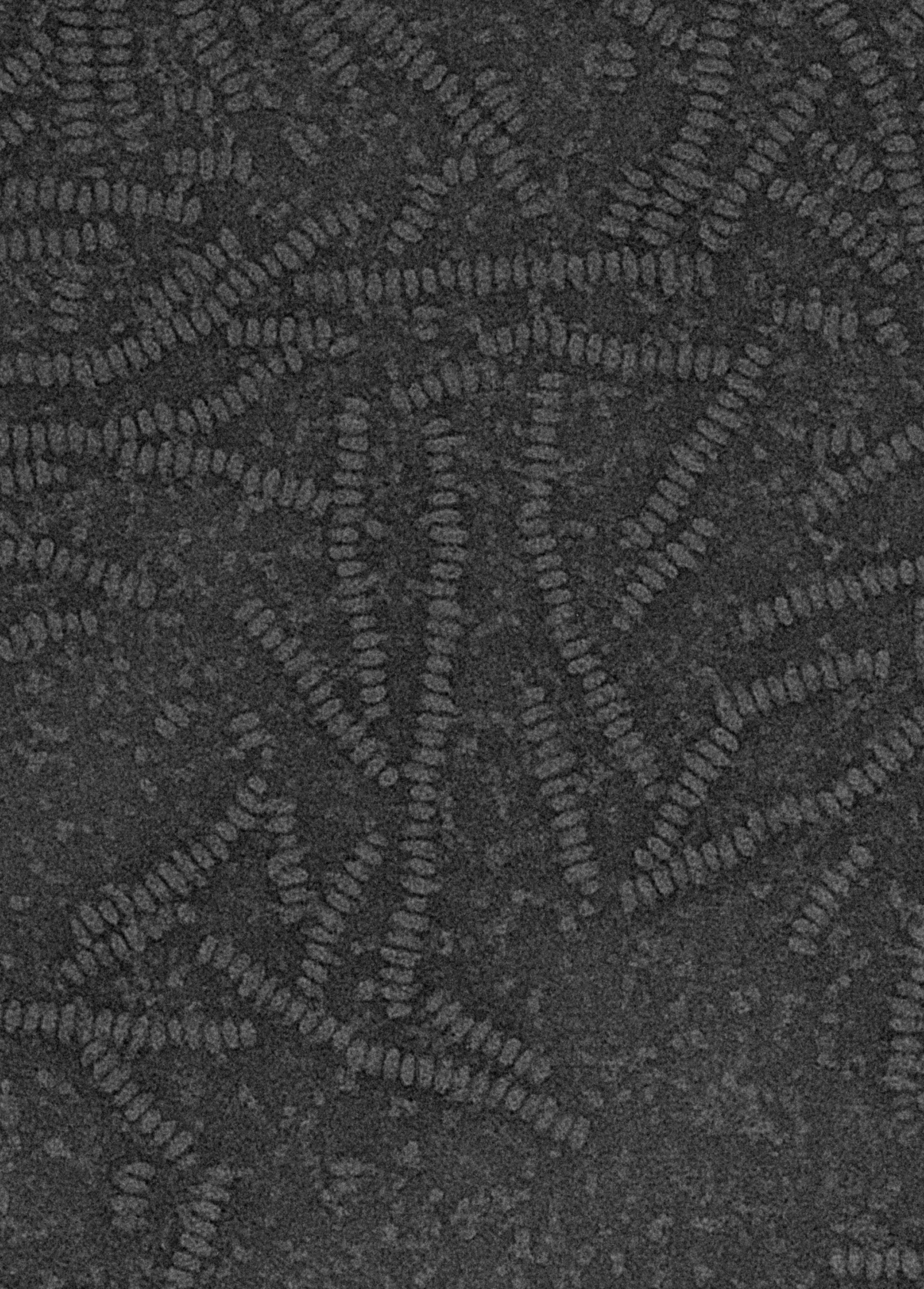

Chapter II

Solubilization of lipids and lipid phases by the styrene-maleic acid copolymer

J. J. Domínguez Pardo†*, J. M. Dörr†, A. Iyer‡, R. C. Cox†, S. Scheidelaar†, M. C. Koorengevel†, V. Subramaniam‡ and J. A. Killian†*

† Membrane Biochemistry & Biophysics, Bijvoet Center for Biomolecular Research, Department of Chemistry, Faculty of Science, Padualaan 8, 3584 CH Utrecht, The Netherlands.
‡ Nanoscale Biophysics Group, FOM Institute AMOLF, Science Park 104, 1098 Amsterdam, The Netherlands

This chapter has been published in Eur. Biophys. J. 46, 91-101. 2017

Abstract

A promising tool in membrane research is the use of the styrene–maleic acid (SMA) copolymer to solubilize membranes in the form of nanodiscs. Since membranes are heterogeneous in composition, it is important to know whether SMA thereby has a preference for solubilization of either specific types of lipids or of specific bilayer phases. Here, we investigated this by performing partial solubilization of model membranes and analyzing the lipid composition of the solubilized fraction. We found that SMA displays no significant lipid preference in homogeneous binary lipid mixtures in the fluid phase, even when using lipids which by themselves show very different solubilization kinetics. By contrast, in heterogeneous phase-separated bilayers, SMA was found to have a strong preference for solubilization of lipids in the fluid phase as compared to those in either a gel phase or a liquid-ordered phase. Together the results suggest that (i) SMA is a reliable tool to characterize native interactions between membrane constituents, (ii) any solubilization preference of SMA is not due to properties of individual lipids but rather due to properties of the membrane or membrane domains in which these lipids reside and (iii) exploiting SMA resistance rather than detergent resistance may be an attractive approach for the isolation of ordered domains from biological membranes.

Introduction

In recent years, the styrene–maleic acid (SMA) copolymer has evolved as an important tool for isolation and characterization of membrane proteins (for review see (Dörr et al. 2016)). SMA has been shown to solubilize biological membranes in the form of nanodiscs allowing the isolation of membrane proteins directly from their native environment without the need for detergent (Long et al. 2013; Dörr et al. 2014; Gulati et al. 2014; Swainsbury et al. 2014; Jamshad et al. 2015; Prabudiansyah et al. 2015). The small size of these so-called "native nanodiscs" enables their characterization by a variety of biophysical approaches (Orwick et al. 2012; Orwick-Rydmark et al. 2012; Dörr et al. 2014; Swainsbury et al. 2014; Jamshad et al. 2015; Vargas et al. 2015; Dörr et al. 2016) Furthermore, the presumed preservation of the annular lipid environment helps to maintain the stability of the embedded proteins and thereby allows the use of SMA as a convenient tool to study preferential lipid–protein interactions, simply by analyzing the lipid composition of purified protein-containing nanodiscs and comparing it with that of the native membrane (Dörr et al. 2014; Swainsbury et al. 2014; Prabudiansyah et al. 2015).

For unambiguous analysis of preferential lipid–protein interactions using SMA, it is however of crucial importance to know whether or not SMA by itself exhibits any lipid preference during solubilization. This can be conveniently investigated by employing synthetic model membrane systems, which allow highly systematic variation of lipid composition. Solubilization of model membranes by SMA results in the formation of styrene–maleic acid lipid particles (SMALPs), which have similar sizes and properties as membrane protein-containing (native) nanodiscs (Dörr et al. 2016). Using such model systems, it has been shown that the interaction of SMA with membranes strongly depends on lipid composition, with the kinetics of solubilization being modulated by e.g. surface charge, lipid packing and lipid chain length (Scheidelaar et al. 2015). This would suggest that SMA might exhibit a lipid preference towards solubilization. However, experiments in which model membranes of an *Escherichia coli* total lipid extract were partially solubilized, showed that the SMA-solubilized fraction exhibits no significant enrichment in specific lipid species (Scheidelaar et al. 2015). Together these results suggest that SMA is promiscuous, and that solubilization is determined by overall properties of the membrane rather than by properties of individual lipids. This was supported by a recent study using ^{31}P NMR (Cuevas Arenas et al. 2016).

So far the lipid mixtures that have been used to study preferential solubilization by SMA represent only a few selected homogeneous lipid mixtures in the fluid phase and no systematic studies have been reported yet on a possible lipid preference of SMA. Also, it has not been investigated whether

SMA exhibits any preference in heterogeneous membranes that exhibit domain formation and that arguably are biologically more relevant than homogeneous fluid bilayers.

To obtain insight into these matters, we here set out to investigate to what extent preferential solubilization of lipids by SMA occurs in simple binary lipid systems forming a single homogeneously-mixed fluid phase and in heterogeneous phase-separated membranes exhibiting coexistence of a fluid phase with either gel or liquid-ordered phase. In order to maximize our "window" for monitoring any potential preferences of the polymer, the following strategy was employed. First, combinations of lipids were selected which on their own would have very different SMA solubilization kinetics. Second, to achieve partial solubilization short incubation times of 1 h were used thereby avoiding full equilibration of the system. This required adjustment of the concentration of SMA for each system individually in order to obtain sufficient material for reliable analysis. Third, multilamellar vesicles (MLVs) were chosen as lipid system, which has the following advantages: (i) MLVs provide a large accessible surface area which diminishes the chance of "all or nothing" effects that may occur for small vesicles, i.e. full solubilization of some membranes and no solubilization of others, (ii) by employing these larger structures any potential curvature effects are avoided, and (iii) the use of these larger structures facilitates the separation of solubilized and non-solubilized material by centrifugation.

The results show that SMA is indeed highly promiscuous with respect to solubilization of lipid species in homogeneous fluid bilayers, but that there is a clear preference for solubilization of the fluid phase in phase-separated bilayers with either a gel phase or a fluid phase. We will discuss the implications of these findings regarding the general applicability of SMA as a tool to determine preferential lipid–protein interactions. We will also discuss the use of SMA for the isolation of SMA-resistant membranes (SRMs) as an alternative to conventionally-studied detergent-resistant membranes (DRMs).

Materials and Methods

Materials

All lipids were purchased from Avanti Polar Lipids (Alabaster, AL). The used lipids were: 1,2-dioleoyl-*sn*-glycero-3-phosphocholine (di-18:1 PC); 1,2-dioleoyl-*sn*-glycero-3-phospho(1'-rac-glycerol) (di-18:1 PG); 1,2-dioleoyl-*sn*-glycero-3-phosphoethanolamine (di-18:1 PE); 1,2-distearoyl-*sn*-glycero-3-phosphocholine (di-18:0 PC); 1,2-dimyristoleoyl-*sn*-glycero-3-phosphocholine (di-14:1 PC); 1,2-di-(9Z-hexadecenoyl)-*sn*-glycero-3-phosphocholine (di-16:1 PC); 1,2-di-(11Z-eicosenoyl)-*sn*-glycero-3-phosphocholine (di-20:1 PC); 1,2-dierucoyl-*sn*-glycero-3-phosphocholine (di-22:1 PC); 1-palmitoyl-2-oleoyl-**sn**-glycero-3-phosphocholine (16:0/18:1 PC); brain sphingomyelin (bSM); cholesterol; 23-(dipyrromethene boron difluoride)-24-norcholesterol (Top-Fluor-cholesterol) and 1,2-dioleoyl-*sn*-glycero-3-phosphoethanolamine-N-(lissamine rhodamine B sulfonyl) (rhodamine-PE).

Xiran 25010, a styrene–maleic anhydride copolymer with a molar ratio of styrene-to-maleic anhydride of 3:1 and a weight average molecular weight of 10 kDa, was a kind gift from Polyscope (Geleen, Netherlands). Xiran 25010 (anhydride copolymer) was converted to the acid form by hydrolysis under base-catalytic conditions as detailed elsewhere (Scheidelaar et al. 2015). All other chemicals used were from Sigma Aldrich (St. Louis, MO) .

Preparation of multilamellar vesicles (MLVs)

Phospholipid stock solutions in chloroform/methanol (9:1 v/v) were mixed in predetermined ratios and the solvent was removed under a stream of N_2. The resulting lipid film was dried in a desiccator under vacuum for at least 1 h. MLVs were obtained by hydrating the lipid films with solubilization buffer (50 mM Tris-HCl, 150 mM NaCl, pH 8.0). The samples were then subjected to 10 freeze–thaw cycles, each consisting of 3 min of freezing in liquid N_2 (–196 °C) and 3 min of thawing in a water bath at 50 °C, well above the gel-to-fluid phase transition temperature (T_m) of the lipids. For vesicles containing di-18:0 PC (T_m = 56 °C (Lewis et al. 1987; Marsh 2013)) the water bath was kept at 60 °C to ensure membrane fluidity.

Turbidimetry experiments

The solubilization of MLVs was monitored by turbidimetry, using a Lambda 18 spectrophotometer (PerkinElmer, Waltham, MA) as described previously (Scheidelaar et al. 2015). Briefly, 700-µL aliquots of 0.5-mM dispersions of MLVs in solubilization buffer were transferred to a quartz cuvette

and equilibrated at the desired temperature for 10 min. Next, different amounts of SMA were added as detailed in the legends of the corresponding figures and the solubilization kinetics were followed at a fixed wavelength of 350 nm by monitoring the decrease of the apparent absorbance. Absorbance values were recorded every 0.4 s.

Analysis and quantification of the lipid composition of solubilized fractions

Partial solubilization of vesicles

To achieve partial solubilization while still obtaining enough lipid material for further analysis, the SMA concentration was tuned for each lipid mixture individually. Accordingly, 700-µL aliquots of 0.5-mM dispersions of MLVs in solubilization buffer were supplemented with an amount of SMA that led to a decrease in apparent absorbance to approximately 50–60 % after 1 h of incubation. Vesicles containing liquid-ordered domains required higher amounts of SMA for sufficient solubilization due to their higher solubilization resistance. Detailed incubation conditions for each sample are specified in the legends of the corresponding figures.

Lipid isolation

After 1 h of incubation with SMA, the samples were cooled down on ice and then transferred to a pre-chilled ultracentrifuge. The non-solubilized material was removed by centrifugation at 115,000 × *g* for 1 h at 4 °C and the supernatant, containing the solubilized lipid material, was collected. The lipids from the supernatant and from an aliquot of non-treated MLVs were extracted according to the method of Bligh and Dyer (Bligh and Dyer 1959) (see Supporting Information) prior to analysis.

Lipid analysis and quantification

The procedure for lipid analysis and quantification was selected depending on the lipid composition of the membrane. Lipids with different headgroups were separated by thin layer chromatography (TLC). Quantification was then achieved by densitometric analysis after copper staining (Dörr et al. 2014; Swainsbury et al. 2014). Phospholipids with the same headgroup but with unsaturated acyl chains of different length were separated by reverse-phase TLC. After iodine staining, each spot was scraped off and the amount of phosphate was determined by the method of Rouser (Rouser et al. 1970). For phospholipids with the same headgroup but with acyl chains differing in degree of unsaturation reverse-phase TLC did not provide sufficient separation. These samples were therefore

quantified by gas chromatography after esterification of the fatty acids (de Smet, C. H. et al. 2012; Dörr et al. 2014). For detailed experimental descriptions see Supporting Information.

Transmission electron microscopy

Size characterization of the SMALPs present in the supernatant fractions resulting from turbidimetry experiments was performed by transmission electron microscopy. To this end, copper grids were prepared following the carbon flotation technique. Briefly, samples were diluted with solubilization buffer to a lipid concentration of 0.5–1 mM and small aliquots were adsorbed on carbon-coated mica. The mica was then transferred to a staining solution containing 2% (w/v) sodium silico tungstate, causing detachment of the carbon film. Subsequently, a copper grid was placed on top of the detached carbon which was recovered and dried under air flow. Images were taken under low dose conditions at a nominal magnification of 49,000 with a T12 electron microscope (FEI, Hillsboro, OR) at an operating voltage of 120 kV using an ORIUS SC1000 camera (Gatan, Inc., Pleasanton, CA). The average size of the SMALPs was estimated manually from 16 well-defined individual particles randomly located through the image based on their maximum diameter using Adobe Illustrator software (San Jose, CA). This procedure was used to avoid potential artefacts such as stain-induced particle aggregation or inhomogeneous particle staining (Wan et al. 2011; Zhang et al. 2011; Scheidelaar et al. 2015)

Fluorescence imaging

Fluorescence microscopy imaging was performed at room temperature using a Nikon A1 confocal microscope (Tokyo, Japan) equipped with a Perfect Focus system. Supported lipid bilayers (SLBs) were prepared in a custom-built chamber following the vesicle fusion procedure (see Supporting Information). Solubilization of SLBs by SMA was assessed under a continuous flow of solubilizing agent solution. Images were taken before addition of SMA and after 5 min of incubation using a 100x oil immersion 1.49-NA objective (Nikon) under identical conditions of laser power and gain for all samples. Top-Fluor cholesterol and rhodamine-PE were imaged sequentially using a 488-nm and 561-nm laser, respectively, to avoid spectral cross-talk. The images were acquired with a resolution of 512 × 512 pixels (pixel size 0.41 × 0.41 µm).

Fluorescence intensities were quantified from intensity histograms using NIS Elements software (Nikon). Intensity values are expressed as an average of the intensities calculated from 5 different snapshots randomly picked from the planar bilayer. A representative video of the solubilization process can be found in the Supporting Information (Video S1).

Results

SMA does not display a preference for individual lipid species when solubilizing homogeneously mixed bilayers.

It was previously demonstrated in model membrane systems that lipid headgroup and acyl chain composition are important determinants for the kinetics of SMA solubilization (Scheidelaar et al. 2015). Here, we investigated whether two lipids that exhibit very different solubilization kinetics will be selectively solubilized by SMA, when homogenously mixed in a lipid bilayer. For this we selected mixtures of di-18:1 PC as "host" lipid with an equimolar amount of different "guest" lipids. The choice of these guest lipids was motivated by our previous observations (Scheidelaar et al. 2015) that (i) lipids with short chains are solubilized faster than lipids with longer acyl chains, most likely as a consequence of the lower number of van der Waals interactions between neighboring chains; (ii) bilayers containing negatively charged lipids exhibit much slower solubilization kinetics than bilayers of zwitterionic lipids, presumably due to electrostatic repulsion by the negative charge of the polymer; (iii) bilayers containing lipids in the gel phase, cone-shaped lipids or unsaturated lipids are solubilized more slowly than bilayers containing cylindrical lipids or saturated lipids in the fluid phase. These latter effects were ascribed to differences in packing density of the acyl chains, with tighter packing hindering the insertion of the polymer and subsequent solubilization.

To obtain insights into a possible selectivity of SMA for certain lipids an approach of partial solubilization of MLVs was used, as illustrated in Figure 1A for a mixture of di-18:1 PC with the anionic lipid di-18:1 PG, which is known to form homogenously-mixed bilayers(Nibu et al. 1995; Marsh 2013). The soluble fraction after incubation with SMA for 1 h, was subjected to electron microscopy (EM) imaging (Figure 1B) and to lipid composition analysis by TLC (Figure 1C). The EM data (Figure 1B) show a homogeneous distribution of particles of a size of 6–8 nm (Table 1), which is at the lower end of the range of commonly reported dimensions of around 10 nm (see e.g. (Orwick et al. 2012; Jamshad et al. 2015; Scheidelaar et al. 2015)). Lipid composition analysis of the solubilized fraction after SMA incubation revealed that PC and PG are present in a similar molar ratio as in the initial vesicles (Figure 2A), indicating non-selective solubilization of both lipids. Considering the electrostatically unfavorable interaction of SMA with negatively charged lipids (Scheidelaar et al. 2015), this result is rather surprising and suggests that SMA does not perturb the bilayer homogeneity.

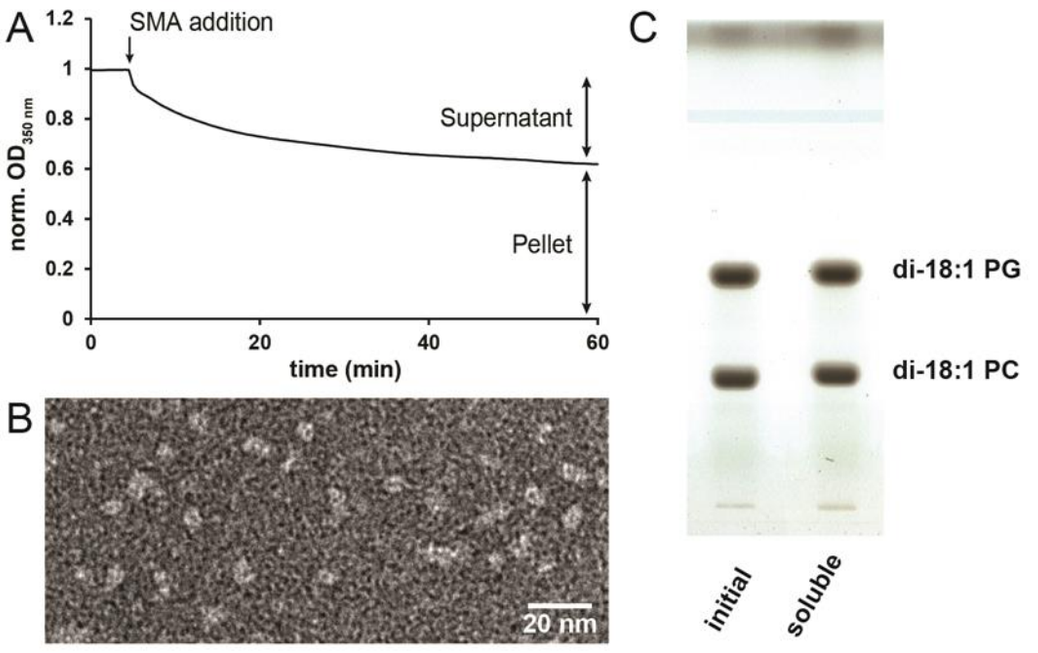

Figure 1. Partial solubilization of vesicles by SMA (*A*) Kinetics of SMA solubilization of MLVs composed of an equimolar mixture of di-18:1 PC and di-18:1 PG (0.5 mM lipid, SMA-to-lipid mass ratio of 0.64) at 25 °C. Data are shown as normalized optical density at 350 nm. (*B*) Visualization of the SMALPs from the supernatant by negative-stain transmission electron microscopy. (*C*) Thin layer chromatography analysis of the lipid composition of lipids extracted from non-treated MLVs as well as the soluble fraction after partial solubilization by SMA.

Similar experiments were performed with other homogeneous lipid mixtures in the fluid phase. The results are summarized in Figure 2A and Table 1, while original solubilization traces and representative EM micrographs can be found in Figure S1. When di-18:1 PC was mixed with the cone-shaped lipid di-18:1 PE, again it was found that SMA does not show a lipid preference (Figure 2A), despite the slower kinetics of solubilization of PC/PE as compared to pure PC bilayers (Scheidelaar et al. 2015). This non-selective solubilization is in line with results from a recent study of a very similar lipid system (Cuevas Arenas et al. 2016). A different result was obtained for mixtures of lipids with varying acyl chain length, where a small preference was observed for solubilization of di-14:1 PC over di-18:1 PC (Figure 2A). To elucidate whether this preference might be related to hydrophobic mismatch effects, we also tested mixtures in which di-14:1 PC was kept as the shorter lipid, while the length difference between the lipid components was either increased or decreased (Figure S2A). In all cases, the results showed a similar small preference for di-14:1 PC, suggesting that this is an artefact related to a particular feature of di-14:1 PC, perhaps being more easily extracted from the membrane due its short unsaturated acyl chains. This hypothesis is supported by the results obtained from partial solubilization of di-18:1 PC/di-22:1 PC membranes (Figure S2B), where the solubilized fraction has a similar lipid composition as the initial vesicles. Finally, a mixture of di-18:1 PC with di-

18:0 PC was tested under conditions where both lipids are in the fluid phase. This was achieved by raising the incubation temperature to 60 °C, above the gel-to-liquid crystalline phase transition temperature of di-18:0 PC. Here, again no preference for either lipid species was observed (Figure 2A).

For all the solubilized fractions corresponding to Figure 2, the formed SMALPs appeared to have a rather similar size in the range of 6–10 nm as visualized by EM imaging (Figure 1B, Figure S1) and as quantified in Table 1. Previously it was reported that the use of relatively low SMA concentrations might result in the formation of larger particles (Vargas et al. 2015; Zhang et al. 2015). However, in our case the different populations of SMALPs were found to be fairly small with a relatively uniform size distribution, despite conditions of relatively low SMA concentrations (SMA-to-lipid mass ratio of 0.3–1.3). Importantly, similar particle sizes were found under conditions of using a higher SMA-to-lipid ratio, longer incubation times, and higher lipid concentrations, which allowed characterization of the particles by both EM and dynamic light scattering (Figure S2, Table S1). Together these data support the validity of our partial solubilization approach.

Overall, the data show that SMA is highly promiscuous with respect to solubilization of lipid species when these are present as homogeneously mixed bilayers in the fluid phase. Whether preferences of SMA solubilization do occur in bilayers with a heterogeneous lipid distribution was investigated next.

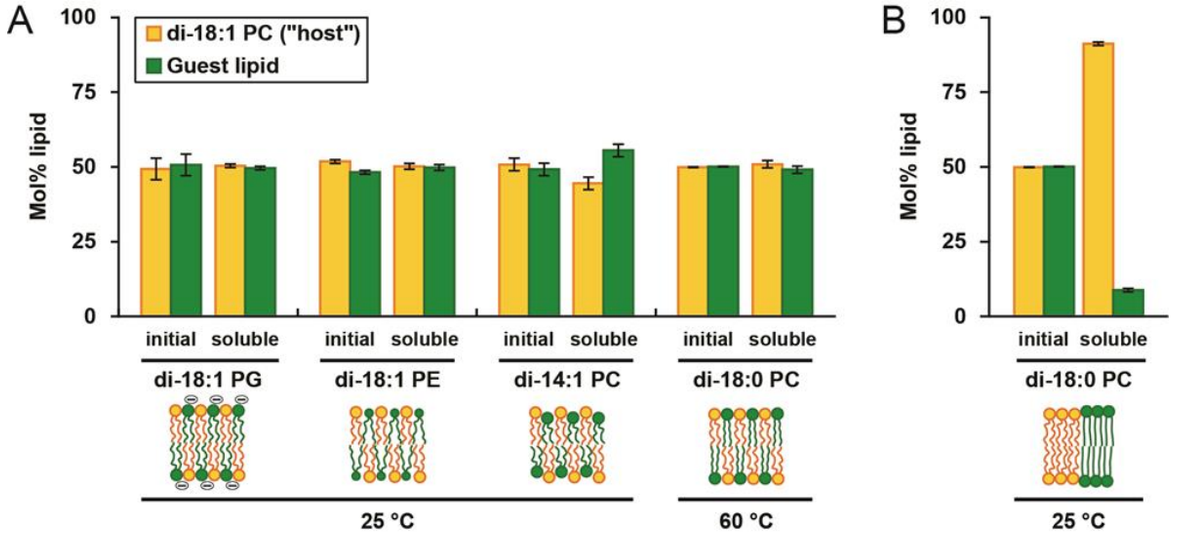

Figure 2. Solubilization preference of SMA in binary lipid systems with different properties assessed by lipid composition analysis after partial solubilization. (*A*) Equimolar mixtures of the zwitterionic unsaturated di-18:1 PC ("host", orange) with different guest lipids (green) under conditions of phase homogeneity. From left to right: anionic di-18:1 PG, cone-shaped di-

18:1 PE, short chain di-14:1 PC and saturated di-18:0 PC. Respective SMA-to-lipid mass ratios at 0.5 mM lipid were 0.64, 1.31, 0.27 and 0.13. Phase homogeneity for di-18:1 PC/di-18:0 PC was achieved by elevating the temperature to 60 °C, above T_m of di-18:0 PC (T_m = 56 °C) (Lewis et al. 1987; Marsh 2013). (B) Equimolar mixture of di-18:1 PC and di-18:0 PC under conditions of phase separation at 25 °C (SMA-to-lipid mass ratio 1.27). Cartoons show the schematic bilayer organization before addition of SMA. Error bars represent the standard deviation of 3 independent experiments.

Lipid mixture (1:1, molar)	Incubation temperature (°C)	Size (nm)
di-18:1 PC/di-18:1 PG	25	6–8
di-18:1 PC/di-18:1 PE	25	8–10
di-18:1 PC/di-14:1 PC	25	6–8
di-18:1 PC/di-18:0 PC	60	8–10
di-18:1 PC/di-18:0 PC	25	6–8

Table 1. Nanodisc size characterization based on analysis of EM data

SMA preferentially solubilizes the fluid phase under conditions where gel phase and fluid phase coexist.

A heterogeneous lipid bilayer can easily be obtained in mixtures of lipids with unsaturated (low T_m) and saturated (high T_m) acyl chains by lowering the temperature well below T_m of the saturated lipid. For instance, in the above-described equimolar mixture of di-18:1 PC and di-18:0 lowering the temperature to 25 °C promotes a situation where gel and fluid (liquid-crystalline) phase coexist (Marsh 2013). Under these conditions, SMA shows a strong preference towards solubilizing the fluid phase, which is mainly constituted by di-18:1 PC (Figure 2B). This result is in accordance with the much faster solubilization kinetics of lipids in the fluid phase as compared to lipids in the gel phase (Scheidelaar et al. 2015; Cuevas Arenas et al. 2016). For bilayers exhibiting phase coexistence, the lipid preferences of SMA under conditions of partial solubilization thus do appear to reflect the differences in solubilization kinetics between the lipids in their respective phases.

SMA preferentially solubilizes the fluid liquid-disordered matrix upon incubation with membranes containing liquid-ordered domains.

The resistance of gel-phase lipids against solubilization by SMA raises the question whether this is a general phenomenon for phases in which the lipids exhibit a high degree of order. This was first

tested by adding SMA to a binary mixture of brain sphingomyelin (bSM) and cholesterol that forms a liquid-ordered (L_o) phase (Sankaram and Thompson 1990; Rodrigo F.M. de Almeida et al. 2003). Addition of an amount of SMA that is generally sufficient to rapidly solubilizes homogeneous bilayers in the fluid phase (SMA-to-lipid mass ratio of 3.5) did not lead to any decrease in apparent absorbance after 1 h for this system (Figure S4), and neither did increasing the SMA concentration or prolonging incubation times (data not shown), indicating a very poor solubilization efficiency of SMA for lipids in the L_o phase. These results resemble those reported for the non-ionic detergent Triton X-100 (TX-100), for which the L_o phase shows a well-described detergent resistance (see e.g. (Patra et al. 1999; Erwin London and Deborah A. Brown 2000; Rinia et al. 2001; Veiga et al. 2001; Sot et al. 2002; El Kirat and Morandat 2007)).

The solubilization potential of SMA was further investigated in an equimolar ternary lipid mixture of di-18:1 PC, bSM and cholesterol. Over a wide temperature range, bilayers of such composition exhibit phase separation, containing L_o domains enriched in sphingomyelin and cholesterol that coexist with a fluid liquid-disordered (L_d) matrix enriched in di-18:1 PC (Rodrigo F.M. de Almeida et al. 2003; Veatch and Keller 2003; Marsh 2013). As shown from the TLC results in Figure 3A and as quantified in Figure 3B, the lipid material solubilized from these membranes after incubation with SMA at 25°C is clearly enriched in di-18:1 PC, while it is depleted in bSM and cholesterol in approximately equimolar amounts. At 4 °C, the SMA-solubilized fraction has a rather similar lipid composition as at 25 °C, while at 37 °C the solubilized fraction resembles the non-treated case more closely (Figure 3B). These results are consistent with a preferential solubilization of the L_d phase over the L_o phase by SMA at lower temperatures, which may be ascribed to tight packing and preferential SM–cholesterol interactions that cause co-segregation from the fluid phase (Sankaram and Thompson 1990; Patra et al. 1999; Veiga et al. 2001; Veatch and Keller 2003). Indeed, in the absence of cholesterol an equimolar mixture of bSM and di-18:1 PC was found to be solubilized in equimolar amounts of both lipids (Figure S5), demonstrating the large effect of cholesterol on lipid organization. At 37 °C, both cholesterol and bSM are more readily solubilized, which are likely to be related to the beginning of a gradual liquid ordered-to-fluid phase transition (McMullen et al. 2004; Lichtenberg et al. 2005). Based on our findings of non-preferential SMA solubilization in homogeneous bilayers (Figure 2A) it is likely that also this phase-separating ternary lipid mixture will be solubilized without a (strong) preference in case it exists in a homogeneous fluid phase. Similar results showing a high predisposition of the SMA copolymer to solubilize the L_d phase over the L_o phase were obtained for a phase-separating ternary lipid mixture of 16:0/18:1 PC, bSM and cholesterol (Figure S6).

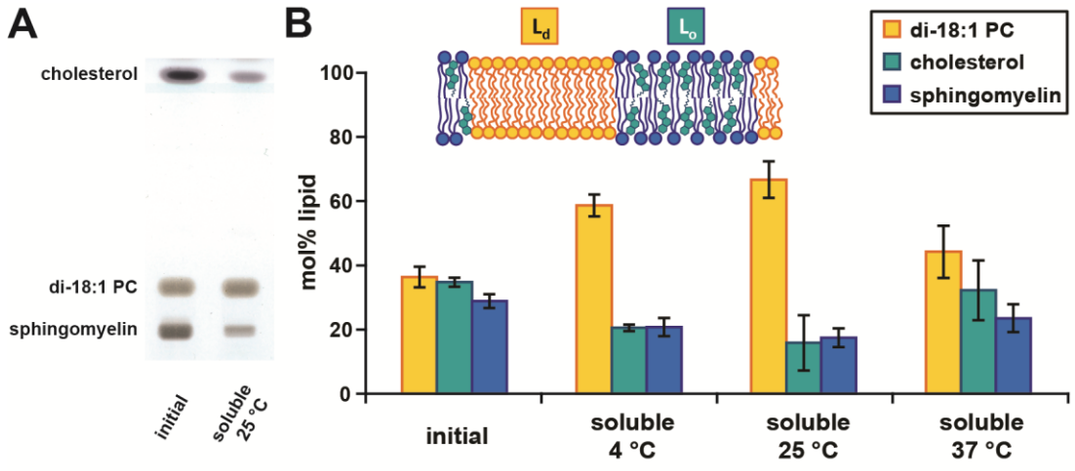

Figure 3. Lipid composition analysis after partial solubilization of MLVs composed of an equimolar ternary lipid mixture of di-18:1 PC, bSM and cholesterol by SMA. The inset shows a simplified schematic cartoon representation. (*A*) TLC plate with lipids extracted from non-treated vesicles and from the soluble fraction after incubation with SMA at 25 °C. (*B*) Quantification of lipid composition shown as mol% lipid (color coding consistent with cartoon) for non-treated vesicles as well as the solubilized fractions after the incubation with SMA (0.5 mM lipid, SMA-to-lipid mass ratio of 3.1) at different temperatures. Error bars represent the standard deviation of 3 independent experiments.

To gain more insight into the mode of action of SMA in phase-separated bilayers, we performed additional experiments where the solubilization of di-18:1 PC/bSM/cholesterol membranes was monitored using fluorescence microscopy. For these experiments we used supported lipid bilayers (SLBs) that were supplemented with a small amount of lipid-derived fluorescent dyes that partition selectively into the L_o or L_d phase (Klymchenko and Kreder 2014). At room temperature, the SLBs showed a clear phase separation, with L_o domains varying in size from 0.1–2 µm (Figure 4A). After 5 min of incubation with 0.1 % (w/v) of SMA, the fluorescence intensity of the L_d probe dropped by more than 50 %, while the fluorescence emitted by the L_o probe decreased only marginally (Figure 4B). When the SMA concentration was increased to 0.5 % (w/v) only background levels of L_d fluorescence could be detected while the L_o fluorescence was still at approximately 40 % of the initial intensity. Importantly, no further decrease in L_o fluorescence was observed when the SMA concentration was further increased to 1% (w/v) (Figure 4B, see also Video S1) or when the sample was allowed to further incubate with the SMA solution for several hours (data not shown). Thus, the L_d phase enriched in di-18:1 PC is efficiently solubilized by SMA while the L_o domains show a high resistance against solubilization, which is in agreement with the experiments performed with vesicles at the same temperature.

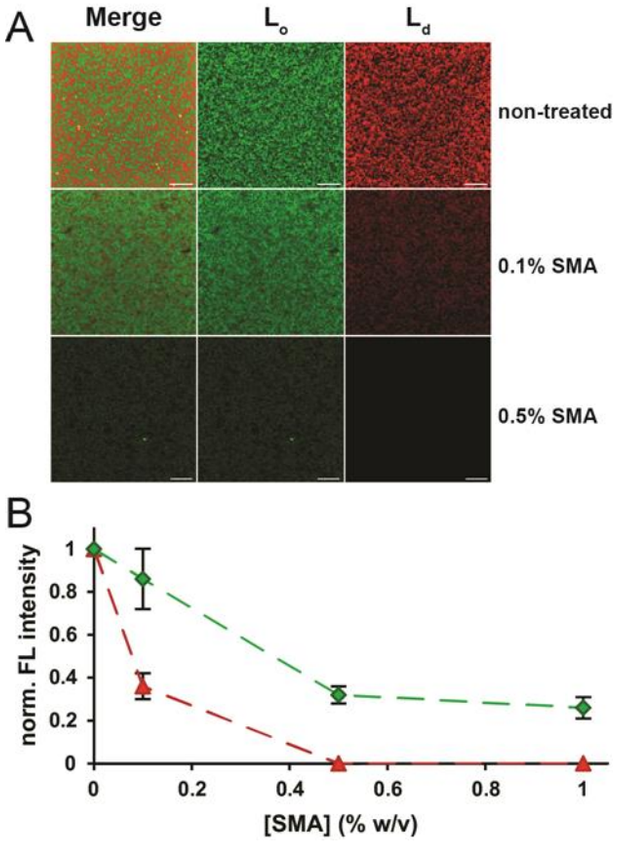

Figure 4. Preferential solubilization in supported lipid bilayers composed of an equimolar ternary lipid mixture of di-18:1 PC, bSM and cholesterol. (*A*) Fluorescence microscopy images are shown as merged (left column) and single channels (green: top-fluor-cholesterol, middle column; red: rhodamine-PE, right column) for non-treated samples and after incubation times of 5 min with different amounts of SMA in solubilization buffer. The scale bars correspond to 10 µm. (*B*) Quantification of the fluorescence intensity in the images from (*A*). Dashed lines are depicted to guide the eye. All experiments were performed at room temperature. Error bars represent the standard deviation of the fluorescence intensity of 5 snapshots randomly picked from the planar bilayer.

Discussion

The experiments described in this study reveal new insights into the process of membrane solubilization by SMA and how it depends on physicochemical properties of individual lipids and those of the membrane or membrane domains they reside in. Here, we will discuss our findings and the implications for the use of SMA as tool to (i) study lipid–protein interactions and (ii) isolate ordered domains from biological or model membranes.

SMA as a tool to study lipid–protein interactions.

To obtain insight into whether SMA by itself has any preference for solubilization of specific lipids, we performed partial solubilization experiments on binary lipid mixtures. The results strongly suggest that under conditions of phase homogeneity there is no significant preference of SMA to solubilize any glycerophospholipid species. This is irrespective of differences in solubilization kinetics of the individual lipids upon changing properties such as headgroup charge, lipid shape, acyl chain saturation or acyl chain length. A potential exception is di-14:1 PC that was found to be incorporated into SMALPs with a slight preference, probably due to its short and unsaturated acyl chains. Importantly, the observed full promiscuity of SMA in solubilizing homogeneous fluid bilayers suggests that SMA by itself does not perturb the bilayer homogeneity. Thus, our findings support the validity of the use of SMA to study preferential lipid–protein interactions of membrane proteins that are extracted from biological membranes (Dörr et al. 2014; Swainsbury et al. 2014; Prabudiansyah et al. 2015). Here, a snapshot view of the interplay of lipids and proteins in biological membranes can be obtained, provided that the proteins reside in a fluid lipid environment.

However, biological membranes in general are heterogeneous and may contain domains that are more ordered (Deborah A. Brown and John K. Rose 1992; Schroeder et al. 1994; Simons and Ikonen 1997). Our experiments with phase-separating lipid bilayers show that distinct solubilization preferences of SMA do arise under conditions of phase coexistence of a fluid phase with either a gel phase or a L_o phase. In both cases, the soluble fractions consisted almost exclusively of lipids that were in the fluid phase. For gel phases it was previously postulated that it is the tight packing of the chains that is responsible for the poor solubilization yield, because it increases the energetic barrier for SMA molecules to penetrate into the bilayer core (Scheidelaar et al. 2015; Cuevas Arenas et al. 2016). The same explanation would hold for the L_o phase, because it displays a similarly high degree of order of the acyl chains (Ipsen et al. 1987). Together these results demonstrate that lipid packing plays a major role in the resistance against solubilization by SMA. What are the implications of these results for the use of SMA for the investigation of preferential lipid–interactions for proteins that reside in either gel phase domains or liquid-ordered domains? Obviously, such proteins will not easily be solubilized into SMALPs. However, they may be isolated as insoluble domains instead, as will be further discussed below. Although analysis of the lipid environment in such a case will not provide a snapshot of the immediate lipid environment, it may nevertheless provide relevant information on the lipid composition of the domains that the protein resides in.

SMA as a tool to isolate ordered domains.

The clear preference of SMA to solubilize the fluid phase under conditions of phase coexistence holds promise for applications for the isolation of SMA-resistant membrane (SRM) domains. On the one hand, these could be applied to domains with a very high protein density, as was recently demonstrated by experiments in which SMA was used to prepare thylakoid membrane fractions that are enriched in specific photosystem complexes (Bell et al. 2015). On the other hand, they could involve approaches similar to those exploiting detergent resistance of certain membrane domains.

Resistance against detergent solubilization is a well-known phenomenon in membrane research, which has been used extensively to prepare DRMs from biological samples (Deborah A. Brown and John K. Rose 1992; Cerneus et al. 1993; Schroeder et al. 1994; Hanado et al. 1995). In particular, TX-100 resistance at low temperatures has been exploited for the isolation of DRM fractions from mammalian plasma membranes. These DRM fractions have been associated to so-called “lipid rafts”, which are postulated to be specific membrane domains that are enriched in (glyco)sphingolipids, cholesterol and specific proteins, and that have important roles in membrane function (Schroeder et al. 1994). The basis of their detergent resistance is ascribed to the ordered nature of the lipid chains in these domains (Schroeder et al. 1994; Simons and Ikonen 1997). Our results with model membranes suggest that SMA may be used in a similar way as conventional detergent to isolate highly-ordered membrane domains in the form of SRMs.

This raises the question how the two approaches to isolate ordered domains from biological membranes would compare. DRMs are unlikely to have the same composition as postulated natively-occurring lipid rafts in the plasma membrane at physiological temperature (Heerklotz 2002; Lichtenberg et al. 2005). One reason for this is that conditions for DRM isolation usually include low temperatures, which will promote phase separation and thereby may cause further deviation from the composition of lipid rafts as they may occur at physiological temperature. Furthermore, by partitioning into the membrane, TX-100 shifts the thermodynamic equilibrium of phase separation (Heerklotz 2002) and thus likely affects the composition of lipid rafts that are isolated in DRMs. Alternatively, TX-100 has been postulated to increase the sizes of these domains (Priyadarshini and London 2011)

It is not known yet to what extent this also holds for SMA. However, there is evidence that suggests that SMA may be less perturbing than detergent. It has been classified as an extraordinarily mild solubilizing agent (Vargas et al. 2015; Cuevas Arenas et al. 2016) having a very low free energy cost for solubilization of lipids from membranes into SMALPs. This is reflected by the native-like bilayer

organization of the solubilized lipids (Jamshad et al. 2015). The results in the present study furthermore indicate that SMA is fully promiscuous in fluid bilayers, which suggests that SMA does not significantly perturb membrane homogeneity. Together, these results suggest that SMA could serve as an alternative for the isolation of highly-ordered membrane domains that may have advantages over conventional methods using cold detergent solutions. However, whether indeed and to what extent SRMs isolated from biological membranes are superior to DRMs remains to be assessed.

Finally, an interesting novel possibility of this application of SMA may lie in the size of ordered domains existing in biological membranes. SMA may be capable of solubilizing very small membrane nanodomains in a conserved bilayer organization in case they are smaller than the average size of the SMALPs. This may for the first time make it possible to solubilize and characterize such small ordered domains directly from native membranes at physiological temperatures.

Conclusions

In this study, we show that in fluid membranes SMA does not exhibit a preference for solubilization of specific lipids, which supports the validity of studying preferential lipid–protein interactions in SMA-bounded nanodiscs derived either from model membranes or from biological membranes. In phase-separated membranes, SMA has a strong preference for solubilization of the fluid phase, with the potential application of isolating ordered domains from biological membranes by exploiting their SMA resistance. Our initial data suggest that the use of SMA for these approaches may be an alternative to cold detergent solutions, which are commonly used for this purpose.

Associated content

Supporting Information

The supporting information includes turbidimetry data of all binary lipid mixtures shown in Figure 2 (Figure S1), a detailed size characterization of SMALPs by dynamic light scattering and EM (Figure S1, Figure S3 and Table S1), analysis of the lipid preference of SMA in di-14:1 PC-containing lipid mixtures (Figure S3), turbidimetry data on the SMA solubilization of membranes in an L_o phase (Figure S4), analysis of the lipid preference of SMA in a binary mixture of di-18:1 PC and bSM (Figure S5), analysis of the lipid preference of SMA in 16:0/18:1-PC/ bSM/ cholesterol lipid mixtures (Figure S6) and a representative video showing the solubilization of phase-separated SLBs upon SMA addition (Video S1).

Corresponding Authors

* J.J.DominguezPardo@uu.nl; J.A.Killian@uu.nl.

Present Addresses

§ Vrije Universiteit Amsterdam, De Boelelaan 1105, 1081 HV Amsterdam, The Netherlands.

Author Contributions

The manuscript was written through contributions of all authors. All authors have given approval to the final version of the manuscript.

Acknowledgements

This work was supported financially by NWO Chemical Sciences, ECHO grant (No. 711-013-005) (J.J.D.P) and by Foundation for Fundamental Research on Matter (FOM), program Nr.126 (S.S.), Nr.127 (A.I., V.S.) as well as by the Seventh Framework Program of the European Union (Initial Training Network "ManiFold," Grant 317371) (J.M.D.). We thank M. R. Hogeboom, J. J. Rietveld , R. M. Hopman and H. Keser for optimizing the lipid solubilization parameters. This work used the platforms of the Grenoble Instruct centre (ISBG;UMS 3518 CNRS-CEA-UJF-EMBL) with support from FRISBI (ANR-10-INSB-05-02) and GRAL (ANR-10-LABX-49-01) within the Grenoble partnership for structural biology (PSB). We are very grateful to Dr. C. Moriscot from the Electron Microscopy platform of the Integrated Structural Biology of Grenoble (ISBG, UMI3265) for performing the TEM imaging and to B. W. M. Kuipers from the University of Utrecht for advice and support in DLS analysis.

References

Bell AJ, Frankel LK, Bricker TM (2015) High Yield Non-detergent Isolation of Photosystem I-Light-harvesting Chlorophyll II Membranes from Spinach Thylakoids. J. Biol. Chem. 290(30):18429–18437.

Bligh EG, Dyer WJ (1959) A rapid method of total lipid extraction and purification. Can. J. Biochem. Physiol. 37(8):911–917

Cerneus DP, Ueffing E, Posthuma G, Strous GJ, van der Ende A (1993) Detergent insolubility of alkaline phosphatase during biosynthetic transport and endocytosis. Role of cholesterol. J. Biol. Chem. 268(5):3150–3155

Cuevas Arenas R, Klingler J, Vargas C, Keller S (2016) Influence of lipid bilayer properties on nanodisc formation mediated by styrene/maleic acid copolymers. Nanoscale 8:15016–15026

de Smet, C. H., Vittone E, Scherer M, Houweling M, Liebisch G, Brouwers JF, de Kroon, A. I. P. M. (2012) The yeast acyltransferase Sct1p regulates fatty acid desaturation by competing with the desaturase Ole1p. Mol. Biol. Cell 23(7):1146–1156.

Deborah A. Brown, John K. Rose (1992) Sorting of GPI-anchored proteins to glycolipid-enriched membrane subdomains during transport to the apical cell surface. Cell 68(3):533–544.

Dörr JM, Koorengevel MC, Schäfer M, Prokofyev AV, Scheidelaar S, van der Cruijsen, Elwin A. W., Dafforn TR, Baldus M, Killian JA (2014) Detergent-free isolation, characterization, and functional reconstitution of a tetrameric K + channel: The power of native nanodiscs. Proc. Natl. Acad. Sci. U. S. A. 111(52):18607–18612.

Dörr JM, Scheidelaar S, Koorengevel MC, Dominguez JJ, Schäfer M, van Walree CA, Killian JA (2016) The styrene–maleic acid copolymer: a versatile tool in membrane research. Eur. Biophys. J. 45(1):3–21.

El Kirat K, Morandat S (2007) Cholesterol modulation of membrane resistance to Triton X-100 explored by atomic force microscopy. Biochim. Biophys. Acta, Biomembr. 1768(9):2300–2309.

Erwin London, Deborah A. Brown (2000) Insolubility of lipids in Triton X-100: physical origin and relationship to sphingolipid/cholesterol membrane domains (rafts). Biochim. Biophys. Acta, Biomembr. 1508(1–2):182–195.

Gulati S, Jamshad M, Knowles TJ, Morrison KA, Downing R, Cant N, Collins R, Koenderink JB, Ford RC, Overduin M, Kerr ID, Dafforn TR, Rothnie AJ (2014) Detergent-free purification of ABC (ATP-binding-cassette) transporters. Biochem. J. 461(2):269–278.

Hanado K, Nishijima M, Akamatsu Y, Pagano RE (1995) Both Sphingolipids and Cholesterol Participate in the Detergent Insolubility of Alkaline Phosphatase, a Glycosylphosphatidylinositol-anchored Protein, in Mammalian Membranes. J. Biol. Chem. 270(11):6254–6260.

Heerklotz H (2002) Triton Promotes Domain Formation in Lipid Raft Mixtures. Biophys. J. 83(5):2693–2701.

Ipsen JH, Karlstrom G, Mouritsen OG, Wennerstrom H, Zuckermann MJ (1987) Phase equilibria in the phosphatidylcholine-cholesterol system. Biochim. Biophys. Acta 905(1):162–172

Jamshad M, Charlton J, Lin Y-P, Routledge SJ, Bawa Z, Knowles TJ, Overduin M, Dekker N, Dafforn TR, Bill RM, Et Al. (2015) G-protein coupled receptor solubilization and purification for biophysical analysis and functional studies, in the total absence of detergent. Biosci. Rep. 35(2):1–10.

Jamshad M, Grimard V, Idini I, Knowles TJ, Dowle MR, Schofield N, Sridhar P, Lin Y, Finka R, Wheatley M, Et Al. (2014) Structural analysis of a nanoparticle containing a lipid bilayer used for detergent-free extraction of membrane proteins. Nano Res. 8(3):774–789.

Klymchenko AS, Kreder R (2014) Fluorescent probes for lipid rafts: from model membranes to living cells. Chem. Biol. 21(1):97–113.

Lewis RN, Mak N, McElhaney RN (1987) A differential scanning calorimetric study of the thermotropic phase behavior of model membranes composed of phosphatidylcholines containing linear saturated fatty acyl chains. Biochemistry 26(19):6118–6126

Lichtenberg D, Goñi FM, Heerklotz H (2005) Detergent-resistant membranes should not be identified with membrane rafts. Trends Biochem. Sci. 30(8):430–436.

Long AR, O'Brien CC, Malhotra K, Schwall CT, Albert AD, Watts A, Alder NN (2013) A detergent-free strategy for the reconstitution of active enzyme complexes from native biological membranes into nanoscale discs. BMC Biotechnol. 13:41.

Marsh D (2013) Handbook of lipid bilayers. Second edition. CRC Press, Boca Raton

McMullen TP, Lewis RN, McElhaney RN (2004) Cholesterol--phospholipid interactions, the liquid-ordered phase and lipid rafts in model and biological membranes. Curr. Opin. Colloid Interface Sci. 8(6):459–468.

Nibu Y, Inoue T, Motoda I (1995) Effect of headgroup type on the miscibility of homologous phospholipids with different acyl chain lengths in hydrated bilayer. Biophys Chem 56(3):273–280

Orwick MC, Judge PJ, Procek J, Lindholm L, Graziadei A, Engel A, Gröbner G, Watts A (2012) Detergent-free formation and physicochemical characterization of nanosized lipid-polymer complexes: Lipodisq. Angew. Chem. Int. Ed. Engl. 51(19):4653–4657.

Orwick-Rydmark M, Lovett JE, Graziadei A, Lindholm L, Hicks MR, Watts A (2012) Detergent-free incorporation of a seven-transmembrane receptor protein into nanosized bilayer Lipodisq particles for functional and biophysical studies. Nano Lett. 12(9):4687–4692.

Patra SK, Alonso A, Arrondo, José, L. R., Goñi FM (1999) Liposomes Containing Sphingomyelin and Cholesterol: Detergent Solubilisation and Infrared Spectroscopic Studies. J. Liposome Res. 9(2):247–260.

Prabudiansyah I, Kusters I, Caforio A, Driessen AJ (2015) Characterization of the annular lipid shell of the Sec translocon. Biochim. Biophys. Acta, Biomembr. 1848(10):2050–2056.

Priyadarshini Pathak, Erwin London (2011) Measurement of Lipid Nanodomain (Raft) Formation and Size in Sphingomyelin/POPC/Cholesterol Vesicles Shows TX-100 and Transmembrane Helices Increase Domain Size by Coalescing Preexisting Nanodomains But Do Not Induce Domain Formation. Biophysical Journal 101(10):2417–2425.

Rinia HA, Snel MM, van der Eerden, J. P., Kruijff B de (2001) Visualizing detergent resistant domains in model membranes with atomic force microscopy. FEBS Lett. 501(1):92–96

Rodrigo F.M. de Almeida, Aleksandre Fedorov, Manuel Prieto (2003) Sphingomyelin/Phosphatidylcholine/Cholesterol Phase Diagram: Boundaries and Composition of Lipid Rafts. Biophysical Journal 85(4):2406–2416.

Rouser G, Fleischer S, Yamamoto A (1970) Two dimensional thin layer chromatographic separation of polar lipids and determination of phospholipids by phosphorus analysis of spots. Lipids 5(5):494–496.

Sankaram MB, Thompson TE (1990) Interaction of cholesterol with various glycerophospholipids and sphingomyelin. Biochemistry 29(47):10670–10675

Scheidelaar S, Koorengevel MC, Dominguez Pardo J, Meeldijk JD, Breukink E, Killian JA (2015) Molecular Model for the Solubilization of Membranes into Nanodisks by Styrene Maleic Acid Copolymers. Biophys. J. 108(2):279–290.

Schroeder R, London E, Brown D (1994) Interactions between saturated acyl chains confer detergent resistance on lipids and glycosylphosphatidylinositol (GPI)-anchored proteins: GPI-anchored proteins in liposomes and cells show similar behavior. Proceedings of the National Academy of Sciences 91(25):12130–12134

Simons K, Ikonen E (1997) Functional rafts in cell membranes. Nature 387(6633):569–572.

Sot J, Collado MI, Arrondo JLR, Alonso A, Goñi FM (2002) Triton X-100-Resistant Bilayers: Effect of Lipid Composition and Relevance to the Raft Phenomenon. Langmuir 18(7):2828–2835.

Swainsbury DJK, Scheidelaar S, van Grondelle R, Killian JA, Jones MR (2014) Bacterial reaction centers purified with styrene maleic Acid copolymer retain native membrane functional properties and display enhanced stability. Angew. Chem. Int. Ed. Engl. 53(44):11803–11807.

Vargas C, Arenas RC, Frotscher E, Keller S (2015) Nanoparticle self-assembly in mixtures of phospholipids with styrene/maleic acid copolymers or fluorinated surfactants. Nanoscale 7(48):20685–20696.

Veatch SL, Keller SL (2003) Separation of Liquid Phases in Giant Vesicles of Ternary Mixtures of Phospholipids and Cholesterol. Biophys. J. 85(5):3074–3083.

Veiga MP, Arrondo JLR, Goñi FM, Alonso A, Marsh D (2001) Interaction of Cholesterol with Sphingomyelin in Mixed Membranes Containing Phosphatidylcholine, Studied by Spin-Label ESR and IR Spectroscopies. A Possible Stabilization of Gel-Phase Sphingolipid Domains by Cholesterol. Biochemistry 40(8):261–2622.

Wan C-PL, Chiu MH, Wu X, Lee SK, Prenner EJ, Weers PMM (2011) Apolipoprotein-induced conversion of phosphatidylcholine bilayer vesicles into nanodisks. Biochim. Biophys. Acta, Biomembr. 1808(3):606–613.

Zhang L, Song J, Cavigiolio G, Ishida BY, Zhang S, Kane JP, Weisgraber KH, Oda MN, Rye K-A, Pownall HJ, Ren G (2011) Morphology and structure of lipoproteins revealed by an optimized negative-staining protocol of electron microscopy. J. Lipid Res. 52(1):175–184.

Zhang R, Sahu ID, Liu L, Osatuke A, Comer RG, Dabney-Smith C, Lorigan GA (2015) Characterizing the structure of lipodisq nanoparticles for membrane protein spectroscopic studies. Biochim. Biophys. Acta, Biomembr. 1848(1):329–333.

Supporting Information

Materials and Methods

Dynamic light scattering

1-mL aliquots of 15 mM dispersions of MLVs were incubated with SMA (SMA-to-lipid mass ratio of approximately 1.8) overnight at the specified temperature (see Table S1). The non-solubilized material was pelleted down by spinning at 115,000 × *g* for 1 h at 4 °C and the supernatant, containing the solubilized lipid material, was collected. Excess SMA was removed from the supernatant using Amicon Ultra 0.5-mL centrifugal filters with a molecular weight cut-off of 30 kDa (Millipore, Darmstadt, Germany). The filtered solution was diluted to 1 mL with solubilization buffer aiming for a final lipid concentration of approximately 10 mM. Dynamic light scattering (DLS) analysis was performed on the dialyzed samples using a Zetasizer Nano ZS (Malvern Instruments, Worcestershire, UK). Samples were measured at least 12 times, each measurement being an average of 20 sub-runs of 15 s. Size–intensity distributions were generated using Zetasizer software Ver. 6.20 and 7.03 and analyzed using the multiple narrow distribution. Hydrodynamic diameters were calculated from the intensity distributions with the assumption that nanodiscs have a spherical shape. All samples showed a polydispersity index (PDI)<0.4.

Transmission electron microscopy

Size characterization of the SMALPs present in the supernatant fractions resulting from DLS experiments was performed by transmission electron microscopy (TEM). To this end, samples were diluted with solubilization buffer to a lipid concentration of 0.5–1 mM and small aliquots were adsorbed on EM grids. The further procedure was as described in the main text.

Lipid extraction

The lipids from solubilized fractions and from the initial vesicles were extracted according to the method by Bligh and Dyer (Bligh and Dyer 1959b). Briefly, 700 µL of sample was mixed with 700 µL of $CHCl_3$ and 1.61 mL of MeOH in a glass tube and the mixture was vortexed vigorously. Next, 700 µL of $CHCl_3$ were added promoting phase separation and the organic phase was recollected. The aqueous phase was mixed once more with 700 µL of $CHCl_3$ and vortexed. The organic phase was again recollected and added to the previous organic fraction obtained. The organic fraction containing the lipids was washed with a buffer solution (Tris 50 mM, EDTA 50 mM, pH 8.0) and mixed with 100 µL of isopropanol. The solvent was evaporated under a stream of N_2 and the resulting lipid films were stored for further use.

Lipid analysis and quantification

For thin layer chromatography, lipids extracted from the solubilized fraction and from the non-treated vesicles were dissolved in 100 µL chloroform/methanol (9:1 v/v) of which 20 µL and 10 µL, respectively, were applied to a high performance thin layer chromatography 10 x 10 cm Silica gel 60 plate (Macherey Nagel, Düren, Germany) using a Linomat 5 automatic TLC device (CAMAG, Muttenz, Germany). The lipids were separated in an ADC2 automatic development chamber (CAMAG), using chloroform/methanol/24% (v/v) ammonia/H_20 (68:28:3:1 v/v/v/v) as the mobile phase. Next, the plate was dried for 5 min under a stream of N_2 and dipped in copper staining solution (10% w/v $CuSO_4$, 8% v/v H_2SO_4 98% w/v and 8% v/v H_3PO_4 85% w/v). The spots were visualized by uniform heating at 130 °C for 15 min on a TLC plate heater (CAMAG) and subsequently quantified. The quantification was based on densitometry comparing the intensity of the lipid spots with a calibration curve on the same plate (Dörr et al. 2014; Swainsbury et al. 2014; Scheidelaar et al. 2015), using the Quantity One software (BioRad, Hercules, CA). In all cases, the amount of lipid in the samples was found to be in the linear range of the calibration curves.For reverse phase-TLC, the lipids extracted from the SMA-induced solubilized fraction and from the non-treated vesicles were dissolved in 100 µL chloroform/methanol (9:1 v/v) and 40 µL of each solution was applied manually to a silica gel C_{18} TLC plate (Millipore, Darmstadt, Germany). Next, the plate was developed in a TLC chamber, where the mobile phase consisted of methanol/dichloromethane/acetic acid (glacial) (80:20:1.5 v/v/v). After development, the plate was dried under a stream of N_2 and immediately placed in an iodine tank to visualize the lipid spots. The spots were scraped off and the total phosphate content in each spot was quantified according to the method of Rouser (Rouser et al. 1970) as follows. Each sample was suspended in 300 µL of $HClO_4$ (70 % w/v) and heated for 1.5 h at 170 °C until organic samples were completely converted to inorganic phosphate. Next, the reaction was cooled down by adding 1 mL of H_2O followed by the addition of 0.4 mL of ascorbic acid (5% w/v)

solution and 0.4 mL of ammonium molybdate (VI) tetrahydrate (1.25 % w/v) solution The samples were agitated and heated in a boiling water bath for 6 min and cooled at room temperature for at least 10 min. Absorbance of the samples was recorded at λ=797 nm, and the total phosphate amount was quantified from a calibration curve.

For gas chromatography, analysis was conducted after subjecting the phospholipids to an acid-catalyzed esterification (de Smet, C. H. et al. 2012) as follows. The lipid films were suspended in 3 mL solution of 2.5 % w/v MeOH in H_2SO_4 (98% w/v) and heated for 2 h at 70°C. The reaction was stopped by adding 3 mL of H_2O and the methylated fatty acids were extracted with 3 mL of hexane. The extraction was repeated and the organic fractions were combined. The organic fraction was washed twice with H_2O after which 100 uL of isopropanol was added. The solvent was then removed under a stream of N_2 stream and the resulting methylated fatty acid films were redissolved in 90 µL of hexane and saved for further analysis. Subsequently, the samples were analyzed using a TRACE GC Ultra (Interscience, Breda, The Netherlands) equipped with a Stabilwax polar column (Thermo Fisher scientific, Waltham, MA) with an internal diameter of 0.31 mm and a film thickness of 0.25 µm. The retention times of different fatty acid methyl esters were assigned by comparison with two standards: GLC 63b (Nu-Check Prep,Elysian, MN), and Bacterial Acid Methyl Ester Mix (Sigma-Aldrich, St.Louis, MO).

Preparation of supported lipid bilayers

Substrate pretreatment

Glass slides were washed in 2 % (w/v) Hellmanex (VWR International, Chicago, IL) at 80 °C for 60 min, rinsed excessively with deionized water and then dried under a stream of N_2. Cleaned slides were then etched for 8 min in a solution of 98 % w/v H_2SO_4 and 30 % w/v H_2O_2 (3:1 v/v). The slides were kept in MilliQ water and used immediately.

Preparation of supported lipid bilayers

Multilamellar vesicles (MLVs) were prepared in solubilization buffer from a mixture of di-18:1 PC, bSM and cholesterol in an equimolar ratio, supplemented with 0.01 mol% rhodamine-PE and 0.05 mol% Top-Fluor cholesterol (see Preparation of MLVs). Large unilamellar vesicles (LUVs) were then obtained by extrusion of the MLV dispersion 21 times through 100-nm polycarbonate membranes at 50 °C. Next, supported lipid bilayers (SLBs) were prepared by vesicle fusion as follows: a custom-built chamber (V = 100 µL) was assembled on top of the pretreated, hydrophilic glass slide. The chamber was then completely filled with a LUV dispersion (250 µM lipid) and equilibrated for 30 min. at room temperature. Subsequently, the unfused vesicles were removed by buffer flow and 2 chamber

volumes of solubilization buffer containing different amounts of either SMA were flowed through the chamber at a flow speed of 50 µL/min using an oil-free pump.

Monitoring the process of solubilization in real time

The process of solubilization of supported bilayers (di-18:1 PC, bSM and cholesterol in an equimolar ratio, supplemented with 0.01 mol% rhodamine-PE and 0.05 mol% Top-Fluor cholesterol) was also monitored in real time for 5 minutes at a constant flow of 1% w/v SMA-containing buffer solution at room temperature.

Results

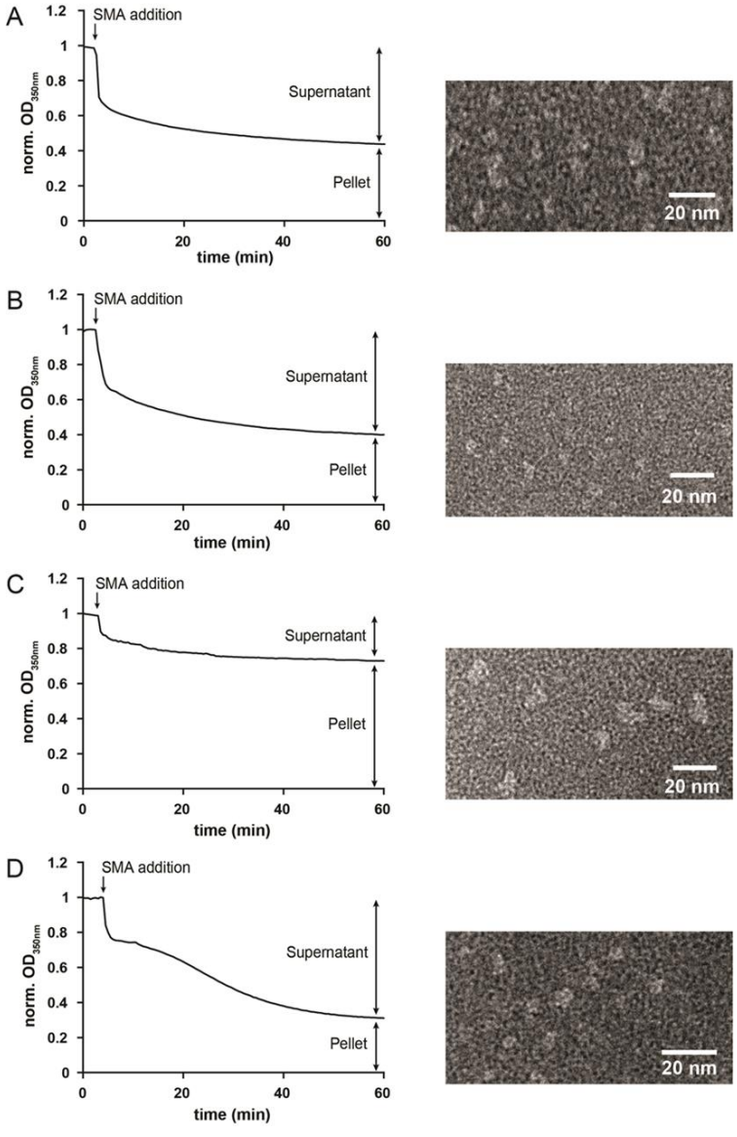

Figure S1: (Left) Kinetics of SMA solubilization of MLVs composed of equimolar lipid mixtures of 18:1-PC with di-18:1 PE (A), di-14:1 PC (B), di-18:0 PC (preparation at 60°C) (C) and di-18:0 PC (D). Solubilization was assessed at 25°C unless specified. Respective SMA-to-lipid mass ratios at 0.5 mM lipid were 1.31, 0.27, 0.13 and 1.27. Data are shown as normalized optical

density (apparent absorbance) at 350 nm. (Right) Visualization of the nanodiscs from the corresponding supernatant fractions by negative-stain transmission electron microscopy.

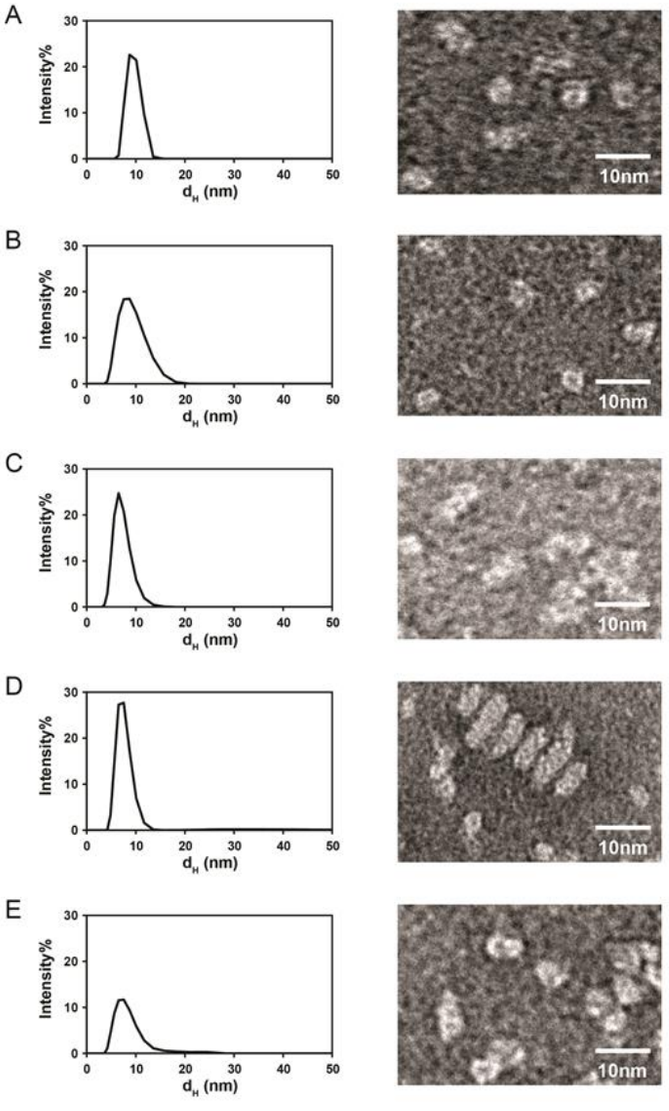

Figure S2. (Left) Size distribution of soluble nanodiscs after removal of non-solubilized material as quantified by dynamic light scattering at 25 °C for equimolar mixtures of di-18:1 PC with di-18:1 PG (A), di-18:1 PE (B), di-14:1 PC (C), di-18:0 PC (preparation at 60°C) (D) and di-18:0 PC (E). The SMA-to-lipid mass ratio was kept constant at 1.8. Samples were prepared at 25 °C unless specified. (Right) Visualization of the SMALPs from the same sample by negative-stain transmission electron microscopy. In D, note the formation of stacks of discs in samples of di-18:1 PC and di-18:0 PC. Such “rouleaux” stacks have been observed before in or nanodiscs bounded by amphipathic proteins (Wan et al. 2011; Zhang et al. 2011) and were ascribed to an artifact resulting from specific interactions of the inorganic complexes of the staining solution with the positively charged choline headgroups.

Lipid mixture (1:1, molar)	Incubation temperature (°C)	Size EM (nm)	Size DLS (nm)*
di-18:1 PC/di-18:1 PG	25	6–8	8.2 ± 0.9
di-18:1 PC/di-18:1 PE	25	5–8	8.8 ± 0.7
di-18:1 PC/di-14:1 PC	25	5–7	8.3 ± 1.0
di-18:1 PC/di-18:0 PC	60	7–9	8.1 ± 0.3
di-18:1 PC/di-18:0 PC	25	6–9	7.2 ± 0.7

Table S1. Nanodisc size characterization.

*Errors reflect the accuracy of the positioning of the peak maximum within 12 consecutive measurements. Note however that the actual size distribution as estimated from the DLS intensity plots in Fig. S2 is several nm.

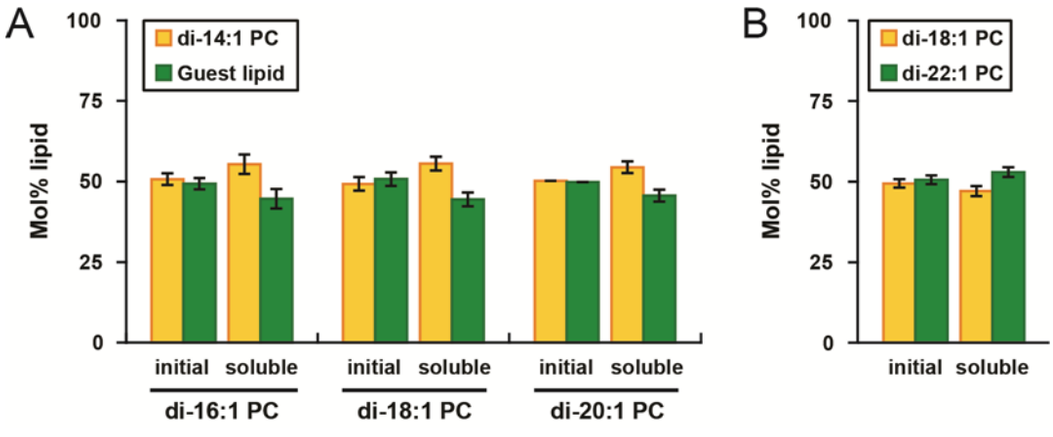

Figure S3. Solubilization preference of SMA in binary lipid systems with different properties assessed by lipid composition analysis after partial solubilization. Analysis was performed by reverse phase TLC (A) Equimolar mixtures of the zwitterionic unsaturated di-14:1 PC ("host", orange) with different guest lipids (green) under conditions of phase homogeneity. From left to right: di-16:1 PC, di-18:1 PC and di-20:1 PC. Respective SMA-to-lipid mass ratios at 0.5 mM lipid were 0.28, 0.27 and 0.26. (B) Solubilization preference of SMA in equimolar mixture of di-18:1 PC and di-22:1: PC at SMA-to-lipid mass ratio of 0.24. Cartoons show the schematic bilayer organization before addition of SMA. Error bars represent the standard deviation of 3 independent experiments.

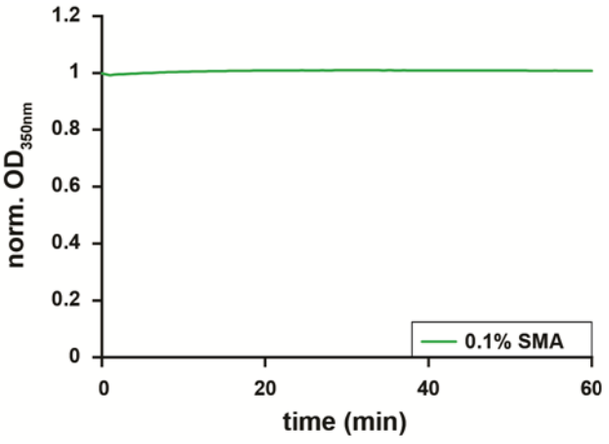

Figure S4. Inefficient SMA solubilization of membranes in the L_o phase. A turbidity trace is shown for MLVs composed of bSM and cholesterol (1:1, molar) that were incubated with SMA for 1 h (SMA-to-lipid mass ratio of 3.5).

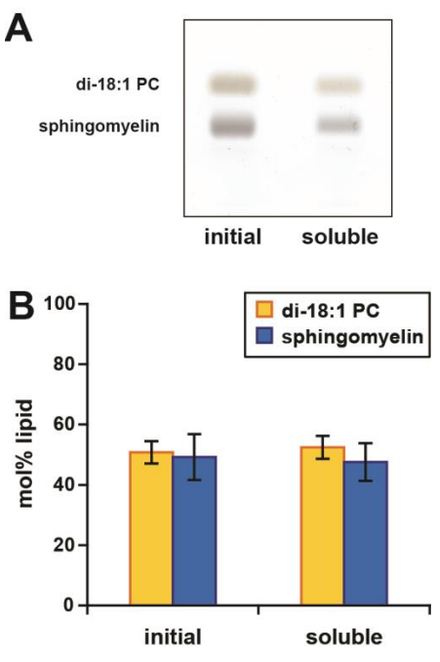

Figure S5. Lipid composition analysis after partial solubilization of MLVs composed of an equimolar binary lipid mixture of di-18:1 PC and brain sphingomyelin. (*A*) TLC plate with lipids extracted from initial vesicles and from the soluble fraction after incubation with SMA at 25 °C. (*B*) Quantification of lipid composition shown as mol% lipid for initial vesicles as well as the solubilized fractions after the incubation with SMA (0.5 mM lipid, SMA-to-lipid mass ratio of 2.6) at 25 °C. Error bars represent the standard deviation of 3 experiments.

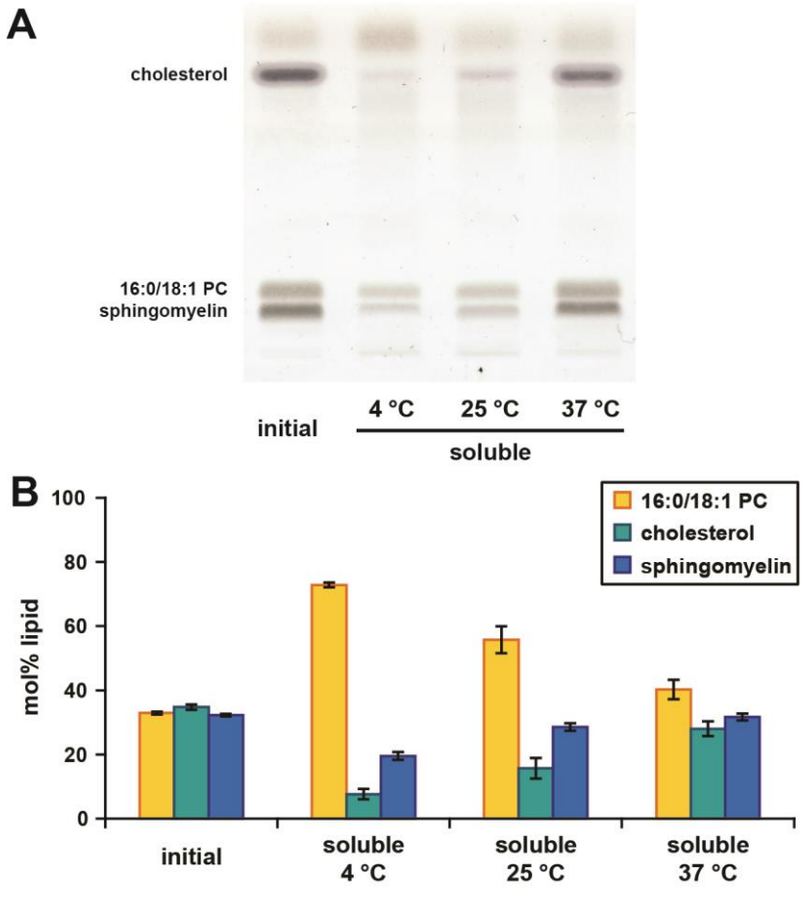

Figure S6. Lipid composition analysis after partial solubilization of MLVs composed of an equimolar ternary lipid mixture of 16:0/18:1 PC, brain sphingomyelin and cholesterol by SMA. (*A*) TLC plate with lipids extracted from initial vesicles and from the soluble fraction after incubation with SMA at 4 °C , 25 °C and 37 °C. (*B*) Quantification of lipid composition shown as mol% lipid for initial vesicles as well as the solubilized fractions after the incubation with SMA at different temperatures (0.5 mM lipid, SMA-to-lipid mass ratio of 3.2). Error bars represent the standard deviation of 3 experiments.

References

Bligh EG, Dyer WJ (1959) A rapid method of total lipid extraction and purification. Can. J. Biochem. Physiol. 37(8):911–917

de Smet, C. H., Vittone E, Scherer M, Houweling M, Liebisch G, Brouwers JF, de Kroon, A. I. P. M. (2012) The yeast acyltransferase Sct1p regulates fatty acid desaturation by competing with the desaturase Ole1p. Mol. Biol. Cell 23(7):1146–1156.

Dörr JM, Koorengevel MC, Schäfer M, Prokofyev AV, Scheidelaar S, van der Cruijsen, Elwin A. W., Dafforn TR, Baldus M, Killian JA (2014) Detergent-free isolation, characterization, and functional

reconstitution of a tetrameric K + channel: The power of native nanodiscs. Proc. Natl. Acad. Sci. U. S. A. 111(52):18607–18612.

Rouser G, Fleischer S, Yamamoto A (1970) Two dimensional thin layer chromatographic separation of polar lipids and determination of phospholipids by phosphorus analysis of spots. Lipids 5(5):494–496.

Scheidelaar S, Koorengevel MC, Dominguez Pardo J, Meeldijk JD, Breukink E, Killian JA (2015) Molecular Model for the Solubilization of Membranes into Nanodisks by Styrene Maleic Acid Copolymers. Biophys. J. 108(2):279–290.

Swainsbury DJK, Scheidelaar S, van Grondelle R, Killian JA, Jones MR (2014) Bacterial reaction centers purified with styrene maleic Acid copolymer retain native membrane functional properties and display enhanced stability. Angew. Chem. Int. Ed. Engl. 53(44):11803–11807.

Wan C-PL, Chiu MH, Wu X, Lee SK, Prenner EJ, Weers PMM (2011) Apolipoprotein-induced conversion of phosphatidylcholine bilayer vesicles into nanodisks. Biochim. Biophys. Acta, Biomembr. 1808(3):606–613.

Zhang L, Song J, Cavigiolio G, Ishida BY, Zhang S, Kane JP, Weisgraber KH, Oda MN, Rye K-A, Pownall HJ, Ren G (2011) Morphology and structure of lipoproteins revealed by an optimized negative-staining protocol of electron microscopy. J. Lipid Res. 52(1):175–184.

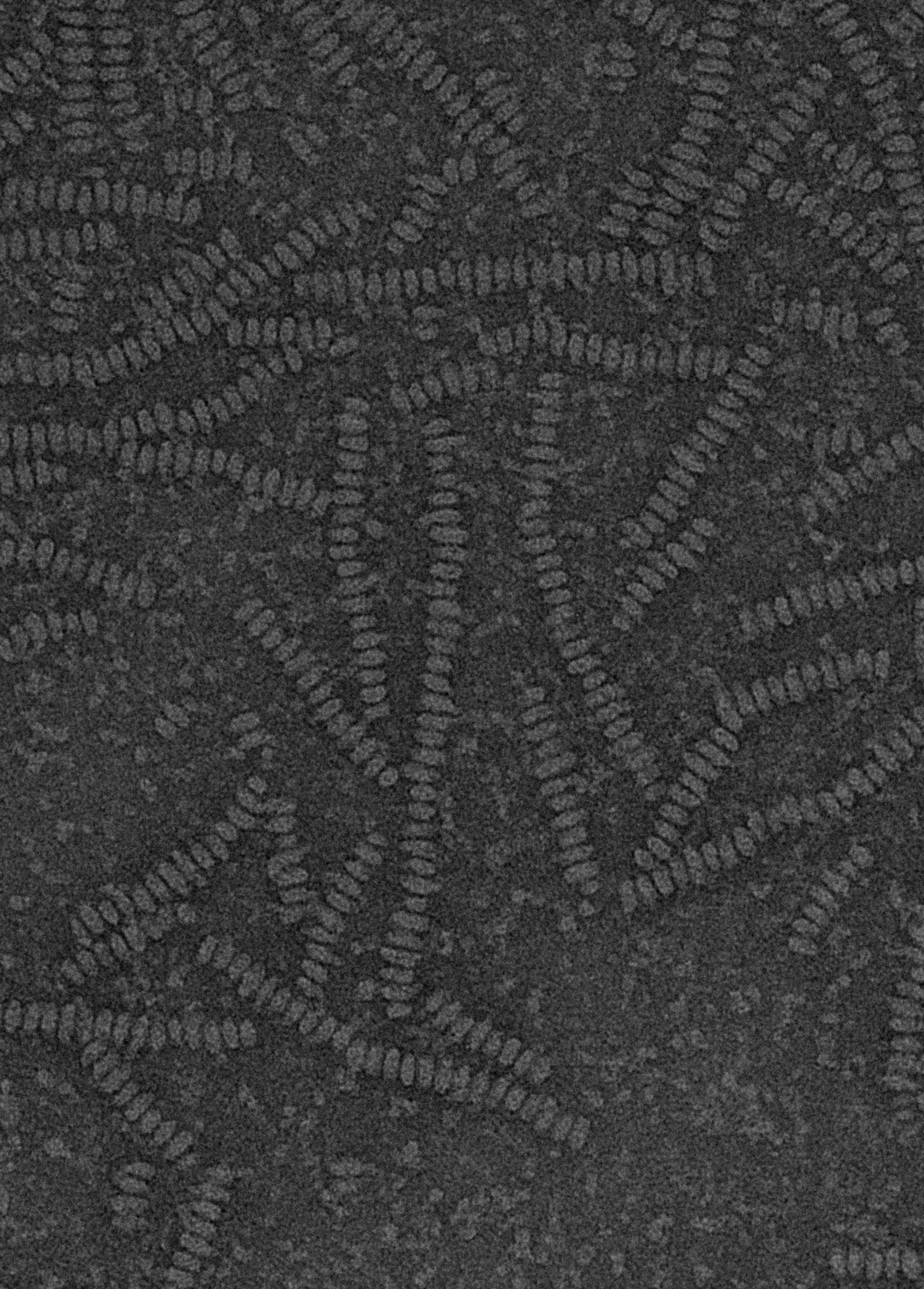

Chapter III

Thermotropic properties of phosphatidylcholine nanodiscs bounded by styrene-maleic acid copolymers

J.J. Dominguez Pardo[†*], J.M. Dörr, M.F. Renne, T. Ould-Braham, M.C.Koorengevel, M.J van Steenbergen [‡], J.A. Killian[†*]

[†] Membrane Biochemistry and Biophysics, Bijvoet Center for Biomolecular Research, Department of Chemistry, Faculty of Science, Padualaan 8, 3584 CH Utrecht,
The Netherlands.
[‡] Department of Pharmaceutics, Utrecht Institute for Pharmaceutical Sciences (UIPS), Faculty of Science, Utrecht University, PO Box 80082, 3508 TB Utrecht,
The Netherlands

This chapter is has been published in Chem. and Phys. of lipids 208, 58-64, 2017.

Abstract

Styrene-maleic acid copolymers (SMA) have been gaining interest in the field of membrane research due to their ability to solubilize membranes into nanodics. The SMA molecules act as an amphipathic belt that surrounds the nanodiscs, whereby the hydrophobic styrene moieties can insert in between the lipid acyl chains. Here we used SMA variants with different styrene-to-maleic acid ratio (i.e. 2:1, 3:1 and 4:1) to investigate how lipid packing in the nanodiscs is affected by the presence of the polymers and how it depends on polymer composition. This was done by analyzing the thermotropic properties of a series of saturated phosphatidylcholines in nanodiscs using laurdan fluorescence and differential scanning calorimetry. In all cases it was found that the temperature of the main phase transition (T_m) of the lipids in the nanodiscs is downshifted and that its cooperativity is strongly reduced as compared to the situation in vesicles. These effects were least pronounced for lipids in nanodiscs bounded by SMA 2:1. Unexpected trends were observed for the calorimetric enthalpy of the transition, suggesting that the polymer itself contributes, possibly by rearranging around the nanodiscs when the lipids adopt the fluid phase. Finally, distinct differences in morphology were observed for nanodiscs at relatively high polymer concentrations, depending on the SMA variant used. Overall, the results suggest that the extent of preservation of native thermodynamic properties of the lipids as well as the stability of the nanodiscs at high polymer concentrations is better for SMA 2:1 than for the other SMA variants.

Introduction

Styrene-maleic acid copolymers (SMA) are rapidly gaining interest as tools in membrane protein research due to their capacity of solubilizing biological membranes into nanodiscs without the need for detergents. These so-called “native nanodiscs” thus enclose membrane proteins embedded in a lipid bilayer (for review see (Dorr et al. 2016)), while retaining native protein-lipid interactions (Long et al. 2013; Dörr et al. 2014; Swainsbury et al. 2014; Prabudiansyah et al. 2015). SMA variants are commercially available differing in average length of the polymer and in average styrene-to-maleic acid ratio. The variants most frequently used in literature are SMA 2:1 (styrene-to-maleic acid ratio of 2:1) (Dörr et al. 2014; Swainsbury et al. 2014; Jamshad et al. 2015) and SMA 3:1 (Orwick et al. 2012; Cuevas Arenas et al. 2016; Dominguez Pardo et al. 2017) of approximately ~10 kDa. Studies in model membranes showed that the SMA 2:1 variant is slightly more efficient in solubilization than SMA 3:1, while both are significantly more efficient than SMA 4:1 (Scheidelaar et al. 2016). Similar results were reported for solubilization of proteins from *E.coli* (Morrison et al., 2016).

A general advantage of using SMA-bounded nanodiscs for membrane protein research is that the bilayer environment reflects the organization of the lipids in the native membrane (Orwick et al. 2012; Jamshad et al. 2015). However, for studies on membrane protein structure and function it is also important to know to what extent the packing of the lipids in the nanodiscs is preserved and resembles that in the native membrane. Previous reports showed that SMA molecules behave as a belt encircling the nanodiscs, where the styrene units intercalate between the lipid acyl chains (Orwick et al. 2012; Jamshad et al. 2015). This intercalation will affect lipid packing and it is thus likely that the properties of the nanodiscs and packing of the lipids will be affected by the composition of the SMA molecules that form the belt. This is supported by the recent observation that SMA composition affects the functional properties of proteins in purified nanodiscs (Morrison et al., 2016).

A convenient way of monitoring the extent to which native lipid packing properties are preserved in nanodiscs is by investigating the thermotropic behavior of the enclosed lipids as compared to that of lipids in vesicles (Shaw et al. 2004; Denisov et al. 2005; Orwick et al. 2012; Jamshad et al. 2015; Tanaka et al. 2015). In order to gain insight into the effect of polymer composition on the properties of the formed nanodiscs and in particular on the extent to which native membrane properties are preserved, we here directly compared the effects of different polymer variants on the thermotropic properties of SMA-bounded nanodiscs. Such a direct comparison is essential, because it is becoming increasingly clear that the properties of nanodiscs are dependent on precise experimental conditions, and can vary for example with SMA concentration (Cuevas Arenas et al. 2016; Oluwole et al. 2017).

To allow comprehensive and systematic comparison, we studied a series of saturated phosphatidylcholine lipids in SMA-nanodiscs by laurdan fluorescence and DSC analysis. Briefly, we found that lipids in SMA 2:1-nanodiscs retain to a higher extent the thermodynamic properties of the native membrane as compared to lipids in SMA 3:1-nanodiscs under a variety of experimental conditions. Moreoever, upon varying the SMA concentration both the thermodynamic properties and the morphology of the nanodiscs were best retained in SMA 2:1-nanodiscs. These results are discussed in terms of the membrane interactions of the styrene units in SMA and how they may depend on the phase state of the lipids.

Materials and Methods

Materials

The following lipids where purchased from Avanti Polar Lipids (Alabaster, AL, USA): 1,2-dipentadecanoyl-sn-glycero-3-phosphocholine (di-15:0 PC), 1,2-dipalmitoyl-sn-glycero-3-phosphocholine (di-16:0 PC), 1,2diheptadecanoyl-sn-glycero-3-phosphocholine (di-17:0 PC) ,1,2-distearoyl-*sn*-glycero-3-phosphocholine (di-18:0 PC) and 1,2-diarachidoyl-*sn*-glycero-3-phosphocholine (di-20:0 PC). The SMA copolymers, Xiran 20010 (molar ratio of styrene-to-maleic anhydride of 4:1), Xiran 25010 (molar ratio of styrene-to-maleic anhydride of 3:1) and Xiran 30010 (molar ratio of styrene- to- maleic anhydride of 2:1), all with a weight average molecular weight of ~10 kDa, were a kind gift from Polyscope Polymers (Geleen, The Netherlands). The polymers were converted to the acid form by hydrolysis under base-catalyzed conditions as detailed before (Stefan Scheidelaar et al. 2015). Laurdan (6-dodecanoyl-2-dimethylaminonaphtalene) and all other chemicals were purchased from Sigma Aldrich (St.Louis, MO).

Preparation of multilamellar vesicles (MLVs)

Phospholipid stock solutions were prepared in chloroform/methanol (9:1 v/v) in concentrations of either 5 mM or 20 mM (for DSC measurements), based on the analysis of total phosphate (Rouser et al. 1970). A 5-mM laurdan stock solution was prepared in ethanol/chloroform (1:1 v/v). Aliquots from the phospholipid stock solutions and from the laurdan stock solutions, if required, were taken and the solvent was removed under a stream of N_2. The resulting lipid film was dried in a desiccator under vacuum for at least 1 h. Multilamellar vesicles (MLVs) were obtained by hydrating the lipid films with buffer (50 mM Tris-HCl, 150 mM NaCl, pH 8.0) to a final concentration of 0.5 mM or 20 mM (for DSC measurements). The samples were then subjected to 10 freeze-thaw cycles, each consisting of 3 min freezing in liquid N_2 (-196°C) and 3 min thawing in a water bath above T_m of the lipids (Marsh 2013).

Preparation of nanodiscs

Dispersions of MLVs containing either 0.5 mM or 20 mM lipid were incubated with SMA (SMA-to-lipid mass ratios used for solubilization are detailed in the legends of each figure) for 1h at the phase transition temperature (T_m) of the lipid components (Lewis et al. 1987; Marsh 2013). After incubation with SMA, the samples were placed in an Optima Max ultracentrifuge (Beckman-Coulter, Brea, CA). Traces of non-solubilized material were removed by centrifugation at 115,000 × *g* for 1 h at 4°C.

Laurdan fluorescence

Laurdan fluoresence was measured using a Varian Cary Eclipse fluorescence spectrophotometer (Santa Clara, CA). 1-mL aliquots of ~0.5 mM phosphatidylcholine nanodisc solutions (lipid-to-laurdan molar ratio of 200:1) were placed in a 10-mm quartz cuvette and excited at 340 nm. The excitation and emission slits were adjusted to 5 nm. Emission spectra were recorded in the range of 400-550 nm at a speed of 60 nm/min. The temperature was controlled with a Peltier cuvette holder (Santa Clara, CA) in the range of 5-70 °C. Exact temperatures of the samples were obtained from a thermosensor dipped inside the cuvette. Generalized polarization parameters defined as GP= (I_{440nm}-I_{490nm})/(I_{440nm}+I_{490nm}) (Parasassi et al. 1991) were obtained as function of temperature. Phase transition midpoints were determined by nonlinear least-squares fitting using a sigmoidal fitting function (Kemmer and Keller 2010). GP values were obtained from a single heating scan. For selected samples additional heating cycles were performed as a control and negligible differences in the GP curves were observed.

Differential scanning calorimetry

DSC measurements were performed using a Discovery DSC (TA Instruments, Newcastle, DE) calorimeter. 10-µL aliquots of nanodisc solutions or MLV dispersions containing ~20 mM lipids were placed in hermetic Tzero pans (TA Instruments, Newcastle, DE). Heating curves were recorded in the ranges of 5-70 °C at a scan rate of 5 °C/min at least 3 times. Calorimetric enthalpies (ΔH_{cal}) were determined from the area under the peak of the main phase transition using Trios software (TA Instruments, Newcastle, DE). The calorimetric enthalpies reported represent the average obtained from the 2nd and the 3rd heat scan from 2 independent samples. Error bars reported for both T_m and ΔH_{cal} values correspond to the average from the 2nd and 3rd heating cycles from 2 independent samples. The full width at half height of the peaks ($\Delta T_{1/2}$) were determined manually using Adobe Illustrator software (San José, CA). For determination of the calorimetric enthalpy, the total lipid material contained in the calorimetric pans was recovered by perforating the pans in a glass tube containing 1-mL of water. The tubes were vortexed vigorously in order to assure that all lipids were

extracted from the pans. Next, the total lipid was quantified in triplicate by applying a phosphate analysis (Rouser et al. 1970) on 200- µL aliquots of the resulting nanodisc solutions or MLV dispersions.

Transmission electron microscopy

Size characterization of di-16:0 PC and di-18:0 PC nanodiscs was performed by transmission electron microscopy (TEM). 1-mL aliquots of 0.5 mM nanodisc solutions were adsorbed on carbon-coated mica following the carbon flotation technique and stained with a staining solution containing 2% (w/v) sodium silicotungstate as detailed before (Dominguez Pardo et al. 2017). Images were taken under low dose conditions at a nominal magnification of 49,000 with a T12 electron microscope (FEI, Hillsboro, OR) at an operating voltage of 120 kV using an ORIUS SC1000 camera (Gatan, Inc., Pleasanton, CA). The average size of the nanodiscs was estimated from at least 25 well-defined individual particles. The maximum diameter was determined using Adobe Illustrator software (San Jose, CA).

Results

Native thermotropic lipid properties are better retained in SMA 2:1 nanodiscs than in SMA 3:1 nanodiscs

Shifts in phospholipid phase behavior can be conveniently followed by incorporating amphipathic solvatochromic dyes, such as laurdan, into lipid membranes. Laurdan probes are extremely sensitive to solvent relaxation and can be used to track changes in membrane fluidity based on a shift in emission maximum. Briefly, when the temperature is raised above the main gel-to-fluid phase transition temperature (T_m) of the lipid constituents of the membrane, a spectral shift of the emission maximum takes place from 440 nm to 490 nm (Parasassi et al. 1991).

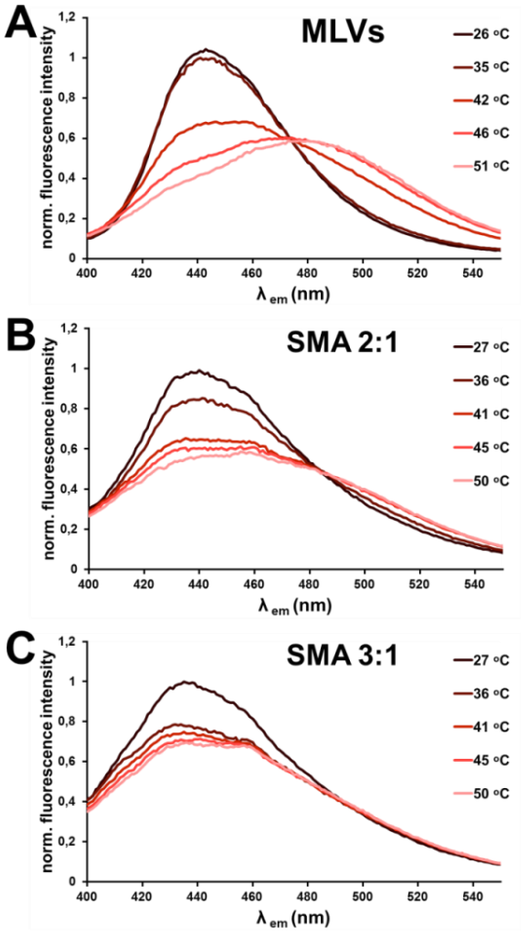

Figure.1 Normalized fluorescence emission of laurdan molecules incorporated in di-16:0 PC self-assemblies: A) MLVs, B) SMA 2:1 nanodiscs and C) SMA 3:1 nanodiscs. Spectra were recorded using an excitation wavelength of 340 nm. The data shown correspond to the spectra obtained during the first heating cycle. Nanodiscs were obtained at a SMA-to-lipid mass ratio of ~1.7.

This is illustrated in **Figure 1A** where laurdan is incorporated into di-16:0 PC MLVs, which have a T_m of around 41°C (Lewis, Ruthven N. A. H. et al. 1987). Below T_m, at 26 °C and 35 °C, the emission maximum is at 440 nm. At 42 °C, the intensity of the emitted fluorescence is decreased at 440 nm but is increased at 490 nm. At higher temperatures of 46 °C and 51 °C, the emission maximum is completely shifted to ~490 nm. Insight into the relative amount of gel and fluid phase present can be obtained by calculating the generalized polarization (GP) values from the maximum intensities of the two emission peaks (Parasassi et al. 1991). As shown in **Figure 2 (green line)** for di-16:0 PC MLVs the GP values slightly decrease as the temperature is raised, with a sharp inflection around T_m, indicating

that phase interconversion is taking place with a high degree of cooperativity (Parasassi et al. 1994). By applying non-linear regression analysis T_m was found to be ~41°C.

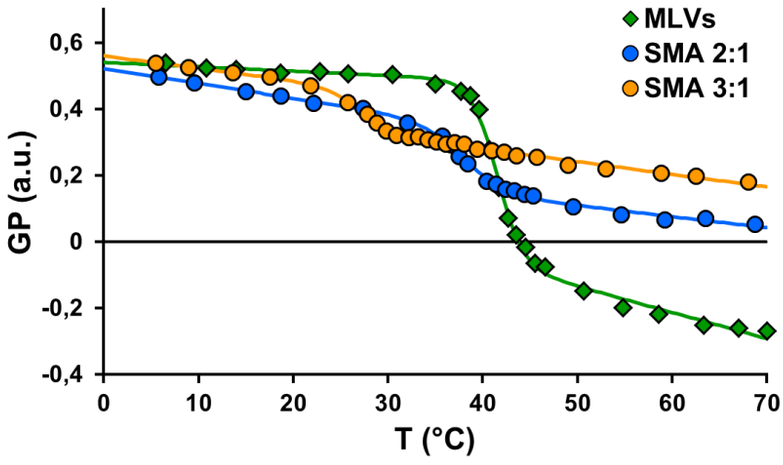

Figure 2. Laurdan generalized polarization (GP) values of di-16:0 PC self-assembled in MLVs (green squares), SMA 2:1 nanodiscs (blue circles) and SMA 3:1 nanodiscs (orange circles). Solid lines indicate a sigmoidal fit. Nanodiscs were obtained at a SMA-to-lipid mass ratio of ~1.7.

The same experimental approach was used for nanodiscs obtained after addition of SMA to di-16:0-PC MLVs. We inititally focussed on SMA 2:1 and SMA 3:1, as they are the commonly used SMA variants in literature. As shown in **Figure 1 B,** for SMA 2:1 a decrease in the emission at 440 nm is observed that now begins already at lower temperatures in the range of 27 °C to 36 °C. In addition, there is no clear peak appearing at 490 nm upon further increasing the temperature. Similar but more pronounced effects are observed for di-16:0 PC SMA 3:1 nanodiscs (**Figure 1C).** These results are attributed to a blue shift of the emission wavelength that is particularly pronounced in the fluid phase (Parasassi et al. 1993) and that can be ascribed to a decrease in i) the motility of laurdan molecules or ii) the polarity of the solvent (Parasassi et al. 1993; Parasassi et al. 1994). Here it is possible that both factors are involved as a result of binding of SMA molecules to the surface of the nanodiscs, which may impede the motility of the lipids (Cuevas Arenas et al. 2016b) while at the same time insertion of styrene moieties will decrease the polarity.

Analysis of the GP curves observed for laurdan in the nanodiscs reveals that for SMA 2:1 nanodiscs the phase transition occurs at ~38 °C and for SMA 3:1 nanodiscs at ~27 °C (**Figure 2**). The decreased steepness of the slope of the inflection curve around T_m suggests a decrease in the cooperativity of the transition. This effect is more pronounced for SMA 3:1 nanodiscs than for SMA 2:1 nanodiscs.

Furthermore, the higher GP values of SMA 2:1 nanodiscs and particularly SMA 3:1 nanodiscs in the fluid phase suggest a less hydrated or more ordered environment than for MLVs. Similar results were obtained when the lipid acyl chain length was varied from 15 to 18 C-atoms (see GP curves in **Figure S1**). Overall, the Laurdan data show a downshift in T_m of ~3–5 °C for saturated phosphatidylcholines organized in SMA 2:1 nanodiscs as compared to MLVs (**Table 1**, left column), while the same lipids assembled in SMA 3:1 nanodiscs show a downshift of ~14–17 °C. In addition, the SMA 3:1 nanodiscs exhibit a further increased broadening of the phase transition and a less hydrated environment in the fluid phase as compared to SMA 2:1 nanodiscs for all lipids tested

Phospholipid	Self-assembly	T_m (°C) Laurdan	T_m (°C) DSC	$\Delta T_{½}$ (°C) DSC
di-15:0 PC	MLVs	34.3	33.3 ± 0.1	0.7 ± 0.1
	SMA 2:1	28.6	29.2 ± 0.2	4.0 ± 0.2
	SMA 3:1	ND*	21.6 ± 0.4	6.6 ± 0.4
di-16:0 PC	MLVs	41.4	40.8 ± 0.1	0.5 ± 0.1
	SMA 2:1	38.0	37.4 ± 0.2	3.8 ± 0.2
	SMA 3:1	27.1	29.4 ± 0.2	5.1 ± 0.1
di-17:0 PC	MLVs	48.1	48.3 ± 0.1	0.4 ± 0.1
	SMA 2:1	44.1	46.5 ± 2.0	3.3 ± 0.1
	SMA 3:1	34.1	36.1 ± 0.6	5.6 ± 0.1
di-18:0 PC	MLVs	53.3	54.0 ± 0.1	0.4 ± 0.1
	SMA 2:1	48.7	50.9 ± 0.1	2.9 ± 0.1
	SMA 3:1	36.5	42.3 ± 0.2	5.5 ± 0.1

* No clear transition is visible.

Table. 1 T_m values and peak widths at half maximum ($\Delta T_{½}$) of saturated phosphatidylcholine self-assemblies measured by laurdan fluorescence and DSC. DSC data are given as averages of the 2nd and 3rd heating cycle from 2 independent samples, with errors representing the standard deviation.

The laurdan fluorescence data were complemented with differential scanning calorimetry (DSC) analysis. DSC has the advantage of being a high precision technique which does not require the addition of fluorophores that may perturb the phase equilibrium of the membrane. As shown in **Figure 3**, DSC thermograms of di-16:0 PC MLVs display a sharp peak with a maximum corresponding to T_m at ~41 °C. SMA 2:1 nanodiscs and SMA 3:1 nanodiscs both exhibit a lowering of T_m with the downshift being more pronounced in SMA 3:1 nanodiscs, as was also observed for PC lipids with shorter and longer chain lengths (**Figure S2**). The T_m values show downshifts of approximately ~2–4

°C in T_m of lipids in SMA 2:1 nanodiscs and of ~11–13 °C in SMA 3:1 nanodiscs (**Table 1,** middle column). These shifts are slightly less than those observed with laurdan fluorescence, most likely due to differences in experimental conditions, but nevertheless the results are qualitatively similar.

DSC analysis also provides insight into the cooperativity of the gel-to-fluid phase transition. The narrow peak width at half maximum ($\Delta T_{1/2}$) observed for di-16:0 PC phospholipids in MLVs indicates a high degree of cooperativity (Biltonen and Lichtenberg 1993), while the heat curves of both nanodisc samples show a clear broadening, suggesting a notable loss in the cooperativity (Shaw et al. 2004; Denisov et al. 2005; Orwick et al. 2012). The broadening is more pronounced in SMA 3:1 nanodiscs as compared to SMA 2:1 nanodiscs, as was also observed for other lipids **(Figure S2)**. These results, as quantified in **Table 1**, are fully consistent with the observed effects of the polymers on the steepness of the inflection points in the laurdan GP-curves (Fig. 2 and S1).

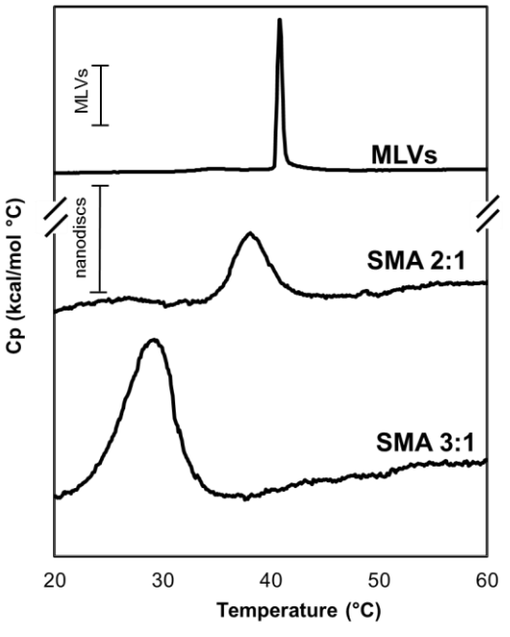

Figure3. Representative differential scanning calorimetry (DSC) thermograms of di-16:0 PC lipids self-assembled in MLVs, SMA 2:1 nanodiscs and SMA 3:1 nanodiscs. Nanodiscs were obtained at a SMA-to-lipid mass ratio of ~1.7. The inserted scale bar at the top (MLVs) corresponds to 5 kcal/mol °C while the bar at the bottom (nanodiscs) corresponds to 0.5 kcal/mol °C.

Calorimetric enthalpy values of the gel-to-fluid phase transition may be determined by multiple processes

Another characteristic property of the gel-to-fluid phase transition is the molar calorimetric enthalpy (ΔH_{cal}) associated with the melting process. As displayed in **Table 2**, the ΔH_{cal} values for MLVs of lipids

increase with lipid chain length, in line with previously reported data (Lewis, Ruthven N. A. H. et al. 1987; Goto et al. 2009; Marsh 2013). For all lipids, a dramatic loss in calorimetric enthalpy is observed when present in SMA-bounded nanodiscs. For SMA 2:1 nanodiscs ΔH_{cal} is approximately 20% of ΔH_{cal} found in MLVs (**Table 2**). Rather surprisingly, the loss of ΔH_{cal} is less dramatic in SMA 3:1-nanodiscs, where ~45-50 % of the value is retained.

ΔH_{cal} (kcal/mol)	**di-15:0 PC**	**di-16:0 PC**	**di-17:0 PC**	**di-18:0 PC**
MLVs	7.2 ± 0.2	7.6 ± 0.1	9.4 ± 0.4	10.0 ± 0.6
SMA 2:1	1.4 ± 0.1	1.5 ± 0.2	1.8 ± 0.2	1.8 ± 0.1
SMA 3:1	3.2 ± 0.3	3.8 ± 0.1	4.8 ± 0.6	4.5 ± 0.1

Table. 2 Calorimetric enthalpies (ΔH_{cal}) of the gel-to-fluid phase transition of saturated phosphatidylcholines. Data are given as averages obtained from the 2nd and 3rd heating cycle from 2 independent samples, with errors representing the standard deviation.

To obtain further insight into the origin of this somewhat puzzling observation we decided to extend the systematic approach by going to system of lipids with an even longer chain length. As shown in **Figure 4**, di- 20:0 PC MLVs exhibit a narrow, highly cooperative gel-to-fluid phase transition while the SMA 2:1-nanodiscs again show a broadening and a small downshift in T_m. Interestingly, a remarkable feature now occurs in the thermogram obtained for SMA 3:1-nanodiscs, where the main phase transition appears to be split into two peaks. Identical thermograms were obtained upon repeated heating showing complete reversibility of this transition. A similar, reversible effect of apparent multiple transitions was detected upon extending the data-set to include nanodiscs of SMA 4:1 copolymers, as shown for di-18:0 PC nanodiscs (**Figure S3**). These results suggest that interpretation of effects on ΔH_{cal} in these nanodiscs is not straightforward, and that possibly SMA molecules themselves contribute to the enthalpy of the transition. We will further elaborate on these effects in the discussion.

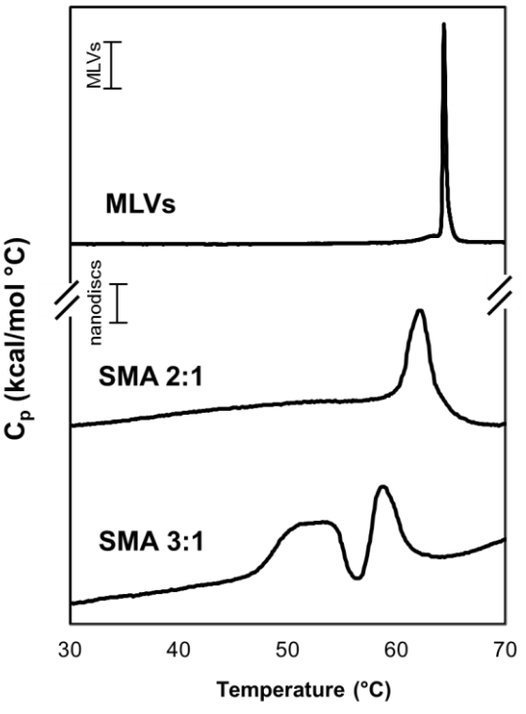

Figure 4. Representative differential scanning calorimetry (DSC) thermograms of di-20:0 PC. Nanodiscs were obtained at a SMA-to-lipid mass ratio of ~1.7. The inserted bars at the top (MLVs) correspond to 5 kcal/mol °C and the inserted bars at the bottom (nanodiscs) correspond to 0.5 kcal/mol

Thermotropic properties are more sensitive to polymer concentration in nanodiscs bounded by SMA 3:1 or SMA 4:1 than in nanodiscs bounded by SMA 2:1

Next it was investigated to what extent the SMA-to-lipid ratio at which the nanodiscs are obtained may affect the thermotropic properties of the lipids in the nanodiscs. As shown in **Figure 5A**, T_m of di-16:0 PC is shifted to lower temperatures as the SMA-to-lipid ratio increases. Importantly, this concentration effect seems to be less pronounced in SMA 2:1-nanodiscs than in SMA 3:1-nanodiscs and SMA 4:1-nanodiscs.

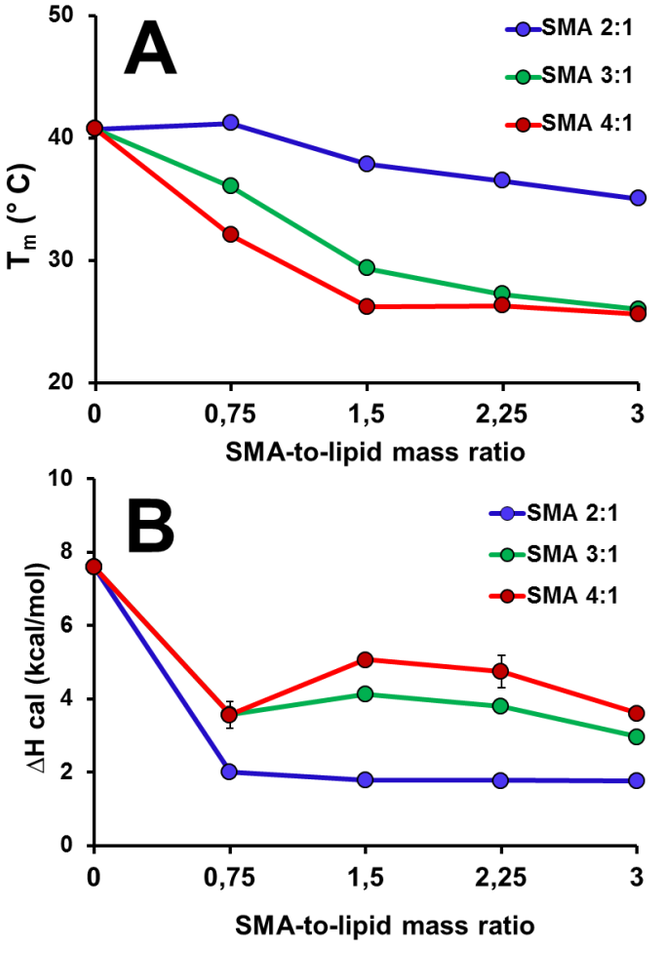

Figure 5. Variation in A) T_m and B) ΔH_{cal} of the gel-to-fluid phase transition of di-16:0 PC lipids in nanodiscs bounded by SMA 2:1 (blue circles) SMA 3:1 (green circles) or SMA 4:1 (red circles). Data are given as averages obtained from the 2nd and 3rd heating cycle from 2 independent samples. Errors representing the standard deviation are covered by the markers.

For all samples also the calorimetric enthalpy values of the gel-to-fluid transition were determined and these are shown in **Figure 5B**. The results show that ΔH_{cal} corresponding to di-16:0 PC lipids bounded by SMA 2:1 is low and rather constant, independent of the SMA concentration used for solubilization. When either the SMA 3:1 or the SMA 4:1 variant are used, the values of ΔH_{cal} are larger and fluctuate. This fluctuation of the ΔH_{cal} values may indicate that i) other factors may be contributing energetically to the phase transition of lipids or ii) the morphology of the nanodiscs is affected by the concentration of SMA.

Morphological integrity is better preserved in nanodiscs bounded by SMA 2:1 than in nanodiscs bounded by SMA 3:1 or SMA 4:1

Finally it was investigated how the SMA variants affect the size and morphology of the nanodiscs and whether this depends on the concentration of the polymer. As illustrated in **Figure 6,** nanodiscs bounded by SMA 2:1 form well-defined nanodiscs at all polymer concentrations with a somewhat inhomogeneous size distribution of approximately d~9—18 nm. A remarkable feature here is the formation of phospholipid stacks. These are also known as "rouleaux" stacks and have been observed before in nanodiscs bounded by SMA molecules and MSP-like proteins (Zhang et al. 2011; Dominguez Pardo et al. 2017), where they were ascribed to an artefact resulting from the interaction between positively-charged choline head groups with the negatively-charged inorganic crystals from the staining solution. These stacks are also observed in nanodiscs bounded by SMA 3:1, where they can be seen most clearly at lower polymer concentrations (SMA-to-lipid mass ratio of 0.75 and 1.5). Here the nanodiscs are still well-defined and a size distribution is observed of 9—16 nm, similar as for SMA 2:1 nanodiscs. At higher concentrations of SMA 3:1 (SMA-to-lipid mass ratio > 1.5) the morphological integrity of the nanodiscs is affected, as shown by the formation of nanoscopic aggregates. Remarkably, EM micrographs of nanodiscs bounded by SMA 4:1 revealed a much higher degree of polydispersity as compared to the other SMA analogues and a higher tendency to aggregate. The presence of circular structures is ascribed to artifacts during the preparation of the grids. Stacks of nanodiscs are not observed in micrographs of SMA 4:1 nanodiscs. Together these data suggest that SMA 3:1 and in particular SMA 4:1 are less prone than SMA 2:1 to form well defined circular-shaped nanodiscs and that SMA 2:1-nanodiscs "allow" a high amount of SMA in solution without affecting their morphological integrity.

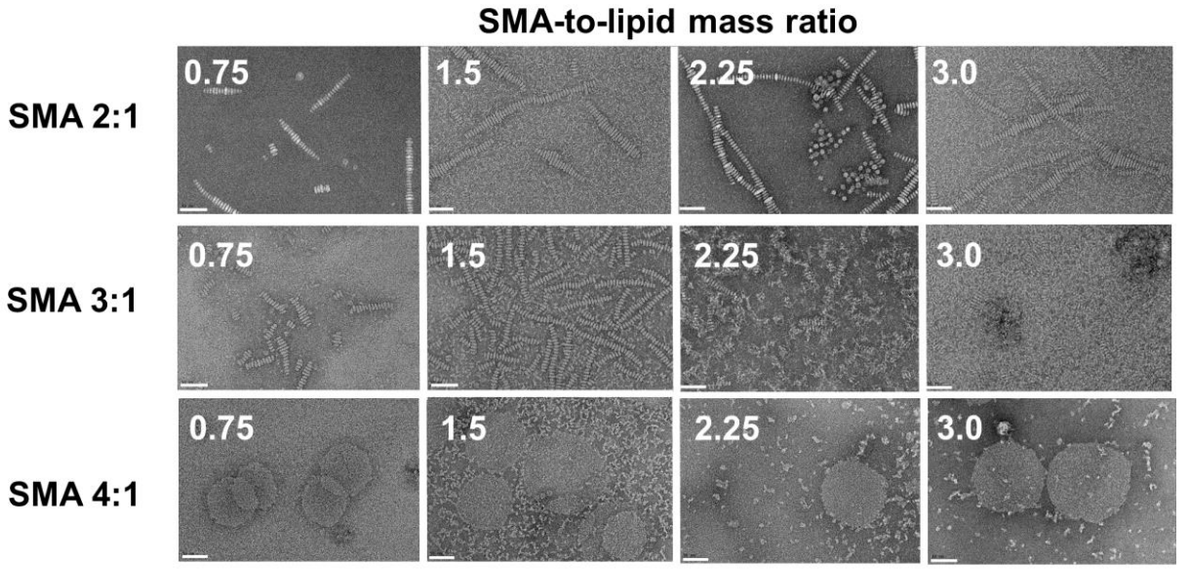

Figure 6. Negative-stain transmission electron micrographs of di-16:0 PC nanodiscs bounded by SMA 2:1 (top), SMA 3:1 (middle) or SMA 4:1 (bottom). The scale bar corresponds to 50 nm. Nanodiscs were obtained at different SMA-to-lipid mass ratio as indicated in the figure

Similar differences in behavior between the SMA analogues were found using dynamic light scattering. These experiments (Figure S 4) revealed rather homogeneous hydrodynamic diameter distributions for nanodiscs bounded by either SMA 2:1 and SMA 3:1 (d~9—12 nm), and a heterogeneous size distribution for SMA 4:1 nanodiscs at the various SMA concentrations.

Discussion

In this study we analyzed the thermotropic properties of saturated phosphatidylcholines in nanodiscs that are bounded by SMA with a styrene-to-maleic acid ratio of 2:1, 3:1 or 4:1. Laurdan fluorescence as well as DSC results for lipids with varying acyl chain length showed that the native main phase transition temperature (T_m) of the lipids is downshifted in the SMA-bounded nanodiscs as compared to the situation in large multilamellar vesicles, and that the cooperativity of the gel-to-fluid phase transition is highly reduced. Nevertheless, native-like properties seemed best preserved in SMA 2:1 nanodiscs, where in all lipid systems the effects on T_m and broadening were least profound. In theory, a likely explanation would be that SMA 2:1 nanodiscs have a somewhat larger size than SMA 3:1 or SMA 4:1 nanodiscs. However, EM and DLS analyses in the present study gave no indication for this. Even though the size distribution in all samples was somewhat heterogeneous, it is unlikely that the differences in effect of the polymers can be ascribed to a difference in size of the nanodiscs. We

speculate that these effects are due to differences in polymer composition. SMA 3:1 and SMA 4:1 have a more inhomogeneous distribution of styrene and maleic acid units along their sequence as compared to SMA 2:1 (Scheidelaar et al. 2016). This would result in a more inhomogeneous membrane partitioning and thus might explain the larger broadening and lower T_m for SMA 3:1 and SMA 4:1 nanodiscs as compared to SMA 2:1 nanodiscs. Further DSC analysis resulted in a remarkable observation that SMA 2:1 nanodiscs have the lowest calorimetric enthalpy, as was observed for all phosphatidylcholines tested when compared with SMA 3:1 and for di-16:0 PC lipids at different concentrations of SMA 2:1, SMA 3:1 or SMA 4:1. This effect would be consistent with a smaller size of the SMA 2:1 nanodiscs, in analogy to effects observed for MSP nanodiscs, where it was found that the calorimetric enthalpy in nanodiscs systematically increases with increasing size of the nanodiscs (Denisov et al. 2005). We speculate that also these effects are due to differences in polymer composition. Using nanodiscs bounded by SMA 3:1 it has been shown that insertion of styrenes into gel phase lipids is thermodynamically more favorable than insertion into fluid phase lipids, demonstrating that there are differences in polymer–lipid interactions as function of the phase state of the lipids in the nanodiscs (Cuevas Arenas et al. 2016). Indeed, insertion of the styrenes inbetween the lipid acyl chains can be expected to be less favorable for lipids in a fluid phase than for lipids in a gel phase, because in the fluid phase the chains will occupy more space causing steric hindrance. This effect will become stronger when the lipids are longer and when there is a higher density of styrenes. We therefore propose that the relatively large enthalpy for SMA 3:1 and SMA 4:1 nanodiscs is due a change in organization of the polymer around the rim of the nanodisc, which accompanies phase interconversion and which energetically contributes to the transition. This might also be the basis for the complex thermograms obtained for di-20:0 PC SMA 3:1-nanodiscs and for di-18:0 PC SMA 4:1-nanodiscs, where the main peak of the thermogram is split into two peaks. If there indeed is such a contribution, then this would imply that calculations of the cooperative unit as number of lipids participating in the phase transition (Orwick et al. 2012; Oluwole et al. 2017) are not useful in SMA-nanodiscs, because they are based on broadening and enthalpy values of a lipid melting transition only. It must be noted that this energetic contribution cannot be interpreted as a gel-to-ripple phase pretransition since such ripples exclusively occur in pure extended lipid bilayer systems (i.e MLVs or supported lipid bilayers) and they are easily abolished by the presence of membrane-interacting molecules (Heimburg 2000). Furthermore, the pretransition can be considered as a macroscopic reorganization of lipids and since the periodicity of the ripples is at least ~5 times larger than the size of nanodiscs (Czajkowsky et al. 1995; Heimburg 2000) their presence in nanodiscs is highly improbable.

Another relevant finding in this manuscript is that the morphological integrity of the nanodiscs can be affected by increasing concentrations of SMA, depending on the hydrophobicity of the polymer. For SMA 2:1 nanodiscs no notable effect of varying the SMA concentration was observed, but for SMA 3:1 at higher SMA concentration regular discs could no longer be observed. Based on both EM and DLS analysis, SMA 4:1 nanodiscs do not appear to self-assemble in regular circular nanodiscs at any SMA concentration, but rather tend to form aggregates. Thus, the term nanodiscs may be incorrect for solubilized SMA 4:1 particles.

In conclusion, the data presented here suggest that the SMA 2:1 polymer is able to preserve native lipid packing properties in the nanodiscs to a higher extent than the SMA 3:1 polymer. Together with recent studies showing that SMA 2:1 is also more efficient in solubilizing membranes (Morrison et al. 2016; Scheidelaar et al. 2016), this supports the notion that SMA 2:1 is more suitable as tool for characterization of membrane proteins in native nanodiscs.

Acknowledgements

This work was supported financially by NWO Chemical Sciences, ECHO grants No. 711-013-005 (J.J.D.P) and 711-013-004 (M.F.R) and by the Seventh Framework Program of the European Union (Initial Training Network “ManiFold,” Grant 317371) (J.M.D). This work used the platforms of the Grenoble Instruct centre (ISBG;UMS 3518 CNRS-CEA-UJF-EMBL) with support from FRISBI (ANR-10-INSB-05-02) and GRAL (ANR-10-LABX-49-01) within the Grenoble partnership for structural biology (PSB). We thank Stefan Scheidelaar and Cornelis A. Van Walree (both from Utrecht University) for helpful discussions. We are very grateful to Dr. C. Moriscot from the Electron Microscopy platform of the Integrated Structural Biology of Grenoble (ISBG, UMI3265) for performing the TEM imaging.

References

Biltonen RL, Lichtenberg D (1993) The use of differential scanning calorimetry as a tool to characterize liposome preparations. Chem Phys Lipids 64:129–142.

Cuevas Arenas R, Klingler J, Vargas C, Keller S (2016) Influence of lipid bilayer properties on nanodisc formation mediated by styrene/maleic acid copolymers. Nanoscale 8:15016–15026.

Czajkowsky DM, Huang C, Shao Z (1995) Ripple phase in asymmetric unilamellar bilayers with saturated and unsaturated phospholipids. Biochemistry 34:12501–12505.

Denisov IG, McLean MA, Shaw AW, Grinkova YV, Sligar SG (2005) Thermotropic phase transition in soluble nanoscale lipid bilayers. J Phys Chem B 109:15580–15588.

Dominguez Pardo JJ, Dorr JM, Iyer A, Cox RC, Scheidelaar S, Koorengevel MC, Subramaniam V, Killian JA (2017) Solubilization of lipids and lipid phases by the styrene-maleic acid copolymer. Eur Biophys J 46:91–101.

Dorr JM, Koorengevel MC, Schafer M, Prokofyev AV, Scheidelaar S, van der Cruijsen, Elwin A W, Dafforn TR, Baldus M, Killian JA (2014) Detergent-free isolation, characterization, and functional reconstitution of a tetrameric K+ channel: the power of native nanodiscs. Proc Natl Acad Sci U S A 111:18607–18612.

Dorr JM, Scheidelaar S, Koorengevel MC, Dominguez JJ, Schafer M, van Walree CA, Killian JA (2016) The styrene-maleic acid copolymer: a versatile tool in membrane research. Eur Biophys J 45:3–21.

Dörr JM, Koorengevel MC, Schäfer M, Prokofyev AV, Scheidelaar S, van der Cruijsen, Elwin A. W., Dafforn TR, Baldus M, Killian JA (2014) Detergent-free isolation, characterization, and functional reconstitution of a tetrameric K + channel: The power of native nanodiscs. Proc. Natl. Acad. Sci. U. S. A. 111:18607–18612.

Goto M, Ishida S, Tamai N, Matsuki H, Kaneshina S (2009) Chain asymmetry alters thermotropic and barotropic properties of phospholipid bilayer membranes. Chem Phys Lipids 161:65–76.

Heimburg T (2000) A Model for the Lipid Pretransition: Coupling of Ripple Formation with the Chain-Melting Transition. Biophysical Journal 78:1154–1165.

Jamshad M, Grimard V, Idini I, Knowles TJ, Dowle MR, Schofield N, Sridhar P, Lin Y, Finka R, Wheatley M, Thomas ORT, Palmer RE, Overduin M, Govaerts C, Ruysschaert J-M, Edler KJ, Dafforn TR (2015) Structural analysis of a nanoparticle containing a lipid bilayer used for detergent-free extraction of membrane proteins. Nano Res. 8:774–789.

Kemmer G, Keller S (2010) Nonlinear least-squares data fitting in Excel spreadsheets. Nat Protoc 5:267–281.

Lewis RN, Mak N, McElhaney RN (1987) A differential scanning calorimetric study of the thermotropic phase behavior of model membranes composed of phosphatidylcholines containing linear saturated fatty acyl chains. Biochemistry 26:6118–6126

Lewis, Ruthven N. A. H., Mak N, McElhaney RN (1987) A differential scanning calorimetric study of the thermotropic phase behavior of model membranes composed of phosphatidylcholines containing linear saturated fatty acyl chains. Biochemistry 26:6118–6126.

Long AR, O'Brien CC, Malhotra K, Schwall CT, Albert AD, Watts A, Alder NN (2013) A detergent-free strategy for the reconstitution of active enzyme complexes from native biological membranes into nanoscale discs. BMC Biotechnol 13:41.

Marsh D (2013) Handbook of lipid bilayers. Second edition. CRC Press, Boca Raton

Morrison KA, Akram A, Mathews A, Khan ZA, Patel JH, Zhou C, Hardy DJ, Moore-Kelly C, Patel R, Odiba V, Knowles T, Javed M-U-H, Chmel NP, Dafforn TR, Rothnie AJ (2016) Membrane protein extraction and purification using styrene-maleic acid (SMA) co-polymer: Effect of variations in polymer structure. Biochem J.

Oluwole AO, Danielczak B, Meister A, Babalola JO, Vargas C, Keller S (2017) Solubilization of Membrane Proteins into Functional Lipid-Bilayer Nanodiscs Using a Diisobutylene/Maleic Acid Copolymer. Angew Chem Int Ed Engl 56:1919–1924.

Orwick MC, Judge PJ, Procek J, Lindholm L, Graziadei A, Engel A, Grobner G, Watts A (2012) Detergent-free formation and physicochemical characterization of nanosized lipid-polymer complexes: Lipodisq. Angew Chem Int Ed Engl 51:4653–4657.

Parasassi T, Stasio G de, Ravagnan G, Rusch RM, Gratton E (1991) Quantitation of lipid phases in phospholipid vesicles by the generalized polarization of Laurdan fluorescence. Biophysical Journal 60:179–189.

Parasassi T, Ravagnan G, Rusch RM, Gratton E (1993) Modulation and dynamics of phase properties in phospholipid mixtures detected by laurdan fluorescence. Photochem Photobiol 57:403–410.

Parasassi T, Di Stefano M, Loiero M, Ravagnan G, Gratton E (1994) Influence of cholesterol on phospholipid bilayers phase domains as detected by Laurdan fluorescence. Biophysical Journal 66:120–132.

Prabudiansyah I, Kusters I, Caforio A, Driessen AJM (2015) Characterization of the annular lipid shell of the Sec translocon. Biochim Biophys Acta 1848:2050–2056.

Rouser G, Fleischer S, Yamamoto A (1970) Two dimensional thin layer chromatographic separation of polar lipids and determination of phospholipids by phosphorus analysis of spots. Lipids 5:494–496.

Scheidelaar S, Koorengevel MC, van Walree CA, Dominguez JJ, Dorr JM, Killian JA (2016) Effect of Polymer Composition and pH on Membrane Solubilization by Styrene-Maleic Acid Copolymers. Biophysical Journal 111:1974–1986.

Shaw AW, McLean MA, Sligar SG (2004) Phospholipid phase transitions in homogeneous nanometer scale bilayer discs. FEBS Lett 556:260–264.

Stefan Scheidelaar, Martijn C. Koorengevel, Juan Dominguez Pardo, Johannes D. Meeldijk, Eefjan Breukink, J. Antoinette Killian (2015) Molecular Model for the Solubilization of Membranes into Nanodisks by Styrene Maleic Acid Copolymers. Biophysical Journal 108:279–290.

Swainsbury DJK, Scheidelaar S, van Grondelle R, Killian JA, Jones MR (2014) Bacterial reaction centers purified with styrene maleic acid copolymer retain native membrane functional properties and display enhanced stability. Angew Chem Int Ed Engl 53:11803–11807.

Tanaka M, Hosotani A, Tachibana Y, Nakano M, Iwasaki K, Kawakami T, Mukai T (2015) Preparation and Characterization of Reconstituted Lipid-Synthetic Polymer Discoidal Particles. Langmuir 31:12719–12726.

Zhang L, Song J, Cavigiolio G, Ishida BY, Zhang S, Kane JP, Weisgraber KH, Oda MN, Rye K-A, Pownall HJ, Ren G (2011) Morphology and structure of lipoproteins revealed by an optimized negative-staining protocol of electron microscopy. J Lipid Res 52:175–184..

Supporting information

Materials and Methods

Dynamic light scattering

1-mL aliquots of ~20 mM nanodisc solutions (SMA-to-lipid mass ratios used for solubilization are detailed in the legends of each figure) were placed in a plastic cuvette and measured by dynamic light scattering (DLS) in a Zetasizer Nano ZS (Malvern Instruments, Worcestershire, UK). Samples were measured at least 12 times, each measurement being an average of 20 sub-runs of 15 s. Size–intensity distributions were generated using Zetasizer software Ver. 6.20 and 7.03 and analyzed using the multiple narrow distribution. Hydrodynamic diameters were calculated from the intensity distributions with the assumption that nanodiscs have a spherical shape.

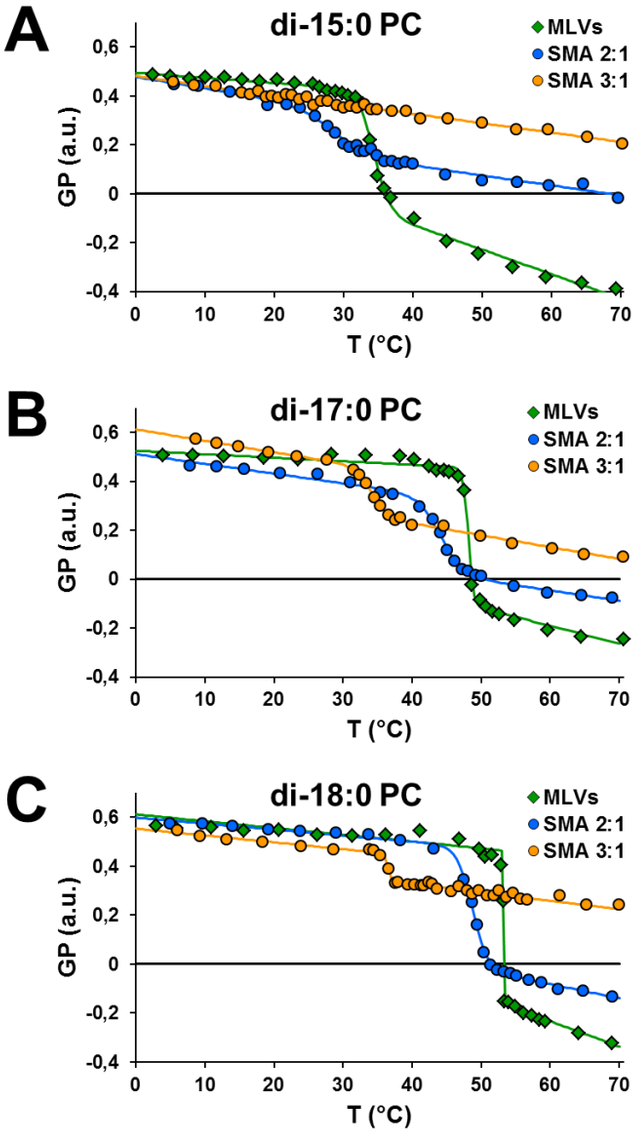

Figure S1. Laurdan generalized polarization (GP) values of di-15:0 PC (A), di-17:0 PC (B) and di-18:0 PC (C) lipids self-assembled in MLVs (green squares), SMA 2:1-nanodiscs (blue circles) and SMA 3:1-nanodiscs (orange circles). Solid lines indicate a sigmoidal fit. Nanodiscs were obtained at a SMA-to-lipid mass ratio of ~1.7.

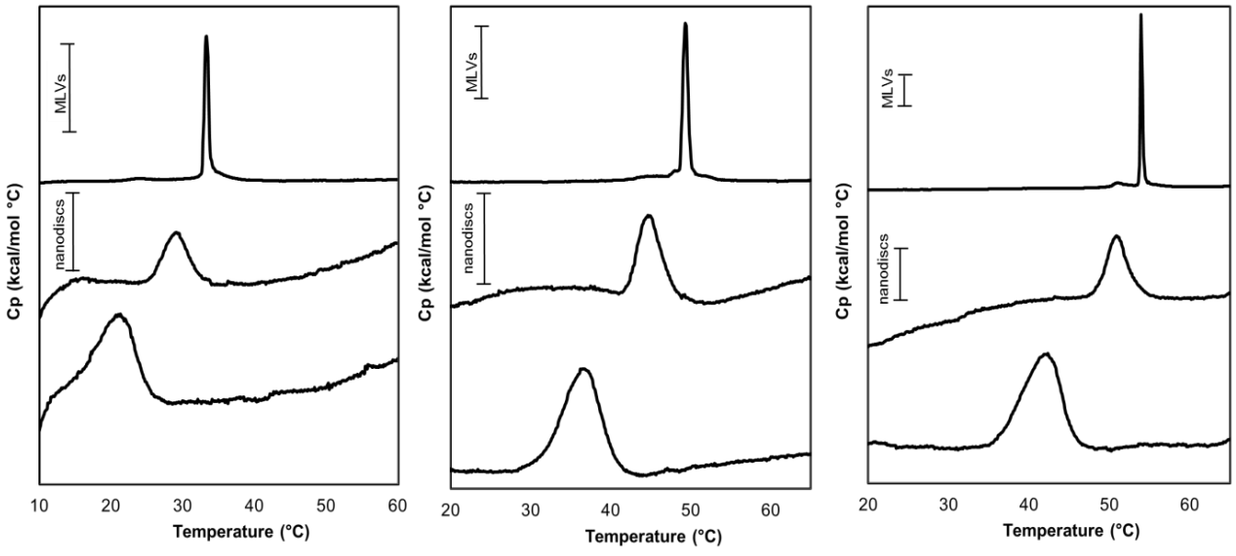

Figure S2. Representative differential scanning calorimetry (DSC) thermograms of di-15:0 PC (A), di-17:0 PC (B) and di-18:0 PC (C) lipids self-assembled in MLVs, SMA 2:1-nanodiscs and SMA 3:1-nanodiscs. Nanodiscs were obtained at a SMA-to-lipid mass ratio of ~1.7. The inserted bars at the top (MLVs) correspond to 5 kcal/mol °C and the inserted bars at the bottom (nanodiscs) correspond to 0.5 kcal/mol °C.

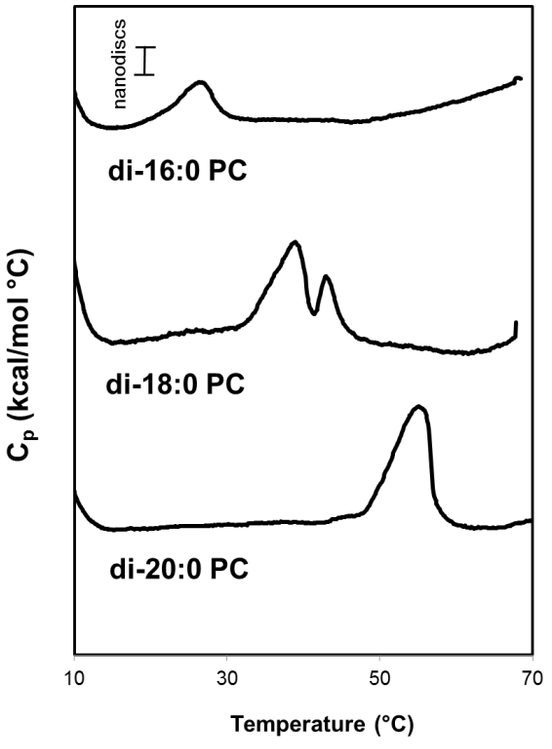

Figure S3. Representative differential scanning calorimetry (DSC) thermograms of di-16:0 PC, di-18:0 PC and di-20:0 PC nanodiscs bound by SMA 4:1 molecules. Nanodiscs were obtained at a SMA-to-lipid mass ratio of ~1.7. The inserted bar correspond to 0.5 kcl/mol °C.

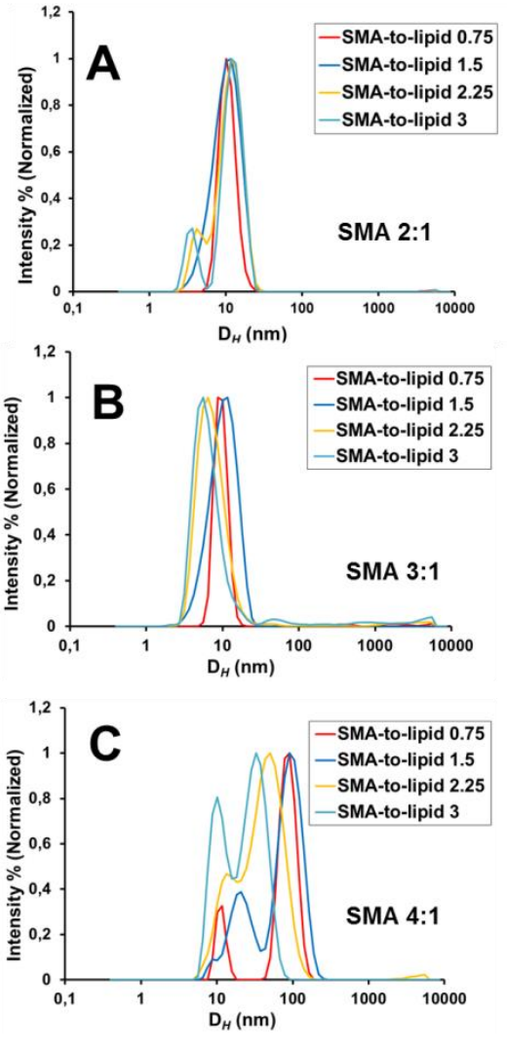

Figure S4. Size distribution of soluble nanodiscs after removal of non-solubilized material as quantified by dynamic light scattering of di-16:0 PC-nanodiscs bounded by (A) SMA 2:1, (B) SMA 3:1 and (C) SMA 4:1 at the indicated different SMA-to-lipid mass ratios. All experiments were performed at T=25 °C.

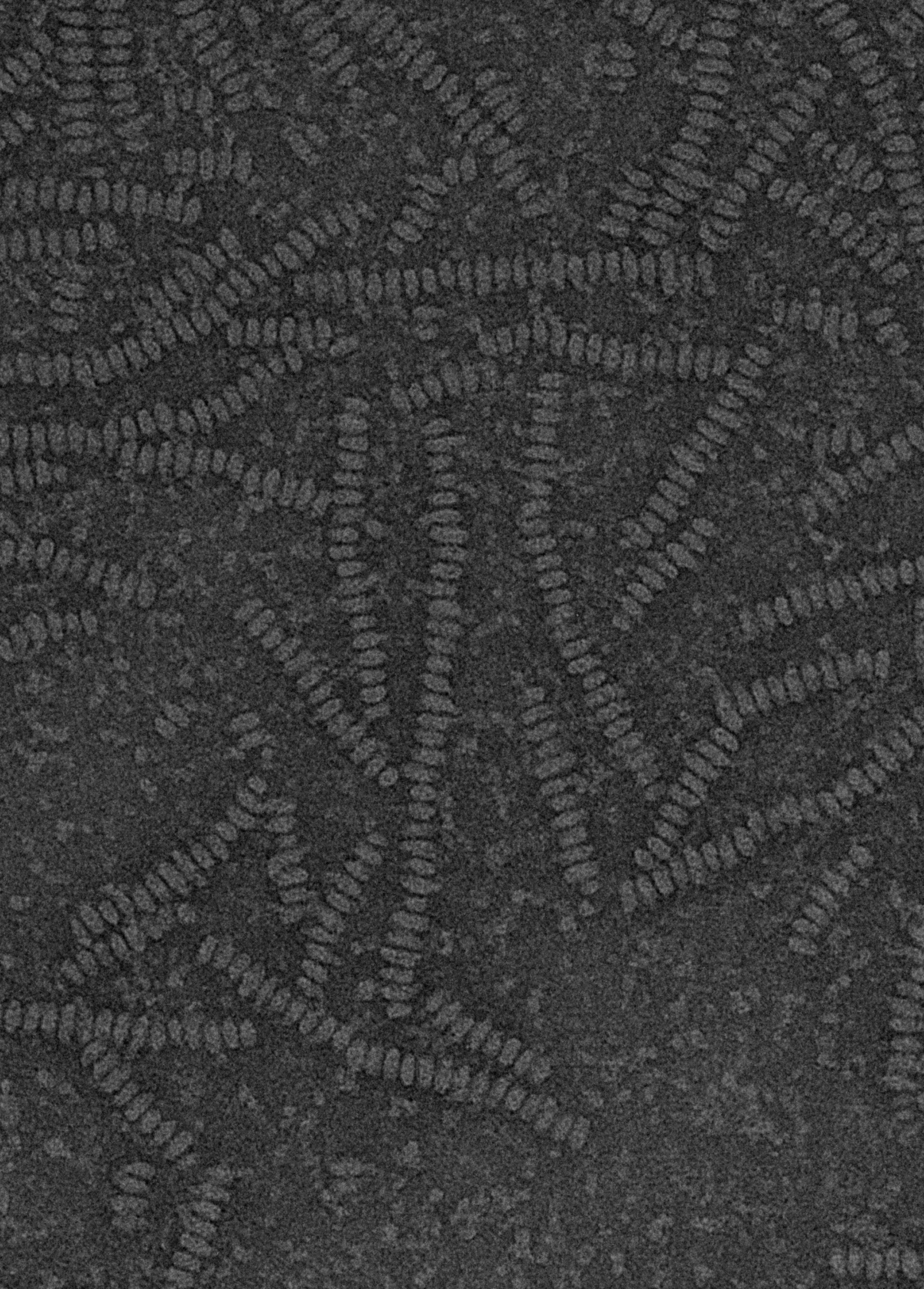

Chapter IV

Styrene-maleic acid-wrapped nanodiscs allow expansion of enclosed lipid material

J. J. Domínguez Pardo†*, C. A. van Walree†, M. Egmond†, M. C. Koorengevel† and J. A. Killian†*

†Membrane Biochemistry & Biophysics, Bijvoet Center for Biomolecular Research, Department of Chemistry, Faculty of Science, Padualaan 8, 3584 CH Utrecht, The Netherlands.

This chapter is under preparation for submission

Abstract

Styrene-maleic acid (SMA) copolymers behave as amphipathic belts encircling lipids in the form of nanodiscs. However, it is unclear whether SMA behaves as a flexible and dynamic band or as a stiff belt which rigidly holds the nanodisc together, thereby interfering with the dynamic behavior of co-purified membrane proteins. Here, we aimed to obtain insight into the flexibility of the SMA belt by making use of synthetic azobenzene-containing phospholipids, incorporated into di-16:0 PC nanodiscs. Azobenzene lipids undergo geometric isomerization upon exposure to light at 365 nm, resulting in the formation of *cis*-isomers that occupy a larger geometric area than the *trans*-isomers. The resistance of the azo-groups against photoisomerization was tested in nanodiscs for different SMA variants and compared with that in large unilamellar vesicles (LUVs). The results showed that azolipids isomerize to the same extent in nanodiscs and in LUVs. This serves as an indication that SMA polymers behave as rather flexible belts, allowing expansion of the enclosed lipid material or of entrapped proteins. The increase in nanodisc diameter upon photoisomerization of the embedded azobenzene lipids is estimated to be approximately ~2 nm.

Introduction

Styrene-maleic acid (SMA) copolymers are in the spotlight of membrane protein (MP) research due to their ability to solubilize lipid membranes into nanodiscs (for reviews see e.g. (Dörr et al., 2016; Esmaili and Overduin, 2017)). It has been suggested that SMA molecules behave as a belt surrounding the enclosed lipid material while styrene units intercalate between adjacent lipids (Dominguez Pardo et al., 2017; Grethen et al., 2017; Jamshad et al., 2015; Orwick et al., 2012). However, it is under dispute whether the interaction of SMA with a lipid membrane has an ordering or disordering effect on the enclosed lipids. EPR experiments conducted with spin-labeled stearic acid (C11-label) in di-14:0 PC nanodiscs indicated an overall increase in order between C8—C12 while the adjacent methylene groups remained unperturbed (Orwick et al., 2012). On the other hand, TEMPO EPR (Orwick et al., 2012) and DSC analysis (Dominguez Pardo et al., 2017; Grethen et al., 2017; Jamshad et al., 2015; Orwick et al., 2012) on di-14:0 PC nanodiscs revealed a melting of the lipids below the melting phase transition temperature ($T<T_m$) and a decrease in the cooperativity between lipids participating in the gel-to-fluid phase transition, suggesting a disordering effect. Whether or not SMA behaves like a stiff belt can be important for the activity of enclosed proteins, since protein conformational changes often involve changes in molecular area that the nanodiscs must be able to accommodate.

Here, we aim to gain insight into the flexibility of the SMA belt by studying the behavior of synthetic di-{9-[(4-phenylazo)-phenoxy]-nonyl} phosphate (i.e Azo-9P, see also forthcoming Figure. 1A) lipids in nanodiscs. In brief, the azobenzenes attached to these lipids undergo geometric isomerization upon exposure of light at 365 nm (for reviews see (Bandara and Burdette, 2012; Beharry and Woolley, 2011)), resulting in *cis*-isomers that occupy a larger geometric volume as compared to *trans*-isomers (Elbing et al., 2008; Nakayama et al., 1997). Whether isomerization of azobenzene is hindered or not will depend on the rigidity of the SMA belt. Isomer conversion can be tracked by UV/Vis spectroscopy as a decrease in A_{350nm} and a small increase in A_{450nm}. First, we will show that this approach is valid by demonstrating that the degree of isomerization (*Xcis*) and the isomerization rate (*k*) of Azo-9P lipids in phosphatidylcholine vesicular self-assemblies are affected by both the temperature and by the lateral pressure in the hydrocarbon region of the membrane. We then will show that efficient isomerization occurs in SMA-bounded nanodiscs, indicating that they consist of dynamic particles despite the higher order of the lipid chains in the nanodisc (Jamshad et al., 2015; Orwick et al., 2012). Based on molecular geometry, we estimate that SMA permits an increase in circumference of approximately ~6.3 nm and thus behaves as a rather flexible belt.

Materials and methods

Materials

1,2-dipalmitoleoyl-**sn**-glycero-3-phosphocholine (di-16:0 PC), 1,2-dipalmitoleoyl-**sn**-glycero-3-phosphocholine (di-16:1 PC) and 1-oleoyl-2-hydroxy-**sn**-glycero-3-phosphocholine (lyso-18:1 PC) were purchased from Avanti Polar Lipids (Alabaster, AL, USA). Xiran 30010 (SMA 2:1, styrene-to-maleic anhydride molar ratio of 2:1) and Xiran 25010 (SMA 3:1, styrene-to-maleic anhydride molar ratio of 3:1) both with a weight average molecular weight of ~10 kDa were obtained as a kind gift from Polyscope Polymers (Geleen, The Netherlands). The polymers were converted to the acid form by hydrolysis under base-catalytic conditions as detailed by Scheidelaar et al (Scheidelaar et al., 2015). 4-Phenylazophenol, 9-bromononan-1-ol and all other chemicals were purchased from Sigma-Aldrich (St. Louis, MO, USA).

Preparation of LUVs

Phospholipid stock solutions were prepared in chloroform/methanol (9:1, v/v) as 10 mM solutions based on the analysis of total phosphate (Rouser et al., 1970). Azo-9P (Kuiper et al., 2003; Kuiper and Engberts, 2004) stock solutions were prepared identically but in methanol/chloroform (1:1, v/v). Aliquots from the phospholipid stock solutions and from the Azo-9P stock solutions, if required, were mixed and the solvent was removed under a stream of N_2. The resulting lipid film was dried in a desiccator under vacuum for at least 1 h. Multilamellar vesicles (MLVs) were obtained by hydrating the lipid films with buffer (50 mM Tris-HCl, 150 mM NaCl, pH 8.0) to a final concentration of 10 mM. The samples were then subjected to 10 freeze-thaw cycles, each consisting of 3 min freezing in liquid N_2 and 3 min thawing in a water bath at 60°C, well above T_m of the lipids (Lewis et al., 1987). Finally, the dispersions of MLVs were extruded at least 10 times through 200 nm polycarbonate filters (Avanti Polar Lipids, Alabaster, USA) at approximately ~50°C, above T_m of the lipids (Lewis et al., 1987).

Preparation of nanodiscs

700 µL aliquots of 10 mM dispersions of LUVs were diluted to 1 mM with solubilization buffer (Tris 50 mM, NaCl 150 mM, Tris-HCl pH=8.0) and mixed with SMA to a final SMA-to-lipid mass ratio of 3.0. The mixture was incubated for at least 15 h above T_m of the lipids and under constant shaking. After solubilization, the samples were placed in an Optima Max ultracentrifuge (Beckman-Coulter, Brea,

CA, USA). Traces of non-solubilized material were removed by centrifugation at 115,000 × *g* for 1 h at 4°C.

Isomerization of Azo-9P

The *trans*-to-*cis* isomerization of Azo-9P was conducted using a SPF-500C spectrofluorometer (SLM Instruments, NY). The quartz cuvette containing the nanodisc solutions or LUV dispersions from the UV-Vis assay was placed in the cuvette holder at the desired temperature and excited at 365 nm for different time periods in the range of 10 s to 120 m (power 250 W).

UV-Vis spectroscopy

UV-Vis scans were performed using a Lambda 18 spectrophotometer (PerkinElmer, Waltham, MA). Briefly, 700 µL aliquots of 1 mM nanodisc solutions or LUVs dispersions were transferred to a quartz cuvette and equilibrated at the desired temperature for 1 min with a cell Peltier element. Scans were recorded in the range of 200 nm to 600 nm at a speed of 240 nm/min. All samples were blanked against identical self-assemblies but without Azo-9P. Data points were obtained every 0.25 s.

Synthesis of Azo-9P

The synthesis of Azo-9P was conducted as detailed by Kuipers and coworkers (Kuiper et al., 2003).
^{1}H NMR (300 MHz, CD_3OD 1:1 v/v): □ = 1.24-1.46 (m, 20 H), 1.59-2.02 (m, 8 H), 3.81 (t, 4 H), 4.02 (t, 4H), 6.97-7.0 (d, *J* = 8.8 Hz, 4 H), 7.4-7.51 (m,6 H), 7.83-7.90 (m, 8 H).
^{13}C NMR (75 MHz, CD_3OD 1:1 v/v): □ = 25.9, 26.1, 29.3, 29.4, 29.6, 29.7, 30.9, 65.7, 68.5, 114.8, 122.6, ,124.8, 129.1, 130.5, 146.9, 152.8, 161.8.
MS (EI^-): *m/z* = 741.

Results and Discussion

Isomerization of Azo-9P is sensitive to temperature and to the physical state of the lipids

Trans—cis isomer conversion of Azo-9P (Figure 1A) can be easily tracked by UV/Vis spectroscopy as an increase in absorbance at 450 nm ($A_{450\ nm}$) and a decrease in absorbance at 350 nm ($A_{350\ nm}$). As detailed in Figure 1B, the band at 350 nm corresponds to strong π—π* transitions in the *trans*-form, while these transitions are downshifted to 310 nm (hypsochromic effect) and weakened in the *cis*-state (Bandara and Burdette, 2012). The band at 450 nm is ascribed to n—π* transitions that are permitted to a higher extent (even though weak) in the *cis*-form than in the *trans*-form. This up-and-down pattern is illustrated in Figure 1C, which shows changes in the absorbance spectra of Azo-9P

upon exposure to light (365 nm) when incorporated in di-16:0 PC LUVs. Experiments were conducted at 50°C, well above T_m of di-16:0 PC (T_m~41°C (Lewis et al., 1987)). At t=0s, the UV/Vis spectra shows a strong absorption peak at 350 nm and a weak absorption peak at 450 nm. The position of the peak at 350 nm for the trans-isomer at t=0 s indicates a homogeneous distribution of *trans*-azobenzene molecules along the lipid membrane and a low degree of chromophore clustering (Kuiper and Engberts, 2004). After 2 minutes of light exposure, A_{350nm} drops to approximately ~40% of its initial value and A_{450nm} increases concomitantly, indicating that isomerization is taking place rather fast. Additionally, the peak at 350 nm is downshifted to 310 nm, further confirming the conversion of the azolipid to the *cis*-state (Einaga et al., 1999; Kuiper and Engberts, 2004). After approximately ~10 min of light exposure no further changes in spectral properties are observed, indicating that the maximal extent of isomerization is reached.

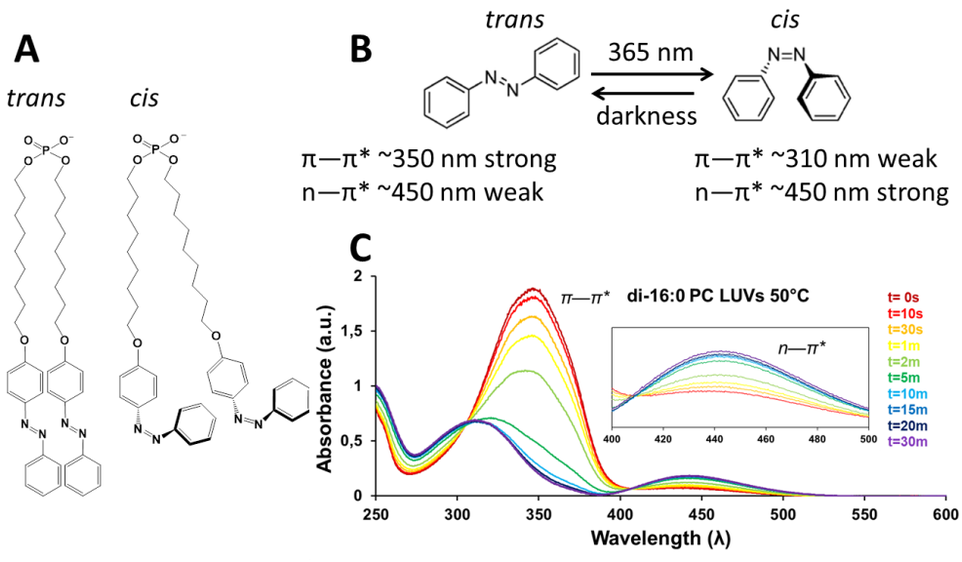

Figure 1. **A**) Molecular structure of *trans*-Azo-9P and *cis*-Azo-9P. **B**) Schematic representation of the isomerization of azobenzene. **C**) Spectra obtained for di-16:0 PC/Azo-9P (9:1 mol). LUVs after light exposure at 350 nm.C) All experiments were conducted at 50 °C.

The presence of two isosbestic points at 50 °C indicates that only two species are involved in the conversion reaction, allowing us to assume first order kinetics for the geometric conversion. Figure 2A shows the *Xcis* values (defined as $1-[A_{350}]_t/[A_{350}]_0$), as function of the exposure time of the sample to the light beam. Data was fitted to equation 2 (SI) to obtain the isomerization rates of Azo-9P (Table 1). It was found that *trans*-to-*cis* isomerization of Azo-9P in di-16:0 PC fluid membranes (50 °C, $T>T_m$) takes place relatively fast with a *k* value of approximately 0.22 min^{-1} (Figure 2, Table 1). The

results furthermore show a high extent of isomerization for *trans*-azobenzene molecules in fluid membranes, with *Xcis* value of ~0.92 after approximately ~10 min of exposure to light.

As illustrated in Fig. 2A and quantified in Table 2, slower isomerization rates were obtained when the isomerization was conducted below T_m at 30 °C and at 20 °C, with *k* values of 0.11 min^{-1} and 0.09 min^{-1} respectively. In addition, lower *Xcis* values of 0.8 and of 0.63, respectively were observed (Table 1). The spectra for both temperatures showed a downshift of the main absorption peak to approximately 330 nm (Figure S1), which may be ascribed to clustering of azobenzene moieties or to a closer contact between chromophores, as a consequence of the tighter lipid packing in gel-phase membranes (Kuiper and Engberts, 2004). Isosbestic points obtained at these lower temperatures were somewhat less well defined than those obtained at 50 °C (Figure 1). Nevertheless, also here the assumption that geometric conversion follows first order kinetics (Whitten et al., 1971), yielded good quality fits (Figure 2A).

The difference in *k* values at the three temperatures tested (Table 2) can be ascribed to changes in temperature (Arrhenius behavior) as well as in the physical state of the lipids, with tighter packing of the lipids or higher viscosity values yielding slower photoiomerization rates. However, this latter may be less likely, since no changes in isomerization rates were found for azobenzene molecules in chloroform/polystyrene mixtures upon variation of viscosity (Serra and Terentjev, 2008). The relatively low degree of isomerization of *trans*-Azo-9P molecules in the gel phase (Table 2) may also at least be partly attributed to the high order parameters and tight packing of the lipids in this phase, as it was found that the bulky *cis*-Azo-9P molecules are difficult to accommodate in solid or highly ordered surfaces (Einaga et al., 1999; Nakayama et al., 1997). Importantly, calorimetric analysis confirmed that also in the presence of *trans*-Azo-9P the lipids are in a gel-phase both at 20°C and at 30°C (Figure S2), demonstrating that Azo-9P has only a mild disturbing effect on the thermotropic properties of its surrounding lipids. However, for the *cis*-form of Azo-9P it is likely that the phase transition becomes more affected, possibly explaining the relatively large difference in *Xcis* value.between 20°C and 30°C.

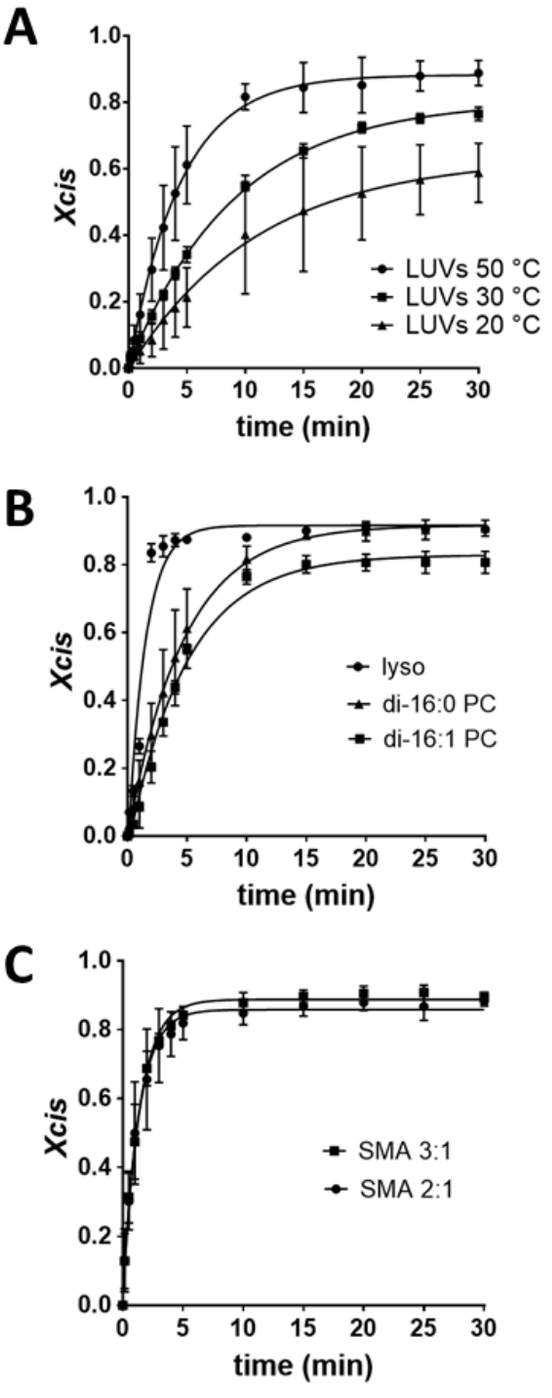

Figure 2. Plot of *Xcis* (isomerization degree) with time (min) of *trans*-Azo-9P in di-16:0 PC at different temperatures (**A**), in LUVs of different lipid composition at 50 °C (**B**), and in di-16:0 PC SMA-bounded nanodiscs at 50 °C (**C**). *Xcis* is defined as 1-$[A_{350}]_t/[A_{350}]_0$. Error bars represent the standard deviation of 3 independent experiments. Data was fitted to equation 2 by using GraphPad Prism™.

Isomerization of Azo-9P is sensitive to the lipid composition of the host membrane

The effect of lipid packing on the rate and extent of isomerization of Azo-9P was further tested by using vesicle preparations in the fluid phase, while keeping the temperature constant but varying the lipid composition. In particular, we used LUVs consisting of the host lipid di-16:0 PC and 20% (mol) of either di-16:1 PC or lyso PC as guest lipid. The azo group in Azo-9P is located at approximately the same depth in the lipid bilayer as the double bonds of di-16:1 PC (Δ9-cis), thus is directly exposed to the high lateral pressure conditions promoted by the kink of the acyl chains. On the other hand, low lateral pressure is expected in the center of the bilayer enriched in lyso PC due its relatively small hydrophobic volume. As shown in Figure 2B and displayed in Table 1, the rate and extent of conversion are lowest for Azo-9P incorporated in vesicles enriched in di-16:1 PC with k 0.20 min^{-1} and *Xcis*~0.83, while the highest rate of interconversion (k 0.69 min^{1}) occurrs for Azo-9P molecules embedded in vesicles enriched in lyso PC lipids. Furthermore, the final extent of isomerization of Azo-9P of *Xcis*~0.92 is rather similar in di-16:0 PC vesicles with or without lyso PC, in line with maximal *Xcis* values reported for di-16:0 PC vesicles.

Overall, these data show that Azo-9P molecules are sensitive to the lipid composition of the membrane whereby a relatively large hydrophobic cross-sectional area of the acyl chains is likely to hamper the accommodation of *cis*-Azo-9P molecules between the lipids.

Self-assembly	Temperature (°C)	Composition	*Xcis* $_{max}$	*k* (min^{-1})
LUVs	20	di-16:0 PC	0.63±0.06	0.09±0.02
LUVs	30	di-16:0 PC	0.80±0.01	0.11±0.01
LUVs	50	di-16:0 PC	0.88±0.02	0.22±0.02
LUVs	50	di-16:0 PC/lyso PC (8:2 mol)	0.92±0.02	0.69±0.09
LUVs	50	di-16:0 PC/di-16:1 PC (8:2 mol)	0.83±0.01	0.20±0.01
SMA 2:1	50	di-16:0 PC	0.86±0.02	0.75±0.09
SMA 3:1	50	di-16:0 PC	0.89±0.01	0.72±0.05

Table.1. Isomerization rate values (*k*) and isomerization degree values (*X*cis) obtained from the isomerization of *trans*-Azo-9P in different self-assemblies. All samples contained ~10 mol% Azo-9P except nanodiscs that contained approximately ~2 mol % Azo-9P. Error bars represent the standard deviation of 2 independent experiments.

Azo-9P molecules incorporated in SMA-nanodiscs isomerize fast and to a very high extent

The sensitivity of isomerization rates and *Xcis* values of Azo-9P to steric hindrance conditions was then employed to elucidate to what extent SMA-bounded nanodiscs are able to accommodate an increase in area of enclosed molecules in the acyl chain region. As shown in Figure 2B, the isomerization rates of Azo-9P in di-16:0 PC nanodiscs bounded by either SMA 2:1 or SMA 3:1 both are extremely fast, with isomerization rates of 0.75 min^{-1} and 0.72 min^{-1} respectively. Furthermore, as shown in Figure 2B and displayed in Table 1, azolipids in nanodiscs reach similar *X*cis values regardless of the nature of the polymer belt, with values of 0.86 for SMA 2:1 nanodiscs and 0.89 by SMA 3:1 nanodiscs. These results indicate that geometric changes are very easily accomodated in the presence of SMA.

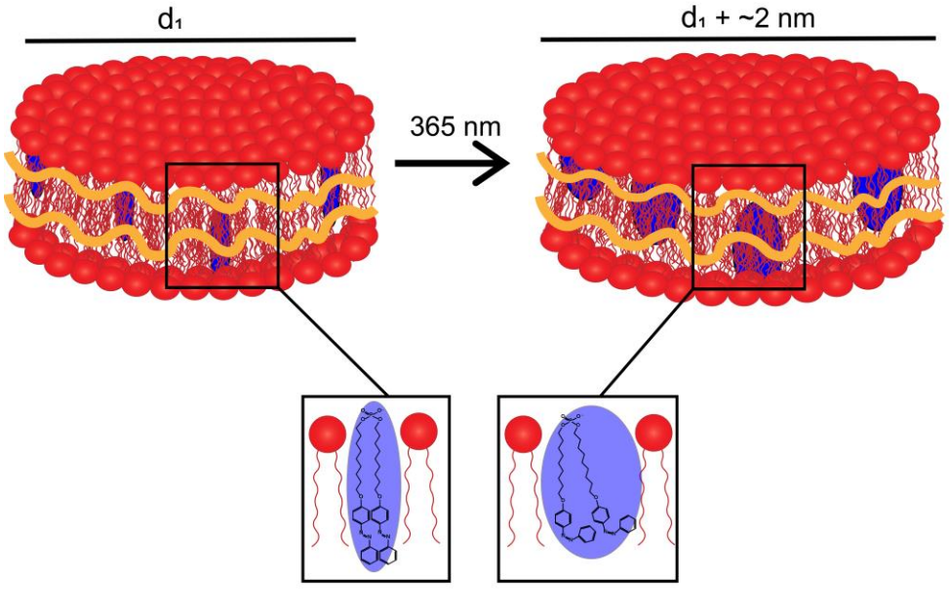

Figure 3. Illustration of the isomerization of trans-Azo-9P lipids embedded in nanodiscs upon light exposure at 365 nm. Inset illustrates the increase in the area of the azolipids after isomerization.

SMA belts can accommodate changes in area of the nanodiscs

In order to estimate the area increase in SMA-wrapped nanodiscs promoted by the isomerization of the enclosed azolipids, first it is necessary to calculate the amount of azolipids solubilized by the SMA preparations. This was estimated from the ratio between initial A_{350} (light exposure t=0 min) values obtained for LUVs and nanodiscs. The results showed that SMA 2:1 nanodiscs contained 1.7±0.2 mol% of Azo-9P while SMA 3:1 nanodiscs contained 1.9±1 mol% of Azo-9P (Table S1). Previous reports estimated that the nanodiscs are constituted by ~200 lipids (Jamshad et al., 2015; Orwick et al., 2012), thus each will contain about 4 azobenzene lipids. We estimated a difference in width between 2 H-atoms in Azo-9P molecules (in identical position, e.g. ortho) in adjacent aromatic rings of ~4.8 Å and ~7.3 Å for the *trans* and the *cis*-isomeric form, respectively. Assuming rapid reorientation of the lipids around their long axis, this 2.5Å difference per azogroup then would translate into a total diameter increase of ~2 nm for 4 double-chained azo-lipids, as illustrated in Figure 3. This ~ 2 nm increase per nanodisc corresponds to a ~6.3 nm increase in circumference.

Unfortunately a size increase could not be detected by DLS (Figure S3). However, DLS is not the most optimal technique, since DLS analyses are conducted for long periods of time under darkness conditions, thus promoting the returning of Azo-9P to a lowest energetic trans-state. Figure S4 includes the extent to which azobenzene lipids isomerize back when embedded in vesicular self-assemblies. Here it is shown that after 30 min (time for DLS measurement) ~50% of azolipids are present in *trans*-isomeric form, hindering the possibility to track changes in size.

Conclusion

We investigated the sensitivity of alkylated azobenzene molecules (Azo-9P) to changes in lipid phase behavior and in lipid composition of the membrane that they are embedded in. Using self-assembled lipid vesicles we have shown that the isomerization rate and the extent to which Azo-9P isomerizes (*X*cis) are sensitive to packing properties of the surrounding lipids and hence that it is a valid method for monitoring the level of "resistance" that the azogroups encounter against the changes in lateral expansion that accompany *trans-cis* isomerization. Importantly, this study demonstrates that amphipathic SMA belts that surround lipid nanodiscs allow enclosed azobenzene labeled lipids to fully isomerize in short periods of time, showing that SMA-bounded nanodiscs can easily accommodate an increase in geometric area in the acyl chain region. This dynamic character of SMA nanodiscs is in line with the observations of collisional lipid exchange between nanodiscs (Cuevas Arenas et al., 2017), and suggests that nanodiscs may provide a suitable bilayer environment also for flexible proteins that undergo relatively large conformational changes during function.

References

Bandara, H.M.D., Burdette, S.C., 2012. Photoisomerization in different classes of azobenzene. Chemical Society reviews 41 (5), 1809–1825.

Beharry, A.A., Woolley, G.A., 2011. Azobenzene photoswitches for biomolecules. Chemical Society reviews 40 (8), 4422–4437.

Cuevas Arenas, R., Danielczak, B., Martel, A., Porcar, L., Breyton, C., Ebel, C., Keller, S., 2017. Fast Collisional Lipid Transfer Among Polymer-Bounded Nanodiscs. Scientific reports 8:15016–15026

Dominguez Pardo, J.J., Dörr, J.M., Renne, M.F., Ould-Braham, T., Koorengevel, M.C., van Steenbergen, M.J., Killian, J.A., 2017. Thermotropic properties of phosphatidylcholine nanodiscs bounded by styrene-maleic acid copolymers. Chemistry and physics of lipids 208, 58–64.

Dörr, J.M., Scheidelaar, S., Koorengevel, M.C., Dominguez, J.J., Schäfer, M., van Walree, C.A., Killian, J.A., 2016. The styrene-maleic acid copolymer: a versatile tool in membrane research. European biophysics journal : EBJ 45 (1), 3–21.

Einaga, Y., Sato, O., Iyoda, T., Fujishima, A., Hashimoto, K., 1999. Photofunctional Vesicles Containing Prussian Blue and Azobenzene. Journal of the American Chemical Society 121 (15), 3745–3750.

Elbing, M., Błaszczyk, A., Hänisch, C. von, Mayor, M., Ferri, V., Grave, C., Rampi, M.A., Pace, G., Samorì, P., Shaporenko, A., Zharnikov, M., 2008. Single Component Self-Assembled Monolayers of Aromatic Azo-Biphenyl: Influence of the Packing Tightness on the SAM Structure and Light-Induced Molecular Movements. Adv. Funct. Mater. 18 (19)

Esmaili, M., Overduin, M., 2017. Membrane biology visualized in nanometer-sized discs formed by styrene maleic acid polymers. Biochimica et biophysica acta. 10.1016

Grethen, A., Oluwole, A.O., Danielczak, B., Vargas, C., Keller, S., 2017. Thermodynamics of nanodisc formation mediated by styrene/maleic acid (2:1) copolymer. Scientific reports 7:11517

Jamshad, M., Grimard, V., Idini, I., Knowles, T.J., Dowle, M.R., Schofield, N., Sridhar, P., Lin, Y., Finka, R., Wheatley, M., Thomas, O.R.T., Palmer, R.E., Overduin, M., Govaerts, C., Ruysschaert, J.-M., Edler, K.J., Dafforn, T.R., 2015b. Structural analysis of a nanoparticle containing a lipid bilayer used for detergent-free extraction of membrane proteins. Nano Research 8 (3), 774–789.

Kuiper, J.M., Engberts, J.B.F.N., 2004. H-Aggregation of Azobenzene-Substituted Amphiphiles in Vesicular Membranes. Langmuir : the ACS journal of surfaces and colloids 20 (4), 1152–1160.

Kuiper, J.M., Hulst, R., Engberts, J.B., 2003. A selective and mild synthetic route to dialkyl phosphates. Synthesis 2003 (05), 695–698.

Lewis, R.N., Mak, N., McElhaney, R.N., 1987. A differential scanning calorimetric study of the thermotropic phase behavior of model membranes composed of phosphatidylcholines containing linear saturated fatty acyl chains. Biochemistry 26 (19), 6118–6126.

Nakayama, K., Jiang, L., Iyoda, T., Hashimoto, K., Fujishima, A., 1997. Photo-Induced Structural Transformation on the Surface of Azobenzene Crystals. Japanese Journal of Applied Physics 36 (6S), 3898.

Orwick, M.C., Judge, P.J., Procek, J., Lindholm, L., Graziadei, A., Engel, A., Gröbner, G., Watts, A., 2012. Detergent-free formation and physicochemical characterization of nanosized lipid-polymer complexes: Lipodisq. Angewandte Chemie (International ed. in English) 51 (19),

Rouser, G., Fleischer, S., Yamamoto, A., 1970. Two dimensional thin layer chromatographic separation of polar lipids and determination of phospholipids by phosphorus analysis of spots. Lipids (5), 494–496.

Scheidelaar, S., Koorengevel, M.C., Pardo, J.D., Meeldijk, J.D., Breukink, E., Killian, J.A., 2015. Molecular model for the solubilization of membranes into nanodisks by styrene maleic Acid copolymers. Biophysical Journal 108 (2), 279–290.

Serra, F., Terentjev, E.M., 2008. Effects of Solvent Viscosity and Polarity on the Isomerization of Azobenzene. Macromolecules 41 (3), 981–986.

Whitten, D.G., Wildes, P.D., Pacifici, J.G., Irick, G., 1971. Solvent and substituent on the thermal isomerization of substituted azobenzenes. Flash spectroscopic study. Journal of the American Chemical Society 93 (8), 2004–2008.

Supporting information

Theoretical background

UV/Vis spectra of Azo-9P molecules show the presence of two isosbestic points at λ=310 nm and at λ=410 nm, delimiting two different regions: the reactant region at λ=350 nm and the product region at λ=450 nm. By applying first order kinetics model we obtain:

$$v = -\frac{\partial[A350]}{\partial t} = k[A350] \qquad (1)$$

Where v corresponds to the reaction rate, k corresponds to the reaction rate constant and $[A350]$denotes the absorbance of trans-azobenzene molecules which in our case is a measure of the concentration. By integrating both sides of equation (1) we obtain equation (2).

$$[A350] = [\mathrm{A350}]0\ e^{kt} \qquad (2)$$

Dynamic light scattering

1-mL aliquots of 10 mM nanodisc solutions obtained at a SMA-to-lipid mass ratio of 3.0 were placed in a plastic cuvette and measured by dynamic light scattering (DLS) in a Zetasizer Nano ZS (Malvern Instruments, Worcestershire, UK). Samples were measured at least 12 times, each measurement being an average of 20 sub-runs of 15 s. Size–intensity distributions were generated using Zetasizer software Ver. 6.20 and 7.03 and analyzed using the multiple narrow distribution. Hydrodynamic diameters were calculated from the intensity distributions with the assumption that nanodiscs have a spherical shape.

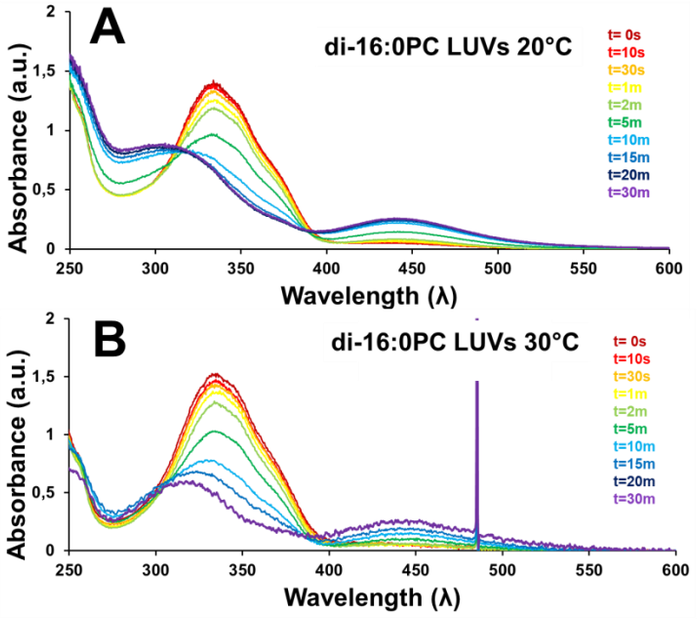

Figure S1. UV-Vis spectra obtained for di-16:0 PC/Azo-9P (9:1 mol) LUVs after light exposure at 365 nm at 20 ^{o}C (A) and at 30 ^{o}C (B). All spectra were obtained at the indicated temperature. Spike at ~485 nm is ascribed to an artifact during the recording of the spectra.

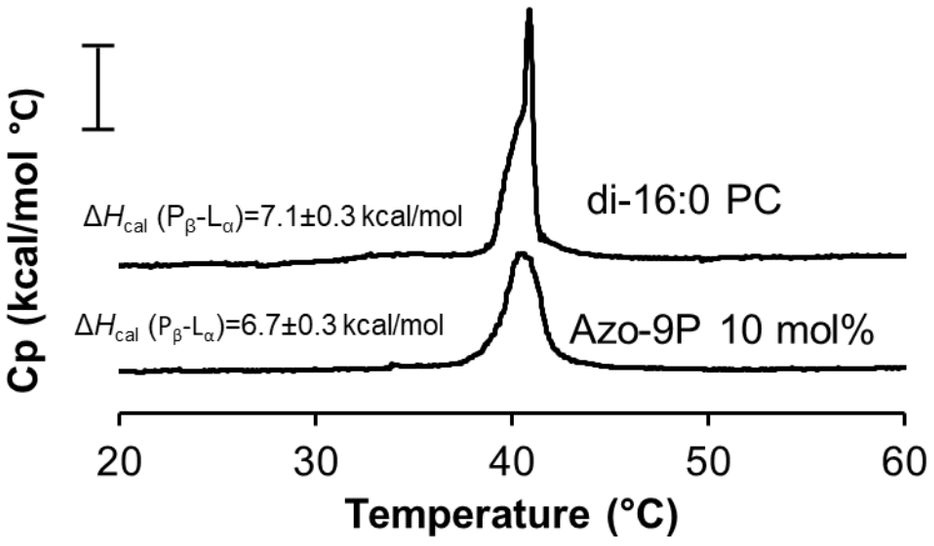

Figure S2. Representative differential scanning calorimetry (DSC) thermograms of di-16:0 PC LUVs (top) and of di-16:0 PC/ Azo-9P (10:1,mol) LUVs (bottom). Figure includes calorimetric enthalpy values of the ripple-to-fluid phase transition of di-16:0 PC lipids in either self-assembly. The inserted scale bar at the top corresponds to 2 kcal/mol.

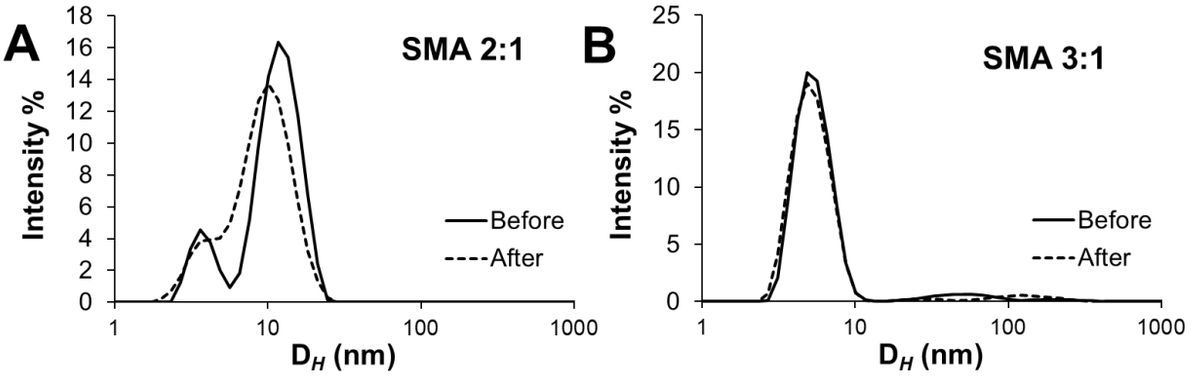

Figure S3. Size distribution of soluble di16:0 PC nanodiscs bounded by either SMA 2:1 (A) or SMA 3:1 (B) before and after exposure to light (365 nm) for 30 min at 50 °C. Data anlyses were performed at T=25 °C.

Di-16:0 PC nanodisc	A_{350} (t=0s)	Azo9P (mol%)

SMA 2:1	0.26±0.03	1.7±0.2
SMA 3:1	0.28±0.16	1.8±1.0

Table S1. Initial absorbance values at 350 nm (A_{350} nm) at isomerization time=0 s and estimated abundance of Azo-9P in SMA-nanodiscs calculated from A_{350} values obtained from LUVs containing 10 mol% Azo-9P. Errors represent the standard deviation of 2 independent experiments.

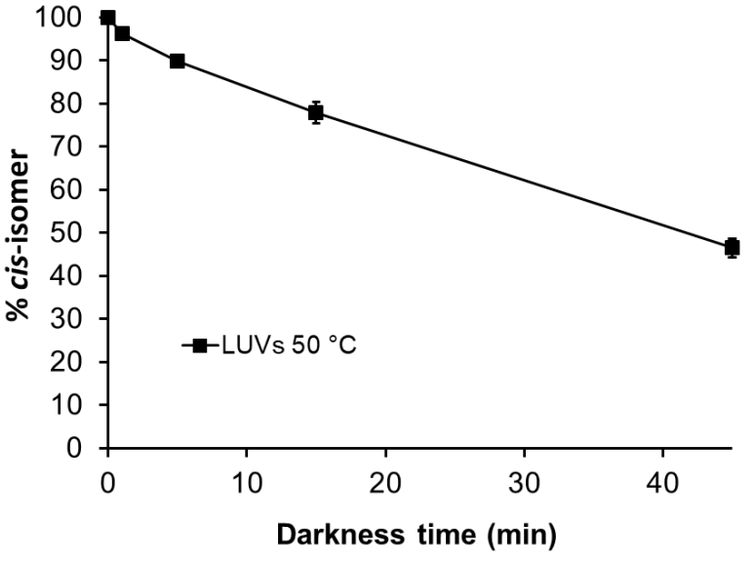

Figure S4. % of *cis*-azobenzenelipid in di-16:0 PC/Azo-9P (10:1,mol) LUVs (squares) after sample incubation in complete darkness at 50 °C. Sample were first exposed to light for 30 min at 50 °C and then stored for back-isomerization. Error bars represent the standard deviation of 2 independent experiments. Final concentration of Azo-9P was kept constant at ~0.1 mM.

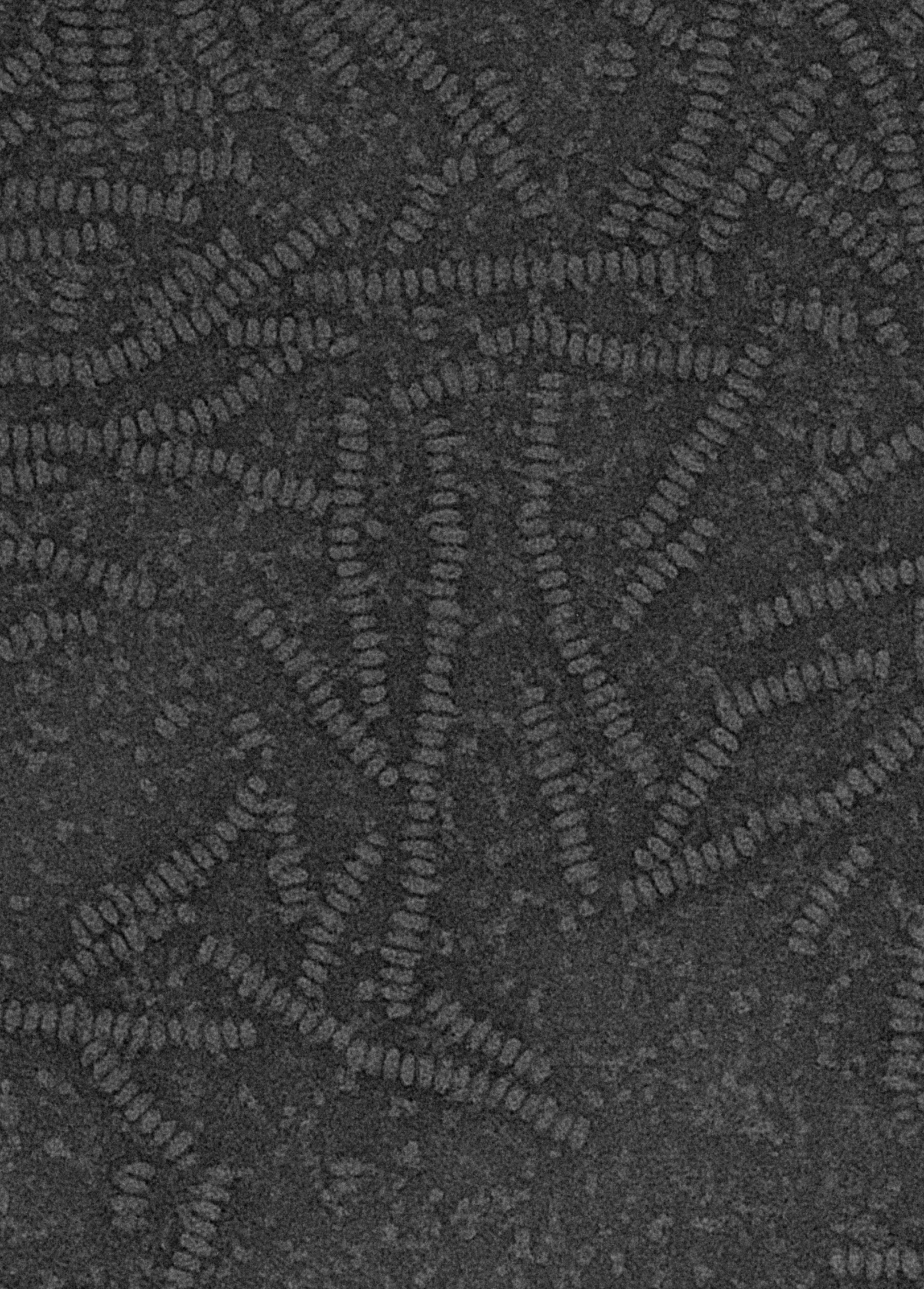

Chapter V

Membrane solubilization by SMA polymers: delineating the role of polymer length

J.J. Domínguez Pardo[†*], M. C. Koorengevel[†], H. Jahn[†], N. Uwugiaren[†], J. Weijers[†], C.A. van Walree[†], M. J van Steenbergen[‡] and J. A. Killian[†*]

[†] Membrane Biochemistry and Biophysics, Bijvoet Center for Biomolecular Research, Department of Chemistry, Faculty of Science, Padualaan 8, 3584 CH Utrecht, The Netherlands.

[‡] Department of Pharmaceutics, Utrecht Institute for Pharmaceutical Sciences (UIPS), Faculty of Science, Utrecht University, PO Box 80082, 3508 TB Utrecht, The Netherlands.

This chapter is under preparation for submission

Abstract

Styrene-maleic acid copolymers have gained interest in membrane research because they allow solubilization and purification of membrane spanning proteins from biological membranes in the form of native-like nanodiscs. However our understanding of the underlying SMA-lipid interactions is hampered by the fact that SMA preparations are very polydisperse. Here, we obtained fractions of the two most commonly used SMA preparations: SMA 2:1 and SMA 3:1 (both of M_w ~10 kD) with different number average molecular weight (M_n) and styrene content. The fractionation is based on the differential solubility of styrene-maleic anhydride (SMAnh) in hexane/acetone mixtures. SMAnh fractions were hydrolyzed to SMA and added to lipid self-assemblies. It was found that SMA fractions inserted in monolayers and solubilized vesicles to a different extent, with the highest efficiency being observed for low M_n SMA polymers. EM and DLS size analyses confirmed the presence of nanodiscs independent of the M_n of the SMA polymers forming the belt and it was shown that the nanodiscs all have approximately the same size. However, the stability of the nanodiscs was strongly affected by the M_n of the polymer rim. Overall, nanodiscs bounded by high M_n SMA polymers were more stable than those bounded by low M_n polymers, as indicated by a better retention of the native lipid thermotropic properties and by slower exchange rates between lipids in nanodiscs. In conclusion, we here present a simple method to separate SMAnh molecules based on their M_n from commercial SMAnh blends, which allowed us to obtain new insights into the importance of SMA length for polymer—lipid interactions.

Introduction

Styrene-maleic acid copolymers (SMA) are in the spotlight of membrane protein research due to their ability to solubilize lipid membranes into nanodiscs (for reviews see (Dörr et al. 2016; Esmaili and Overduin 2017)). SMA-mediated solubilization offers many advantages over conventional solubilization methods based on the use of detergents including retention of the membrane architecture (i.e. lipid bilayer conformation) in nanodiscs (Orwick et al. 2012; Jamshad et al. 2015) and the suitability of nanodisc particles for analysis by biophysical techniques such as NMR (Vargas et al. 2015; Ravula et al. 2017), turbidimetry (Scheidelaar et al. 2015; Dominguez Pardo et al. 2017) and calorimetry (Orwick et al. 2012; Dominguez Pardo et al. 2017; Grethen et al. 2017).

A broad range of SMA polymers differing in composition and in length are commercially available. It has been shown that the composition of the SMA polymers strongly affects the membrane solubilization properties in model membranes (Scheidelaar et al. 2016) as well as in biological membranes (Morrison et al. 2016; Swainsbury et al. 2017) and that it also affects the properties of the resulting nanodiscs (Dominguez Pardo et al. 2017b). Recently, also the effect of polymer length in membrane solubilization has been investigated. It was found that the solubilization of a broad range of membrane spanning proteins (i.e. BmrA, LeuT, ZipA) from *E.coli* membranes was most efficiently conducted by low molecular weight SMA polymers. Similarly, it was found that low molecular weight SMA polymers (approximately ~6—10 kDa) were able to solubilize *R. sphaeroides* monomeric reaction centers approximately ~3x more efficiently than their high molecular weight SMA counterparts (Swainsbury et al. 2017). However, our understanding of the underlying SMA-lipid interactions is hampered by the fact that SMA preparations are very polydisperse and consist of a broad variety of SMA polymers of different length and composition (Scheidelaar et al. 2016).

In order to gain insight into how specific interactions between lipids and SMA polymers affect membrane solubilization and the properties of the resulting nanodiscs, we here prepared SMA fractions from commercial SMA blends based on polymer immiscibility of the non-hydrolyzed form (i.e. styrene-maleic anhydride, SMAnh) in hexane/acetone mixtures. We focused on the two most commonly used SMA preparations: SMA 2:1 (i.e. Xiran 30010) and SMA 3:1 (i.e. Xiran 25010). For each SMAnh preparation we obtained four pools of polymers with different average number molecular weight (M_n) values in the range of 1.1—6.5 kDa and each was hydrolyzed to SMA. It was found that low M_n SMA polymers insert to the highest extent into phosphatidylcholine monolayers. Similarly, the solubilization of phosphatidylcholine vesicles was found to be most efficiently conducted by low M_n SMA. All the SMA polymer fractions were found to yield nanodiscs, with no apparent size correlation with the length or with the composition of the polymer belt. However, the

length of the polymer belt does affect the stability of the enclosed lipids. The highest perturbation of the thermotropic properties of the lipids and the fastest lipid exchange rates between nanodiscs were found when these are bounded by low M_n SMA polymers. Overall, the fragments derived from SMA 2:1 polymers yielded a better stability than the fragments derived from SMA 3:1 polymers. In conclusion, we here present a simple method to separate high M_n and low M_n SMAnh polymers from commercial SMAnh mixtures, providing new insights into the effects of polymer length on membrane solubilization.

Materials and Methods

Materials

1,2-dimyristoyl-***sn***-glycero-3-phosphocholine (di-14:0 PC), 1,2-dipalmitoyl-**sn**-glycero-3-phosphocholine (di-16:0 PC) and 1,2-distearoyl-**sn**-glycero-3-phosphocholine (di-18:0 PC) and 1,2-dimyristoyl-**sn**-glycero-3-phosphoethanolamine-N-(lissamine rhodamine B sulfonyl) were purchased from Avanti Polar Lipids (Alabaster, AL, USA). Styrene-maleic anhydride (SMAnh) copolymers Xiran 30010 (molar ratio of styrene-to-maleic anhydride of 2:1) and Xiran 25010 (molar ratio of styrene-to-maleic anhydride of 3:1), both with a weight average molecular weight of ~10 kDa, were a kind gift from Polyscope Polymers (Geleen, The Netherlands). All other chemicals were purchased from Sigma Aldrich (St.Louis, MO).

Fragmentation of SMA copolymers

SMA copolymers were fragmented by differential solubilization as follows. A 10 % (w/w) solution of SMAnh 2:1 (i.e. X30010) or SMAnh 3:1 (i.e. X25010) in acetone was mixed with an equal volume of hexane to a final 50 % (v/v) concentration and centrifuged for 10 min at 10,000 x *g* at 4 °C leading to the formation of a two-layer system. The bottom layer, denoted the SMAnh P50 fraction, and the upper layer were separated by pipette aspiration and dried by rotary evaporation of the solvent. The residue of the upper layer was dissolved in 10% (w/w) acetone and hexane was added to a final concentration of 80 % (v/v). The resulting mixture was centrifuged for 10 min at 10,000 x *g* at 4 °C leading to the separation of the pellet (denoted the SMAnh P80 fraction) from the supernatant. This procedure was repeated for a final concentration of 90 % (v/v) hexane, yielding the SMAnh P90 fraction, and then for a final concentration of 96.5 % (v/v) hexane yielding the SMAnh P96 fraction (denoted SMAnh P96 instead of SMAnh P96.5 to ease the reading). In order to remove any trapped soluble material in the pellet fractions, an additional washing step was done as follows: 10 % (w/w)

SMAnh solutions consisting of P50, P80, P90 and P96 in acetone were mixed with hexane to a final 51, 81, 91, and 97 % (v/v) hexane concentration respectively. The mixtures were centrifuged for 20 min at 10,000 x *g* at 0 °C. The supernatants were discarded and the pellets were dried by rotary evaporation.

UV-Vis spectroscopy

UV-Vis spectra were obtained for 1 mL aliquots of 0.0125 % (w/v) SMAnh solutions in THF. SMAnh solutions were transferred to a quartz cuvette and equilibrated at 25 °C for 1 minute. Scans were recorded in the range of 240 nm to 290 nm at a speed of 120 nm/min using a Lambda 18 spectrophotometer (PerkinElmer, MA,USA). Data points were obtained every 0.25 s.

Gel permeation chromatography (GPC)

50 µL aliquots of 0.2 % (w/v) SMA solutions in THF were analyzed with a Waters Alliance 2695 system (Milford, MA,USA) and a Waters 2410 RI detector. An Agilent PLgel Mesopore column 8x300 mm (Santa Clara, CA, USA) at a temperature of 30 °C was used with THF at a constant flow rate of 1 mL/min as eluent. Data collection and analysis was done with Empower 3 software (Waters). Number-average molecular weight (M_n) values of the different SMAnh fractions were obtained by relative calibration using polystyrene standards (Saldívar-Guerra and Vivaldo-Lima 2013).

Preparation of SMA fragments

SMAnh fragments were converted to the acid form by alkaline hydrolysis as follows: 10 % (w/v) SMAnh suspensions in water containing 0.6 equivalents of NaOH (NaOH-to-carboxylic acid groups, mol) were introduced in a Certoclav pressure cooker (Traun, Austria) and were subjected to at least 3x15 min autoclave cycles at 125 °C. SMA solutions were further diluted with water if necessary.

Size exclusion chromatography (SEC)

100 µL of 0.5 % (w/v) SMA solutions in 2 mM Britton—Robinson buffer were injected into a manually prepared Sephadex G-75 column (32 cm x 2 cm) equipped with an Akta purification system (Chicago, IL, USA). SEC chromatograms were obtained at a flow rate of 0.2—1 mL/min.

Fourier transform infrared spectroscopy (FTIR)

FTIR spectra were recorded for the different SMAnh fractions using a Perkin-Elmer Spectrum 100 FT-IR spectrometer (Waltham, MA, USA) operated by Perkin-Elmer Spectrum software version 10.4.449. Spectra were collected in the ATR mode. Relative styrene-to-maleic acid ratios were obtained from

the ratio: $A_{680cm-1}/A_{1780cm-1}$ corresponding to the vibration modes of CH-sp^2 bending of monosubtituted benzene at 680 cm^{-1} and to the vibration mode of C=O anhydride stretching at 1780 cm^{-1}.

Lipid monolayer experiments

Surface pressure isotherms versus time were recorded for lipid monolayers formed of either di-14:0 PC or di-18:0 PC upon addition of 20 µL SMA 10% w/v (yielding a final concentration of 0.01 % w/v). Phospholipid monolayers were assembled on a 6.0 x 5.5 cm compartment of a homemade Teflon trough filled with 20 mL buffer (Tris HCl 50 mM, NaCl 150 mM, pH=8.0). Aliquots from 2.5 mM phospholipid stock solutions in chloroform/methanol (9:1 v/v) were carefully added dropwise to the surface of the buffer solution until an initial surface pressure of 25 mN/m was reached. SMA was added after 2 min of stabilization and the increase in surface pressure was recorded for at least 30 min using a MicroTrough XS monolayer system (Kibron, Helsinki, Finland). Surface pressure isotherms presented in this study are a result of the average of 2 independent experiments. All experiments were conducted at room temperature.

Preparation of multilamellar vesicles (MLVs)

Phospholipid stock solutions were prepared in chloroform/methanol (9:1 v/v) in concentrations of 10 mM based on phosphate analysis (Rouser et al. 1970). Aliquots from the phospholipid stock solutions were taken and the solvent was removed under a stream of N_2. The resulting lipid film was dried in a desiccator under vacuum for at least 1 h. Next, the lipid films were hydrated with buffer (Tris 50 mM, NaCl 150 mM, pH 8.0) to the desired final concentration and stabilized for at least 5 minutes at $T>T_m$.The samples were then subjected to 10 freeze-thaw cycles, each consisting of 3 min freezing in liquid N_2 (-196 °C) and 3 min thawing in a water bath at 60 °C, well above T_m of the lipids (Lewis, Ruthven N. A. H. et al. 2002).

Kinetics of solubilization of phosphatidylcholine vesicles

700 µL aliquots of 0.5 mM dispersions of di-14:0 PC MLVs in solubilization buffer (Tris-HCl 50 mM, NaCl 150 mM, pH=8.0) were mixed with SMA 5% (w/v) to a final SMA-to-lipid mass ratio ~3.0. Solubilization kinetics was followed at a fixed wavelength of 350 nm by monitoring the decrease of the apparent absorbance. Solubilization was recorded for 15 minutes at 15 °C, below T_m of di-14:0 PC (T_m~23 °C(Lewis, Ruthven N. A. H. et al. 2002)). The temperature was controlled with a Peltier cuvette holder (Santa Clara, CA, USA). Absorbance values were recorded every 0.4 s.

Preparation of nanodiscs

Dispersions of MLVs in solubilization buffer Tris-HCl 50 mM, NaCl 150 mM, pH 8.0) were mixed with SMA 10% (w/v) (SMA-to-lipid mass ratio ~3.0) overnight at $T>T_m$. The non-solubilized material was pelleted down by spinning at 115,000 × *g* for 1 h at 4 °C and the supernatant, containing the solubilized lipid material, was collected. Both the initial molarity and lipid composition of the dispersions of MLVs are specific for each experiment and are described as follows: nanodisc solutions measured by DLS and DSC analyses were obtained from initial 700 µL aliquots of 20 mM of di-14:0 PC MLVs (DLS) or di-16:0 PC MLVs (DSC). Nanodiscs solutions used in rhodamine dequenching analyses were obtained from initial 100 µL aliquots of 2 mM of di-14:0 PC/ N-rhodamine di-14:0 PE (4:1 mol) MLVs.

Differential scanning calorimetry (DSC)

DSC measurements were performed using a Discovery DSC (TA Instruments, Newcastle, DE) calorimeter. 10-µL aliquots of nanodisc solutions or MLV dispersions containing ~20 mM lipids were placed in hermetic Tzero pans (TA Instruments, Newcastle, DE, USA). Heating curves were recorded in the ranges of 0-70 °C at a scan rate of 5 °C/min at least 3 times. T_m values were obtained at $T_m=Cp_{max}$ using Trios software (TA Instruments, Newcastle, DE, USA). Error bars reported for T_m values correspond to the average from the 2^{nd} and 3^{rd} heating cycles from 2 independent samples.

Dynamic light scattering (DLS)

Dynamic light scattering (DLS) analysis was performed on the samples using a Zetasizer Nano ZS (Malvern Instruments, Worcestershire, UK). 700 µL aliquots of 20 mM of di-14:0 PC nanodisc solutions and 1 mL aliquots of SMA 1% (w/v) in buffer (Tris-HCl 50 mM, NaCl 150 mM, pH 8.0) were measured at least 12 times, each measurement being an average of 20 sub-runs of 15 s. Size–intensity distributions were generated using Zetasizer software Ver. 6.20 and 7.03 and analyzed using the multiple narrow distribution. Hydrodynamic diameters were calculated from the intensity distributions with the assumption that nanodiscs have a spherical shape. All samples showed a polydispersity index (PDI)<0.3.

Transmission electron microscopy

Size characterization of di-14:0 PC nanodiscs was performed by transmission electron microscopy (TEM). Aliquots from the nanodisc solutions used for DLS analyses were diluted to a final 0.5 mM and adsorbed on carbon-coated mica following the carbon flotation technique and stained with a staining solution containing 2% (w/v) sodium silicotungstate as detailed before (Dominguez Pardo et

al. 2017a). Images were taken under low dose conditions at a nominal magnification of 49,000 with a T12 electron microscope (FEI, Hillsboro, OR) at an operating voltage of 120 kV using an ORIUS SC1000 camera (Gatan, Inc., Pleasanton, CA). The average size of the nanodiscs was estimated from at least 15 well-defined individual particles. The maximum diameter was determined using Adobe Illustrator software (San Jose, CA).

Rhodamine fluorescence dequenching

Aliquots of 2 mM of di-14:0 PC/N-rhodamine di 14:0 PE (4:1 mol). MLVs were diluted to a final volume of 1 mL yielding a final N-rhodamine di 14:0 PE concentration of 2.5µM and were placed in a 10 mm quartz cuvette. Next, the solutions were equilibrated for at least 2 minutes at 30 °C by using a Peltier cuvette holder (Santa Clara, CA). Fluorescent nanodiscs were excited at 585 nm and mixed with aliquots of unlabeled di-14:0 PC nanodiscs. Unlabeled nanodiscs were added to a final lipid molar ratio of 1:20 or 1:5 of labeled-to-unlabeled nanodiscs. Rhodamine dequenching was monitored for 15 min using a Varian Cary Eclipse fluorescence spectrophotometer (Santa Clara, CA, USA).

Results

Commercially available SMAnh can be fractionated based on differences in solubility in hexane/acetone mixtures

Commercially available SMAnh copolymers are very heterogeneous and consist of a mixture of polymers of different length and composition. It is expected that these constituents will also exhibit different solubility properties. Here, the fractionation of SMAnh 2:1 and SMAnh 3:1 copolymers was accomplished by differential solubility in mixtures of hexane and acetone. As illustrated in Figure 1A, anhydrous solutions of the polymers (i.e. SMAnh) in acetone were initially mixed with an equal volume of hexane yielding a two-phase system. The bottom phase contained a fraction of the polymer mixture, denoted the SMAnh P50 fraction, which was separated by centrifugation and washed. This procedure was repeated for a final concentration of 80 % hexane, 90% hexane and 96.5 % hexane, yielding respectively the SMAnh P80, SMAnh P90 and SMAnh P96 fractions. As shown in Figure 1B, the yields for both SMAnh 2:1 and SMAnh 3:1 were highest for the SMAnh P50 and the SMAnh P80 fractions, which together contain approximately ~80% of the initial mass of the SMAnh.

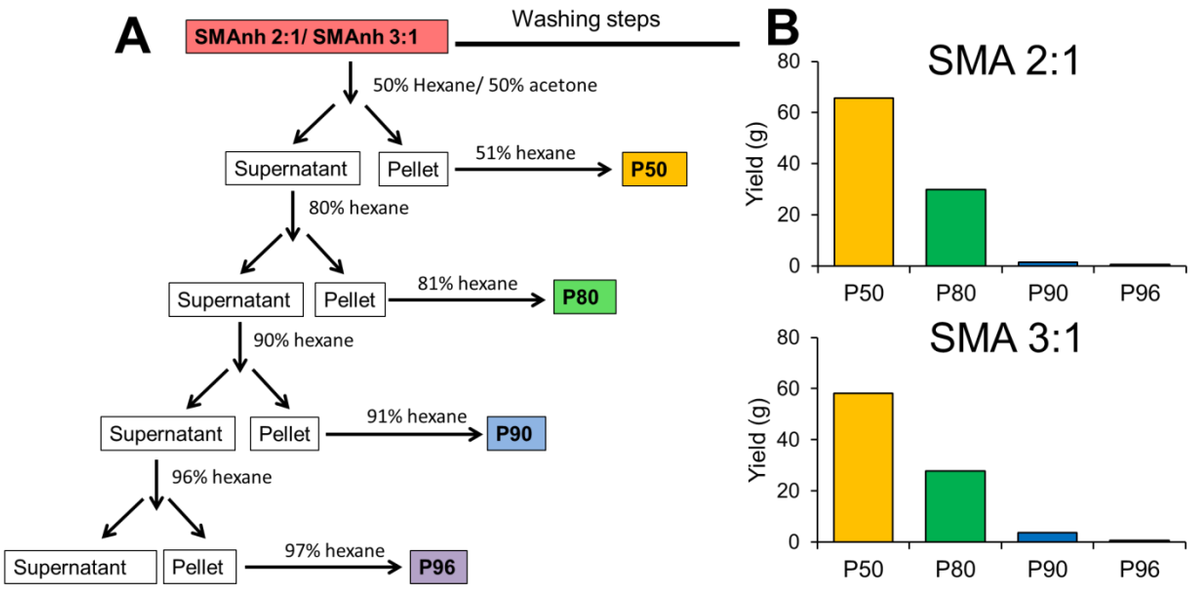

Figure 1. A) Schematic representation of the flowchart for the purification of SMAnh fractions from commercially available SMAnh polymers. Solvent mixtures formed of hexane/acetone are expressed in volume %. B) Yield of the SMAnh fractions expressed in mass (g). The initial mass was 100 g.

Separated fractions of SMAnh mixtures have different length and styrene content

The SMAnh fractions obtained were characterized by gel filtration chromatography (GPC) (Figure 2A and 2B) from which it was possible to determine both their number average molecular weight (M_n) and their polydispersity index (PDI). The M_n and PDI values are displayed in Table 1. SMAnh P50 fractions were found to contain polymers with the highest M_n, while the polymers with lowest M_n were found in the SMAnh P90 fractions and in the SMAnh P96 fractions. The PDI (Table 1) was found to be smaller in the purified fractions than in the non-fractionated material indicating a higher monodispersity.

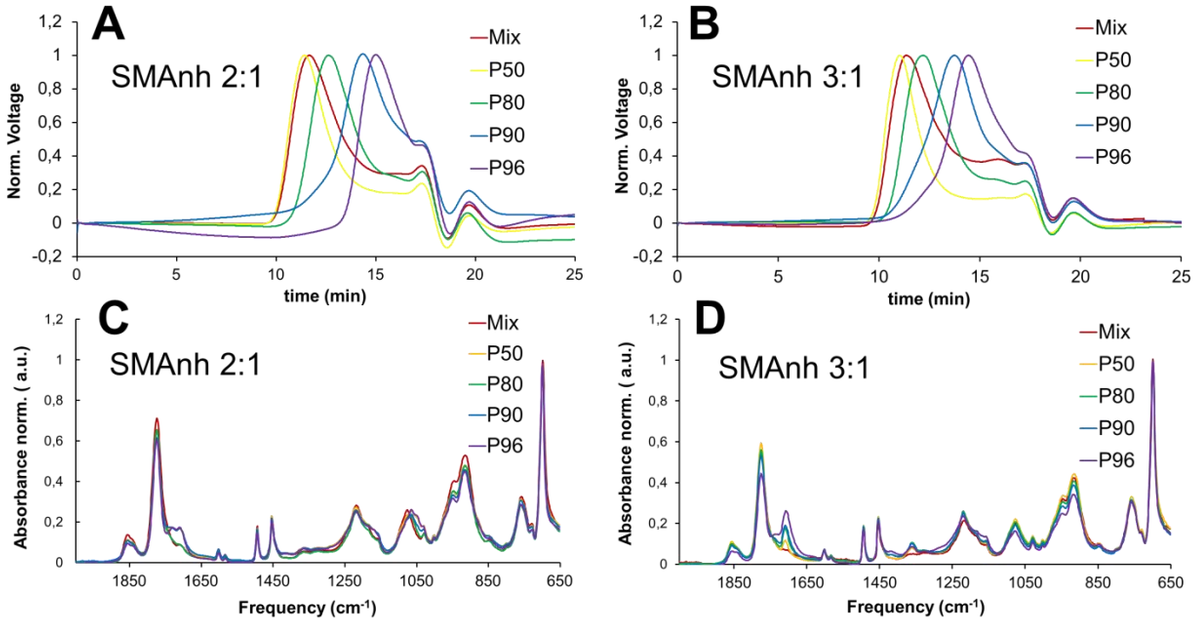

Figure 2. GPC chromatograms of 0.2% (w/v) SMAnh 2:1 (A) and SMAnh 3:1 (B) polymers in THF. FTIR analyses of SMAnh 2:1 (C) and of SMAnh 3:1 (D) polymers. All experiments were conducted at room temperature (~23 °C).

Insight into the composition of the different SMAnh fractions was obtained by FTIR (Figure 2C and 2D). By determining the ratio between the absorbance at 680 cm^{-1} (CH_2= bending monosubtituted benzene) and at 1780 cm^{-1} (C=O stretching, anhydride) it is possible to qualitatively compare the styrene-to-maleic acid ratio's and thus to estimate the relative content of styrene in the SMAnh fractions as compared to that in commercially available SMAnh mixtures. $A_{680cm\text{-}1}/A_{1780cm\text{-}1}$ values are displayed in Table 1.

SMA 2:1	M_n (kDa)	PDI	$Abs_{680cm-1}/Abs_{1780\ cm-1}$
Mix	3.5	2.1	1.48
P50	4.6	2.0	1.41
P80	2.4	1.8	1.55
P90	1.4	1.7	1.57
P96	1.1	2.0	1.98
SMA 3:1	**M_n (kDa)**	**PDI**	**$Abs_{680cm-1}/Abs_{1780\ cm-1}$**
Mix	4.4	2.1	1.77
P50	6.5	2.0	1.54
P80	3.8	1.6	1.66
P90	1.9	1.7	1.77
P96	1.6	1.6	2.1

Table 1. Size characterization and composition analysis of SMAnh polymers. Table includes $A_{650cm-1}/A_{1780cm-1}$ obtained from FTIR spectra represented in Figure 1B, average number molecular weight (M_n) values and polydispersity index values, both obtained from GPC spectra shown in Figure 1A. PDI and M_n values are defined as PDI= $\frac{Mw}{Mn}$ and $Mn = \frac{\sum Ni\ Mi}{Mi}$ respectively.

Interestingly, $A_{680cm-1}/A_{1780cm-1}$ values obtained from SMAnh fractions indicate that the styrene content increases for those fractions that precipitated in solutions with lowest polarity (highest hexane-to-acetone ratio). This was supported by UV/Visible spectroscopy analysis (Figure S2). Here it was found that SMAnh fractions consisting of polymers with lowest M_n gave the highest absorbance values in the range of 240—270 nm, typical for electronic transitions between π—π* orbitals in polyene molecules. Thus it can be concluded that both the composition and the length play a key role in the solubility of the polymer.

SMA purified fractions yield nanodiscs of approximately the same size

The samples (i.e. SMAnh) were next hydrolyzed to yield SMA. The size distributions of the SMA polymers were analyzed by size exclusion chromatography (SEC) (Figure S1) and were found to follow the same trend as those obtained by GPC (Figure 2A and 2B). Then we investigated whether all the SMA fractions are able to solubilize lipid membranes into nanodiscs. EM micrographs (Figure 3) of solubilized lipid vesicles show that nearly all SMA fractions yield nanodiscs with an average size distribution of d~5—13 nm (Table 2), showing no correlation between the size of the nanodiscs and the M_n of the polymer rim. These values are in line with the size values reported previously for similar self-assemblies(Orwick et al. 2012; Jamshad et al. 2015; Scheidelaar et al. 2015; Dominguez

Pardo et al. 2017a). The only exception is the solubilized fraction obtained upon addition of the SMA 3:1 P96 fraction, which does not seem to contain nanodiscs but micrometer-scaled particles. The nature of this self-assembly may be ascribed to the high styrene content of molecules present in the SMA 3:1 P96 fraction (Table 1), leading to the formation of polymer aggregates during sample preparation. Most likely it is an artifact due to sample dehydration, as DLS analyses (described below) of the same sample did not show such large aggregates (Figure S3).

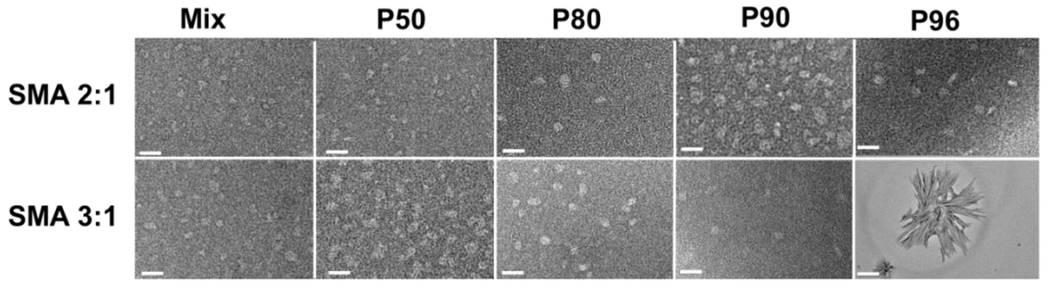

Figure 3. Negative-stain transmission electron micrographs of di-14:0 PC nanodiscs bounded by SMA 2:1 (top) or SMA 3:1 (bottom) polymer variants. The scale bar corresponds to 20 nm except for the SMA 3:1 P96 micrograph that corresponds to 1µm. Nanodiscs were obtained at a SMA-to-lipid mass ratio of 3.0.

DLS measurements on nanodiscs bounded by SMA 3:1-derived polymers (Figure S3) showed similar size distribution values as those reported by EM, in the range of 6—11 nm. For the SMA 3:1 P96 "nanodiscs" an additional scattering peak was obtained at ~60 nm. This may be ascribed the presence of insoluble membrane fragments in very low amounts as supported by its absence in the number-intensity distribution analysis (Figure S4). Remarkably, the nanodiscs bounded by SMA 2:1-derived polymers showed a somewhat smaller average size distribution (~5—7 nm) as compared to the values obtained by EM. One should keep in mind here that the error in the DLS data reflects the position of the maximum and not the actual size distribution, which is much larger. Furthermore, as a general remark we note that all the SMA fractions in solution (in the absence of lipids) scatter light, with an average peak maximum at ~5 nm based on number-size distribution(Figure S5). It is thus possible that the presence of free SMA leads to a down-shift of the size distribution values.

D (nm) SMA 2:1	Mix	P50	P80	P90	P96
	6.9±1.9	8.1±2.2	9.2±2.2	10.2±3.2	10.3±1.4
D (nm) SMA 3:1	**Mix**	**P50**	**P80**	**P90**	**P96**
	7.8±1.3	8.6±3.1	7.6±2.4	8.9±1.9	ND*

Table 2. Average particle diameter values obtain from EM micrographs displayed in Figure 3. Size values reported correspond to the average of at least 13 randomly localized nanodiscs along the EM micropgraph.

Insertion into lipid monolayers is most efficient for SMA fractions containing shortest polymers

A crucial first step in SMA-mediated membrane solubilization is the insertion of SMA into the lipid membrane. The efficiency of this process was investigated for the purified SMA fractions by lipid monolayer experiments. In this case, di-18:0 PC was chosen because it provides a convenient window to compare differences in surface pressure. As shown in Figure 4, addition of SMA fractions leads to a fast increase in surface pressure. For both SMA 2:1 and SMA 3:1 copolymers the surface pressure increase is highest for the fractions containing polymers with lowest M_n values. Interestingly, a plot of the final surface pressure values as function of the M_n of the SMA polymers suggests a linear relationship (Figure 4C). Here, the styrene content does not seem to play a role, as very similar values are found for SMA 2:1 and SMA 3:1 fractions.

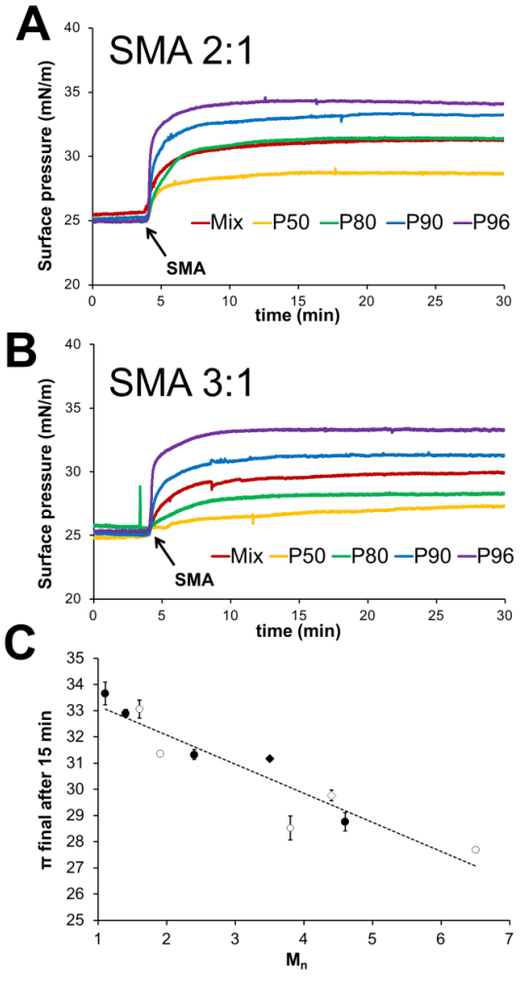

Figure 4. Surface pressure increase in monolayers composed of di-18:0 PC induced by the insertion of SMA molecules obtained from commercial mixtures consisting of SMA 2:1 (A) or SMA 3:1 (B). All surface pressure isotherms were recorded for at least 30 min at 25 °C. Final surface pressure values (t=30 min) against the average number molecular weight of the SMA fractions.(C). Full circles correspond to SMA fractions purified from commercial SMA 2:1 mixtures and empty circles to those purified from commercial SMA 3:1 mixtures. SMA mixtures are indicated by diamonds. Error bars represent the standard deviation of 2 independent experiments.

Solubilization of lipid bilayers is most efficient for SMA fractions containing shortest polymers

Next, the kinetics and efficiency of membrane solubilization by the SMA fractions was investigated by using di-14:0 PC vesicles below the T_m, as described previously (Scheidelaar et al. 2015; Scheidelaar et al. 2016). As shown in Figure 5A and 5B, the solubilization rates appear to follow the same trend as observed for the insertion of the SMA fractions into a lipid monolayer, with low M_n SMA polymers

solubilizing vesicles more efficiently than high M_n SMA polymers. As for the surface pressure isotherms, the final turbidimetry values also appear to hold a linear relation with the M_n values of the SMA fractions regardless of the monomer composition of the polymer (Figure 5C). These findings suggest that the length of SMA plays the most important role in both the insertion of SMA to a lipid surface and in the subsequent solubilization of the membrane, regardless of the overall styrene-to-maleic acid ratio.

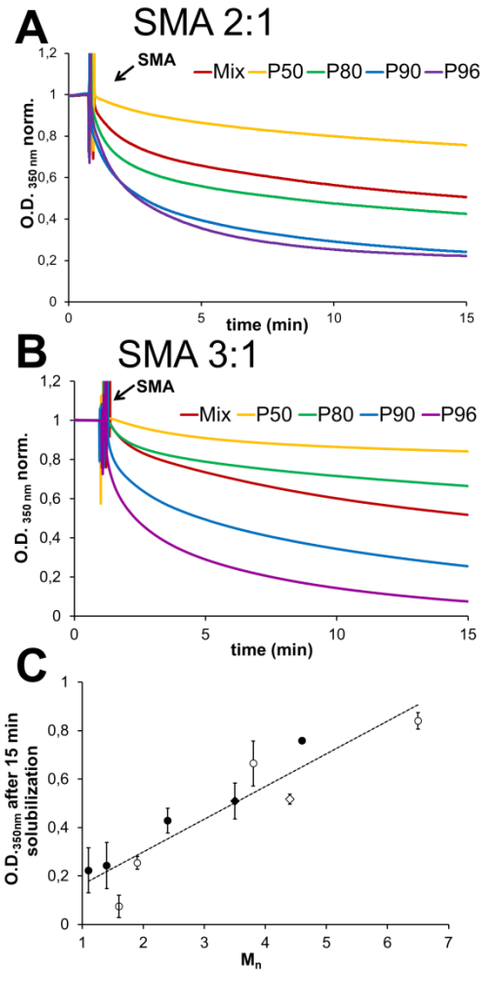

Figure 5. Solubilization kinetics of 0.5 mM di-14:0 PC MLVs induced by SMA copolymers obtained from commercial mixtures consisting of SMA 2:1 (A) or SMA 3:1 (B). Solubilization was conducted at 15 °C at a SMA-to-lipid mass ratio of ~3. Data are shown as normalized optical density at 350 nm. Final $O.D._{350\ nm}$ values (t=30 min) against the average number molecular weight of the SMA fractions. (C). Full circles correspond to SMA fractions purified from commercial SMA 2:1mixtures and empty circles to those purified from commercial SMA 3:1 mixtures. SMA mixtures are indicated by diamonds. Error bars represent the standard deviation of 2 independent experiments

Nanodiscs bounded by long SMA molecules exhibit slower lipid exchange rates than those bounded by short SMA molecules

Next the importance of SMA polymer length for the stability of the nanodiscs was investigated by monitoring the lipid exchange rates. These were studied by making use of the concentration-dependent fluorescence properties of rhodamine. The dye was incorporated at self-quenching concentrations in lipid nanodiscs bounded by different SMA 2:1 and SMA 3:1 fragments, and the increase in fluorescence was monitored upon addition of rhodamine-free nanodiscs. A possibly complicating factor here is that the initial rhodamine fluorescence in nanodiscs at t=0 s seemed to be affected by the length of the SMA belt (Figure S6), being lower for those bounded by low M_n SMA polymers. By contrast, the final fluorescence values appeared to be independent of the polymer length. The reason for these differences is not clear but it may be related to the high extent of membrane insertion of low Mn polymers as will be discussed later. In any case, this finding serves as an indication that SMA-lipid interactions are specific for the length of the polymer belt.

As shown in Figure 6A, nanodiscs bounded by SMA 2:1 fractions containing the longest polymers (SMA 2:1 P50) exhibit slowest dequenching rates upon addition of empty nanodiscs, thus indicating slowest lipid exchange rates between nanodiscs. Dequenching occurs faster when the size of the polymer becomes smaller as illustrated in Figure 6C, where the time required to achieve 50% of total dequenching ($t_{0.5}$) is plotted against the M_n value of the polymer belts. Remarkably, very fast dequenching rates were observed for nanodiscs bounded by SMA 3:1-derived polymers (Figure 6B) in line with previous reports (Arenas et al. 2017). Despite the fast lipid exchange rates observed between SMA 3:1-nanodiscs it was possible to detect slower dequenching rates for nanodiscs bounded by high M_n polymers than for those bounded by low M_n polymers. The clear differences in lipid exchange rates between nanodiscs bounded by polymers derived from SMA 2:1 and from SMA 3:1 commercial blends may be ascribed to the lower thermodynamic stability of SMA 3:1-nanodiscs (Dominguez Pardo et al. 2017b), making them more susceptible to undergo dynamic changes required for lipid exchange.

As a final remark, notably slower lipid exchange rates were obtained when the total excess of empty nanodiscs in solution was lowered to 4x fold (Figure S7). This finding may serve to support the theory that lipid exchange between nanodiscs shows a high Brownian dependence, thus is affected by the amount of particles in solution(Arenas et al. 2017).

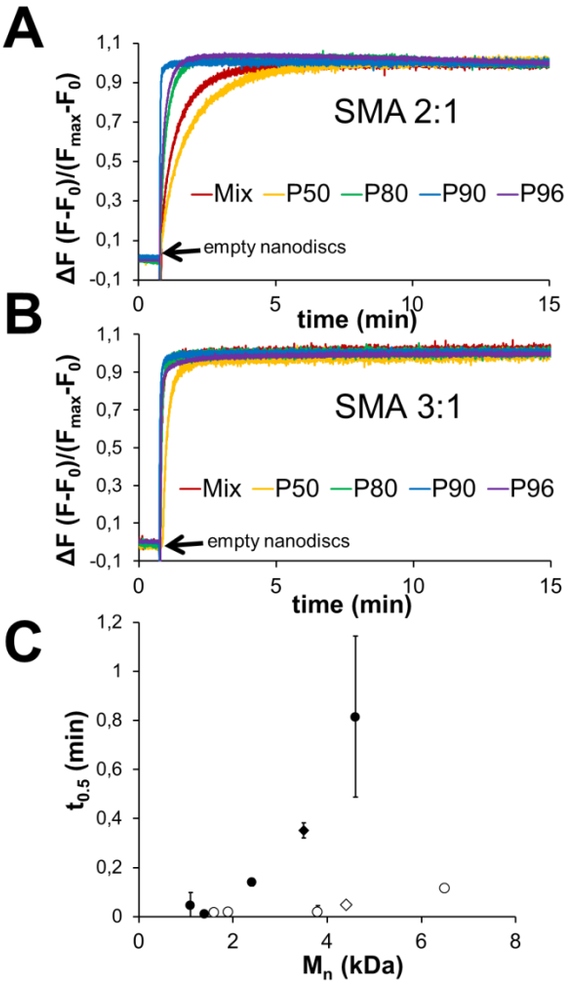

Figure 6. Dequenching of rhodamine-PE in d-14:0 PC nanodiscs (20% mol rhodamine) with time upon addition of unlabeled nanodiscs. Nanodiscs are bounded by SMA polymers obtained from commercial SMA 2:1 mixtures (A) or from SMA 3:1 mixtures (B). Figure includes a plot of the time required to achieve 50% of total lipid exchange ($t_{0.5}$) as function of the average-number polymer weight (C). Full circles correspond to SMA fractions purified from commercial SMA 2:1mixtures and empty circles to those purified from commercial SMA 3:1 mixtures. SMA mixtures are indicated by diamonds. Nanodiscs were obtained at a SMA-to-lipid mass ratio of ~3 and mixed in a ratio (mol) of 20:1 empty nanodiscs/ fluoropohore-loaded. Fluorescence dequenching was recorded for 15 min at λem=585 nm at 30 °C.

Lipids in nanodiscs encircled by long SMA 2:1 molecules retain to a higher extent their native thermotropic properties than those encircled by small SMA molecules

The thermodynamic stability of nanodiscs was further investigated by analyzing the thermotropic properties of the lipids embedded in them. Figure 7A shows that the T_m of di-16:0 PC lipids in nanodiscs bounded by SMA 2:1 mixture is downshifted approximately ~6 °C as compared to that in MLVs. Furthermore a decrease in both the cooperativity and in the calorimetric enthalpy of the gel-

to-fluid phase transition in SMA 2:1 nanodiscs can be observed as compared to that in vesicular self-assemblies in line with results from previous studies (Dominguez Pardo et al. 2017; Grethen et al. 2017). Nanodiscs bounded by SMA 2:1 fractions containing high M_n polymers exhibit similar downshifts in T_m as those bounded by the commercial SMA 2:1 mixture and thus perturb the least the thermodynamic equilibrium of the membrane. By contrast, lipids encircled by SMA 2:1 fractions containing low M_n polymers showed a poor retention of the native thermotropic properties by the lipids. For nanodiscs bounded by SMA 2:1 P90 fragments, additional peaks are observed in the thermograms which may be ascribed to an energetical contribution of the SMA polymer during the melting transition of the lipids, possibly related to the poor thermodynamic stability of the overall nanodisc particle (Dominguez Pardo et al. 2017). For nanodiscs bounded by SMA 2:1 P96 fragments, even a complete loss in cooperativity of the melting phase transition is observed, which may reflect the efficient insertion of these short SMA polymers in lipid systems (Figure 4), leading to a high extent of lipid disordering.

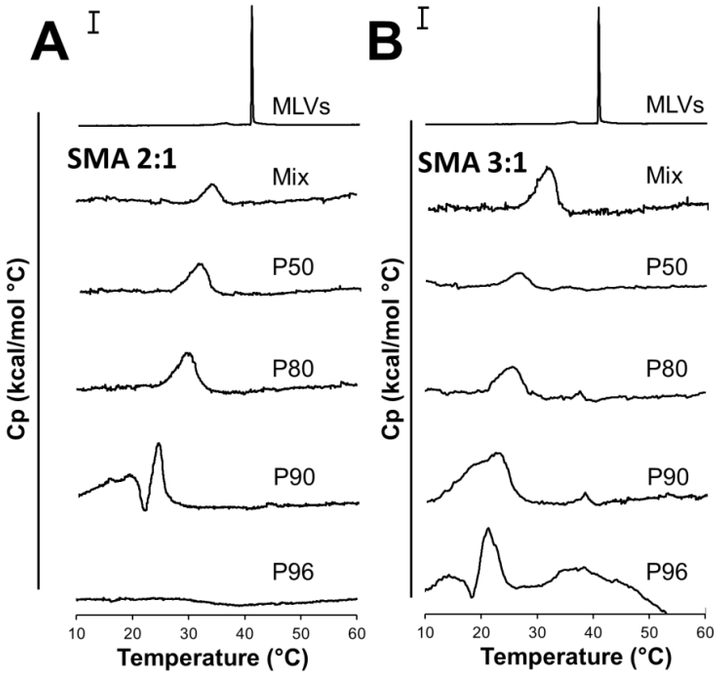

Figure 7. Representative differential scanning calorimetry (DSC) thermograms of di-16:0 PC lipids self-assembled in either MLVs (top) or in nanodiscs bounded by SMA 2:1-derived polymers (A) or by SMA 3:1-derived polymers(B). Nanodiscs were obtained at a SMA-to-lipid mass ratio of ~3.0. The inserted scale bars at the top corresponds to 5 kcal/ mol °C for the thermograms consisting of MLVs and to 0.5 kcal/mol °C for the thermograms consisting of nanodiscs.

The thermograms obtained for nanodiscs bounded by SMA 3:1 are shown in Figure 7B. Also here, it seems that the thermotropic properties of the enclosed lipids are least well retained in nanodiscs

bounded by SMA 3:1-derived polymers with low M_n. This is indicated by the appearance of additional peaks in the thermogram and by a decrease in the cooperativity of the lipids participating in the main gel-to-fluid transition. Overall, these results suggest that nanodiscs are more stable when bounded by long SMA polymers.

Discussion

In recent years the solubilization of lipid membranes by SMA copolymers has been studied extensively using model membrane systems. However these studies were assessed with commercial SMA mixtures that are highly heterogeneous, thus hampering our molecular understanding of SMA—lipid interactions. Here, we aimed to solve this problem by purifying SMAnh fractions from commercial SMAnh blends. When hydrolyzed, it was found by EM analysis that all the SMA fractions except SMA 3:1 P96 were able to yield circular nanodiscs in the range of d 5—13 nm, showing no correlation between the size of the nanodiscs and the M_n of the polymer rim. Importantly, DLS characterization showed that the SMA fractions and the SMA mixtures by themselves also scatter light, resulting in an overall number-size distribution of ~5 nm. This implies that particle analysis by DLS may be biased depending on the SMA concentration and thus EM may be more reliable for size analysis.

By investigating the interaction of SMA fractions with phosphatidylcholine self-assemblies it was found that the size of the polymer molecules constitutes a decisive parameter in achieving efficient membrane insertion and membrane solubilization. The most straightforward explanation for this behavior is that for long polymers it is sterically more difficult to cover a large membrane area such that all hydrophobic phenyl groups can be inserted efficiently.

Analysis of lipid exchange rates showed that lipids in nanodiscs bounded by high M_n polymers exhibit slower exchange rates between lipids in neighboring nanodiscs, as concluded from fluorescence dequenching of rhodamine-labeled lipids in nanodiscs upon addition of nanodiscs with unlabeled lipids. Furthermore, lipids enclosed by high M_n polymers showed a better retention of the native thermotropic properties than those enclosed by low M_n polymers, based on DSC measurements. Low M_n polymers were found to insert more efficiently into lipid monolayers, and thus it is possible that in the nanodiscs they not only shield the hydrophobic lipid acyl chains from the aqueous environment, but they also insert between the lipid headgroups on both surfaces of the nanodiscs. Thereby they will cause more disruption of native lipid—lipid interactions, thus decreasing thermodynamic stability. Remarkably, SMA 3:1 fractions yielded overall less stable nanodiscs than

SMA 2:1 fractions, in agreement with results from previous studies (Dominguez Pardo et al. 2017; Grethen et al. 2017). This behavior may be ascribed to the higher styrene content, but also to the higher chance of obtaining consecutive styrene monomer sequences in the polymer growing chain for SMA 3:1 as compared to SMA 2:1. This could result in a less homogeneous packing of the polymers around the nanodisc, possibly destabilizing the nanodisc.

In conclusion, we here present a simple method to separate high M_n and low M_n SMAnh polymers from commercial SMAnh mixtures, providing new insights into the effects of polymer length on membrane solubilization. The results presented here indicate that SMA 2:1 is recommended over SMA 3:1 polymers for obtaining stable nanodiscs that are suitable for studying specific protein-lipid interactions. Furthermore, the results show that purification of SMAnh commercial blends is a convenient method to obtain purified polymer fractions that offer a wide variety of possibilities depending on the aim of the study. For example, SMA polymers constituting relatively large M_n SMA copolymers offer great advantages in terms of resistance against lipid exchange. On the other hand, polymers constituting small M_n SMA copolymers will ensure fast membrane solubilization, thus shortening the exposure time of the biomembrane to SMA.

Acknowledgements

This work was supported financially by NWO Chemical Sciences, ECHO grants No. 711-013-005 (J.J.D.P). This work used the platforms of the Grenoble Instruct centre (ISBG;UMS 3518 CNRS-CEA-UJF-EMBL) with support from FRISBI (ANR-10-INSB-05-02) and GRAL (ANR-10-LABX-49-01) within the Grenoble partnership for structural biology (PSB). We thank Jonas M. Dörr, Adrian Kopf, Stefan Scheidelaar (all from University of Utrecht, The Netherlands) and Bert Klumperman (Stellenbosch University, South Africa) for helpful discussions. We are very grateful to Dr. Christine Moriscot, Guy Schoehn and Daphna Fenel, all from the Electron Microscopy platform of the Integrated Structural Biology of Grenoble (ISBG, UMI3265) for performing the TEM imaging.

References

Arenas RC, Danielczak B, Martel A, Porcar L, Breyton C, Ebel C, Keller S (2017) Fast Collisional Lipid Transfer Among Polymer-Bounded Nanodiscs. Scientific Reports 8:15016–15026

Dominguez Pardo JJ, Dörr JM, Iyer A, Cox RC, Scheidelaar S, Koorengevel MC, Subramaniam V, Killian JA (2017) Solubilization of lipids and lipid phases by the styrene-maleic acid copolymer. Eur Biophys J 46:91–101.

Dörr JM, Scheidelaar S, Koorengevel MC, Dominguez JJ, Schäfer M, van Walree CA, Killian JA (2016) The styrene-maleic acid copolymer: A versatile tool in membrane research. Eur Biophys J 45:3–21.

Esmaili M, Overduin M (2017) Membrane biology visualized in nanometer-sized discs formed by styrene maleic acid polymers. Biochim Biophys Acta 1860:257–263.

Grethen A, Oluwole AO, Danielczak B, Vargas C, Keller S (2017) Thermodynamics of nanodisc formation mediated by styrene/maleic acid (2:1) copolymer. Scientific Reports 7:11517.

Jamshad M, Grimard V, Idini I, Knowles TJ, Dowle MR, Schofield N, Sridhar P, Lin Y, Finka R, Wheatley M, Thomas ORT, Palmer RE, Overduin M, Govaerts C, Ruysschaert J-M, Edler KJ, Dafforn TR (2015) Structural analysis of a nanoparticle containing a lipid bilayer used for detergent-free extraction of membrane proteins. Nano Res. 8:774–789.

Lewis RNAH, Mak N, McElhaney RN (2002) A differential scanning calorimetric study of the thermotropic phase behavior of model membranes composed of phosphatidylcholines containing linear saturated fatty acyl chains. Biochemistry 26:6118–6126.

Morrison KA, Akram A, Mathews A, Khan ZA, Patel JH, Zhou C, Hardy DJ, Moore-Kelly C, Patel R, Odiba V, Knowles TJ, Javed M-U-H, Chmel NP, Dafforn TR, Rothnie AJ (2016) Membrane protein extraction and purification using styrene-maleic acid (SMA) copolymer: Effect of variations in polymer structure. Biochem J 473:4349–4360.

Orwick MC, Judge PJ, Procek J, Lindholm L, Graziadei A, Engel A, Gröbner G, Watts A (2012) Detergent-free formation and physicochemical characterization of nanosized lipid-polymer complexes: Lipodisq. Angew Chem Int Ed Engl 51:4653–4657.

Pardo JJD, Dörr JM, Renne MF, Ould-Braham T, Koorengevel MC, van Steenbergen MJ, Killian JA (2017) Thermotropic properties of phosphatidylcholine nanodiscs bounded by styrene-maleic acid copolymers. Chemistry and Physics of Lipids.

Ravula T, Ramadugu SK, Di Mauro G, Ramamoorthy A (2017) Bioinspired, Size-Tunable Self-Assembly of Polymer-Lipid Bilayer Nanodiscs. Angew Chem Int Ed Engl 56:11466–11470.

Rouser G, Fleischer S, Yamamoto A (1970) Two dimensional thin layer chromatographic separation of polar lipids and determination of phospholipids by phosphorus analysis of spots. Lipids 5:494–496.

Saldívar-Guerra E, Vivaldo-Lima E (2013) Handbook of Polymer Synthesis, Characterization, and Processing. John Wiley & Sons, Inc, Hoboken, NJ, USA

Scheidelaar S, Koorengevel MC, Pardo JD, Meeldijk JD, Breukink E, Killian JA (2015) Molecular model for the solubilization of membranes into nanodisks by styrene maleic Acid copolymers. Biophys J 108:279–290.

Scheidelaar S, Koorengevel MC, van Walree CA, Dominguez JJ, Dörr JM, Killian JA (2016) Effect of Polymer Composition and pH on Membrane Solubilization by Styrene-Maleic Acid Copolymers. Biophys J 111:1974–1986.

Swainsbury DJK, Scheidelaar S, Foster N, van Grondelle R, Killian JA, Jones MR (2017) The effectiveness of styrene-maleic acid (SMA) copolymers for solubilisation of integral membrane proteins from SMA-accessible and SMA-resistant membranes. Biochim Biophys Acta 1859:2133–2143.

Vargas C, Arenas RC, Frotscher E, Keller S (2015) Nanoparticle self-assembly in mixtures of phospholipids with styrene/maleic acid copolymers or fluorinated surfactants. Nanoscale 7:20685–20696.

Supplementary Information

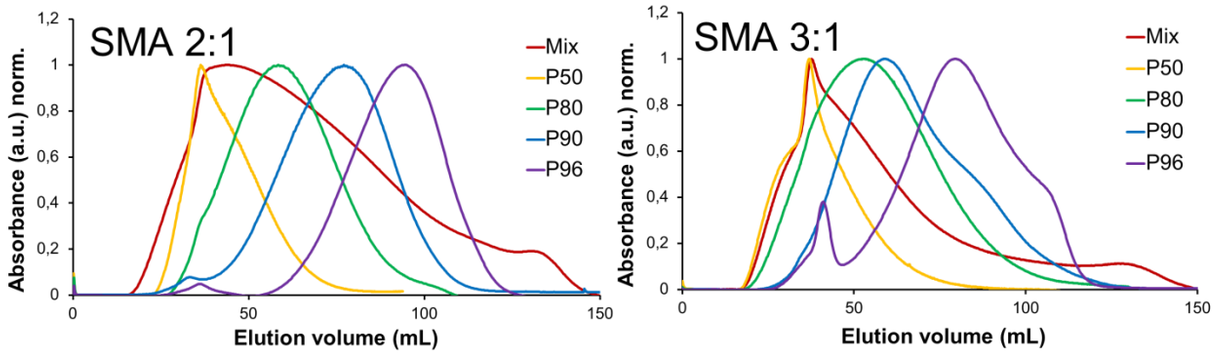

Figure S1. SEC chromatograms of 0.5 % (w/v) SMA copolymers (hydrolyzed form) in 2 mM Britton—Robinson buffer (pH=8.0). For both SMA 2:1 and SMA 3:1 polymers: Non-fractionated: red; P50: orange; P80: green; P90: blue; P96: purple.

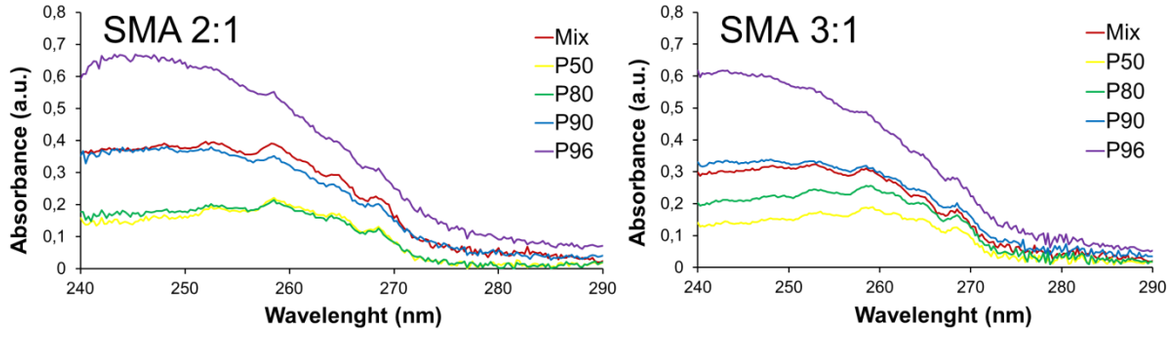

Figure S2. UV-Vis scans of SMAnh copolymers as 0.0125 % (w/v) in THF. Data points were obtained every 0.25 nm at a speed of 120 nm/min. For both SMAnh 2:1 and SMA 3:1nh polymers: Non-fractionated: red; P50: orange; P80: green; P90: blue; P96: purple.

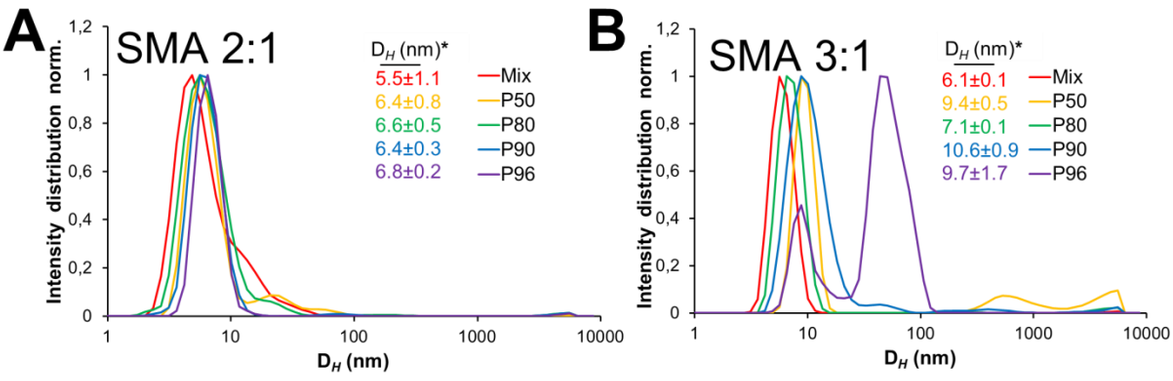

Figure S3. Intensity size distribution of soluble nanodiscs as quantified by dynamic light scattering of di-14:0 PC-nanodiscs bounded by (A) SMA 2:1-derived polymers and (B) SMA 3:1-derived polymers. For both SMA 2:1 and SMA 3:1 polymers: Non-fractionated: red; P50: orange; P80: green; P90: blue; P96: purple. Nanodiscs were obtained at a SMA-to-lipid mass ratio of 3.0. All experiments were performed at T=25 °C.

*Hydrodynamic diameters and errors reflect the positioning of the peak maximum within 6 x16 consecutive measurements. The actual size distribution is several nm.

**Hydrodynamic diameter corresponding to the first peak at D_H~9 nm.

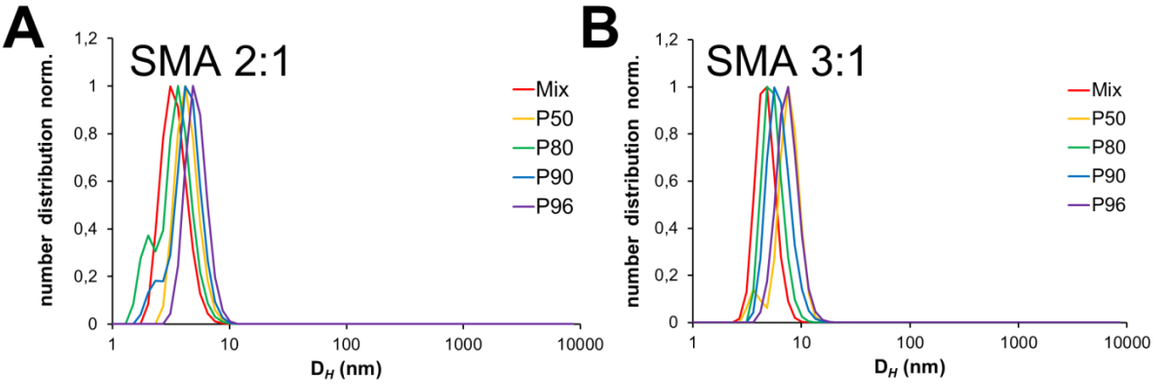

Figure S4. Figure.4. Number size distribution of soluble nanodiscs as quantified by dynamic light scattering of di-14:0 PC-nanodiscs bounded by (A) SMA 2:1-derived polymers and (B) SMA 3:1-derived polymers. For both SMA 2:1 and SMA 3:1 polymers: Non-fractionated: red; P50: orange; P80: green; P90: blue; P96: purple. Nanodiscs were obtained at a SMA-to-lipid mass ratio of 3.0. All experiments were performed at T=25 °C.

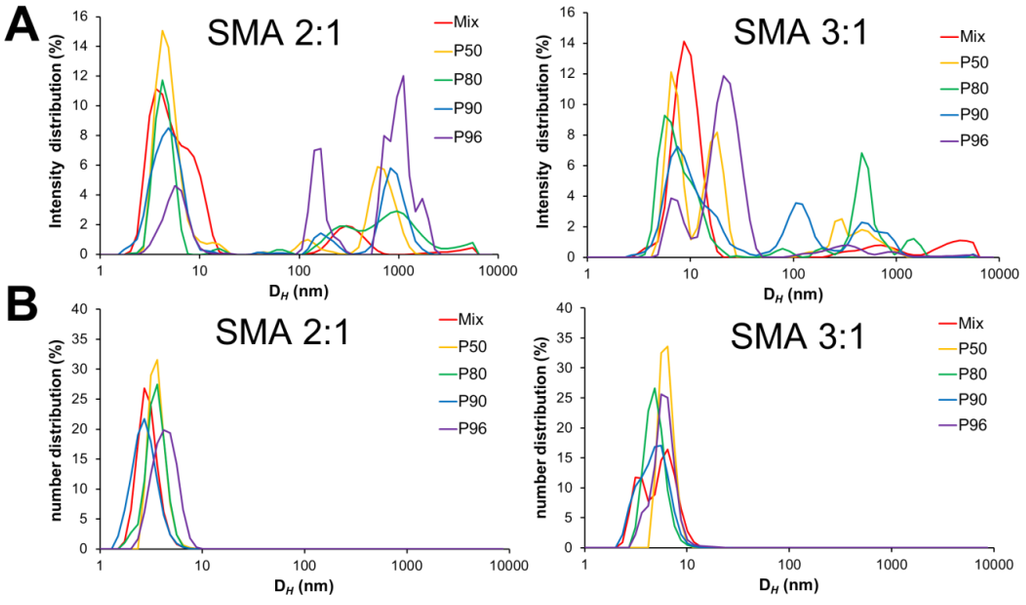

Figure S5. Size distribution of 1 % (w/v) SMA polymers in buffer (Tris 50 mM NaCl 150 mM pH=8.0) expressed as (A) intensity size distribution and (B) number size distribution. For both SMA 2:1 and SMA 3:1 polymers: Non-fractionated: red; P50: orange; P80: green; P90: blue; P96: purple. Nanodiscs were obtained at a SMA-to-lipid mass ratio of 3.0. All experiments were performed at T=25 °C.

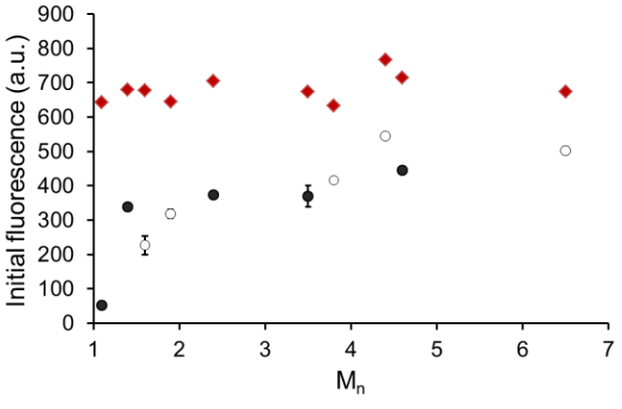

Figure S6. Initial rhodamine fluorescence in nanodiscs bounded to different M_n SMA mixtures and SMA fractions. Nanodiscs consist of di-14:0 PC with 20 % (mol) N-rhodamine di 14:0 PE s. Nanodiscs encircled by SMA 2:1-derived polymers are indicated by full circles while those by SMA 3:1-derived polymers are indicated by empty circles. Fluorescence was measured after 5 minute stabilization at 30 °C at λem=585 nm. Diamonds indicate the fluorescence intensity values obtained after the addition of empty nanodiscs to a solution of labeled nanodiscs in a 20:1 molar ratio (values corresponding to Figure 6A and 6B). Nanodiscs were obtained at a SMA-to-lipid mass ratio of ~3 and mixed in a ratio (mol).

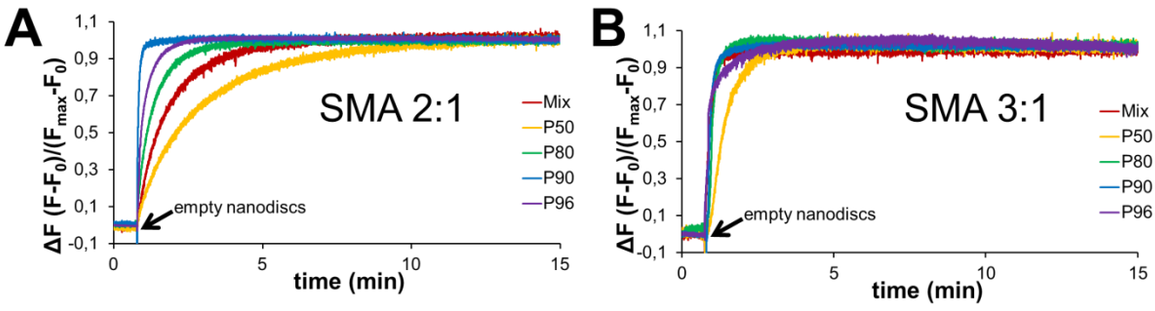

Figure. S7. Dequenching of rhodamine-PE incorporated in di-14:0 PC nanodiscs (20% mol rhodamine) with time upon addition of unlabeled nanodiscs. Nanodiscs are bounded by SMA polymers obtained from commercial SMA 2:1 mixtures (A) or from SMA 3:1 mixtures (B). Nanodiscs were obtained at a SMA-to-lipid mass ratio of ~3 and mixed in a ratio (mol) of 10:1 empty nanodiscs/ fluoropohore-loaded. Fluorescence dequenching was recorded for 15 min at λem=585 nm at 30 °C.

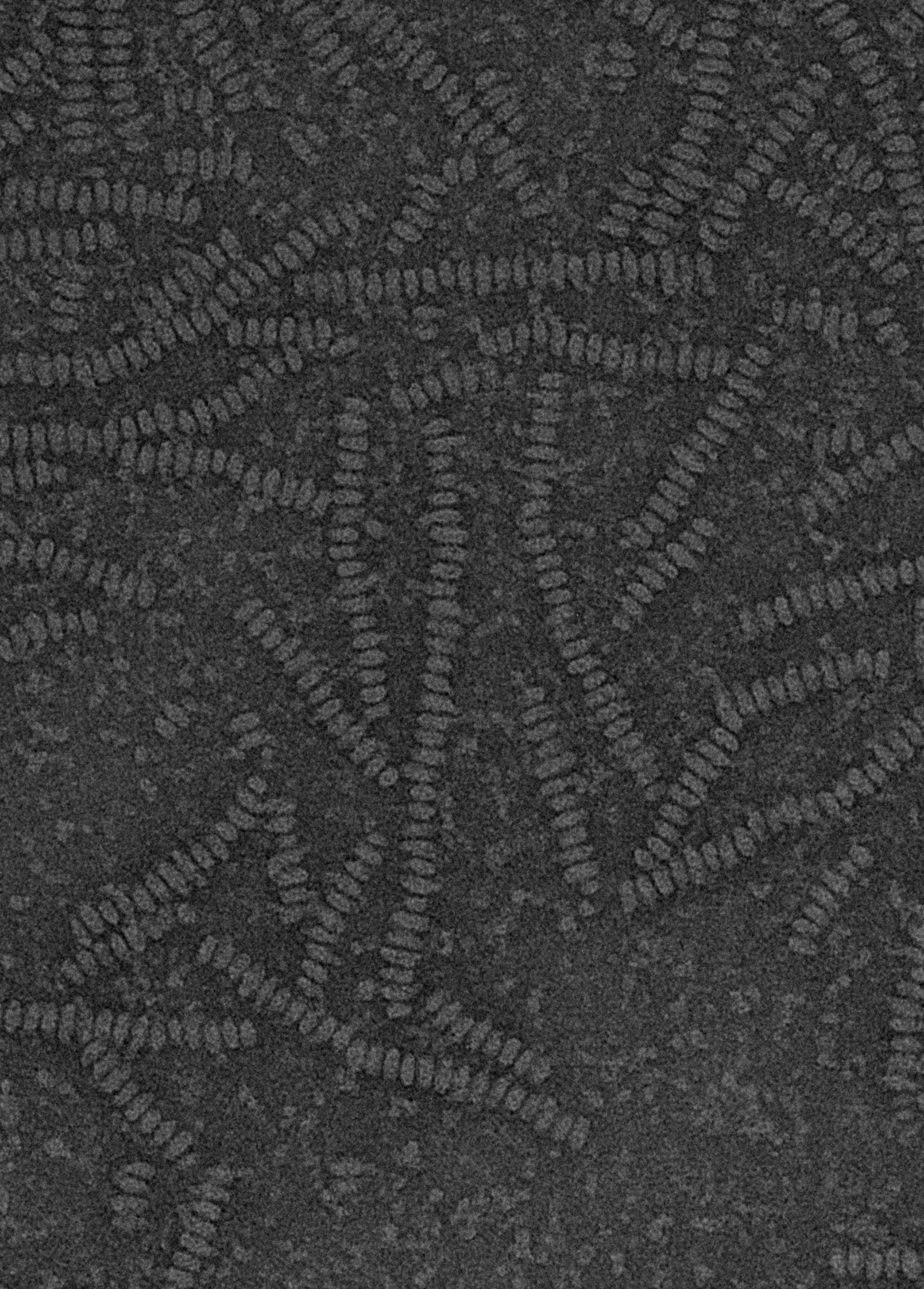

Chapter VI

Discussion

Abstract

In this final chapter we relate the studies to our current knowledge on SMA-mediated membrane solubilization to the experimental data presented in this thesis. The discussion will start with a description of the process of membrane solubilization, including a brief description of the factors affecting the extent of solubilization (e.g. SMA composition, polymer length and pH). Next, the promiscuity of membrane solubilization by SMA copolymers will be described in both model membranes and biological membranes. To conclude, a brief summary will be provided on the different biophysical properties of the nanodiscs (e.g. size, morphology and flexibility of the SMA belt) and on the organization of the lipids enclosed in them. The discussion will include possible limitations of the SMA method.

Solubilization of membranes by SMA

A mechanism of membrane solubilization by SMA was proposed by Scheidelaar and coworkers (Scheidelaar et al. 2015) based on model membrane studies. Here it is suggested that SMA molecules first dock to the outer membrane of vesicles, next they insert in the lipid bilayer and finally they disrupt the membrane resulting in the formation of nanodiscs. Fortunately, most of these steps can be studied by biophysical techniques. For instance, the insertion efficiency of SMA molecules in membranes can be tracked by analyzing the surface pressure increase of self-assembled lipid monolayers and the solubilization kinetics can be easily monitored by turbidimetry. These approaches have been used in **Chapter II** and in **Chapter V**. The efficiency of solubilization of membranes by SMA is affected by several independent parameters that will be discussed below in detail.

Effect of SMA composition on membrane solubilization

SMA variants with low amounts of styrene (SMA 1.4:1, 5kDa) were found to be active in the solubilization of model membranes in a low pH range of 4—5 , yet they yield less efficient solubilization as compared to those with higher styrene content (i.e. SMA 2:1, SMA 3:1), which are the polymers most commonly used in literature (Scheidelaar et al. 2016). This difference was ascribed to the excess charge present in the polymer chain of SMA 1.4:1, stabilizing the polymer in solution and hence hindering binding to the surface of the membrane. On the other hand, SMA variants with very high styrene content (i.e. SMA 4:1) were found to be hardly able to solubilize membranes even at optimum pH. The poor solubilization yield by hydrophobic SMA preparations has been related to the presence of polystyrene segments in the polymer growing chain, hindering the adoption of an uncoiled conformation by the SMA polymer, that is required to stabilize the nanodisc (Scheidelaar et al. 2016). Moreover, in **Chapter III** it is suggested that the presence of polystyrene units in the SMA 4:1 polymer chain has negative implications on the stability and on the morphology of the solubilized particles as will be further discussed below. Importantly, recent studies using *E. coli* membranes (Morrison et al. 2016) and *Rhodobacter sphaeroides* photosynthetic membranes (Swainsbury et al. 2017) showed that a styrene-to-maleic acid ratio of 2:1 or 3:1 also is ideal for membrane protein extraction from biological systems, in line with results on model membranes (Scheidelaar et al. 2016).

Effect of the polymer length on membrane solubilization

An extensive study using most commercially available SMA variants showed that those with relatively low molecular weight (M_w) values of ~7.5—10 kDa yielded the most efficient extraction of LeuT, ZipA

and BmrA membrane spanning proteins from *E. coli* membranes (Morrison et al. 2016). Similar results were obtained from the solubilization of the reaction centres (RCs) from *Rhodobacter sphaeroides* membranes, being solubilized to the highest extent by SMA variants of M_w~ 10 kDa (Swainsbury et al. 2017). However, commercial SMA mixtures consist of a very heterogeneous mixture of SMA molecules of different length and composition, and therefore interpretation of the results may be biased. This problem is partly solved in **Chapter V**. Here, different length SMAnh fractions were purified from commercial SMAnh based on their differential solubility in hexane/acetone mixtures and hydrolyzed to form SMA. It was found that the smallest SMA fractions insert in saturated phosphatidylcholine membranes and solubilize them faster and to a higher extent than their higher Mw SMA analogues.

Effect of pH on membrane solubilization

The maleic acid groups of SMA polymers exhibit two ionization states (two pKa values), depending on the protonation state of the two carboxylic acids. Interestingly, it was found that changes in pH may induce conformational changes in SMA molecules, adapting a random coil or a globular conformation, and hence affecting their interaction with membranes (Scheidelaar et al. 2016). The optimal ratio between both polymer conformations to ensure most efficient membrane solubilization was found in a narrow range of pH values and was found to be specific to each SMA variant (Scheidelaar et al. 2016). Conformational instability of SMA or in extreme case, polymer precipitation can thus be caused by changes in pH but also by the presence of divalent cations (Lee et al. 2016; Oluwole et al. 2017; Ravula et al. 2017b). This is mainly ascribed to the solvation of the negatively charged carboxylate groups by metal ions. Remarkably, a new line of covalently modified SMA preparations have been shown to ensure efficient membrane solubilization and particle stability upon drastic changes in pH and in the presence of high concentrations metal ions (i.e. Ca^{2+} and Mg^{2+}) (Fiori et al. 2017; Ravula et al. 2017b) paving the way for new membrane solubilization procedures.

Promiscuity of SMA copolymers

Scheidelaar et al. showed that the solubilization of *E. coli* total lipid extract vesicles by SMA 3:1 results in non-selective lipid solubilization (Scheidelaar et al. 2015). The general approach here was to use experimental conditions under which partial solubilization occurs and analyzing the composition of the solubilized and non-solubilized fractions after separation by centrifugation. Identical results were obtained when SMA 3:1 was replaced by SMA 2:1 (Dominguez et al., unpublished data), and hence, this fully promiscuous behavior of SMA seems to be independent of the polymer composition. SMA

promiscuity was further investigated in **Chapter II**, where also the phase of the lipids was varied, as will be discussed below.

Solubilization of fluid-phase membranes

As shown in **Chapter II**, the addition of SMA 3:1 copolymers to model membranes consisting of binary mixtures of lipids of different composition results in the non-selective solubilization of the different lipid species. However, the promiscuity of SMA is subject to conditions of lipid phase homogeneity. When SMA is added to membranes with fluid (liquid-crystalline) phase homogeneity, all the lipid species are equally-well solubilized, regardless of the lipid headgroup or acyl chain composition. This is supported by studies where ^{31}P NMR was used to demonstrate full promiscuity of SMA 3:1 in POPC/POPE mixtures (Cuevas Arenas et al. 2016).

Solubilization of gel-phase membranes

In **Chapter II** we show that under conditions of gel-and-fluid phase-coexistence, SMA 3:1 displays a strong preference toward solubilizing fluid-phase lipids. This result is in line with previous kinetic studies where it was found that the solubilization rate of fluid membranes is notably faster than that of gel membranes (Scheidelaar et al. 2015). Furthermore, solubilization of gel-phase membranes by SMA 3:1, while being slower than that of fluid-membranes, appears to be thermodynamically more favorable (Cuevas Arenas et al. 2016), thus serving as an indication that SMA—lipid interactions are affected by the lipid packing of the target membrane.

Solubilization of membranes with liquid-ordered domains

The resistance of SMA against other highly ordered domains, such as liquid ordered-domains is explored in **Chapter II**. Here, it was found that lipids that adopt a liquid-ordered phase (i.e. bSM and cholesterol) are remarkably more resistant against solubilization by SMA than those adopting a liquid-disordered phase (e.g. di-18:1 PC). This resulted in selective solubilization in ternary mixtures of these lipids, where the non-solubilized fractions were found to be enriched in the L_o lipids bSM and cholesterol. These insoluble membrane fractions were termed SMA-resistant membranes (SRMs). The preferential solubilization of L_D (fluid) phases over L_o (ordered) phases was confirmed in **Chapter II** by fluorescence microscopy. Here, supported lipid bilayers consisting of lipids forming liquid-ordered domains and of lipids in the liquid-crystalline phase were supplemented with top-fluor cholesterol (as marker for the L_o phase) and rhodamine-PE (as marker for the L_D phase) and later were mixed with SMA. The results

showed that L_D-lipids were remarkably easier to be solubilized by SMA than L_o-lipids. Membrane resistance against SMA 2:1 has been further investigated in biomembranes of human cells, using a HeLa cell line (Dörr et al. 2017). Here, by making use of different fluorescent protein constructs, it was shown that SMA exhibits different solubilization kinetics of the plasma membrane depending on the lipid specificity of the fluorophore. In brief, when the plasma membrane was labeled with a MARCKS construct that presumable associates with ordered lipid domains, the solubilization was slower than in a situation where the plasma membrane was labeled with an NGL3 construct, that preferentially partitions in the fluid matrix of the membrane (Dörr et al. 2017). This suggests again that model membranes serve as a reliable tool to investigate interactions of SMA with biological membranes. However, it cannot be excluded that the differences in solubilization kinetics between protein constructs in HeLa cells may be due to specific properties of the constructs themselves or related to specific interactions between the fluoropohores and the cytoskeleton.

Controversy: Nanodiscs, native or not native?

One of the most important features of SMA-bounded nanodiscs consists of serving as tool to isolate membrane proteins in their native environment (as “native nanodiscs”) and thus to investigate underlying preferential native protein—lipid interactions. This has been approached by comparing the lipid composition of purified nanodiscs containing membrane spanning proteins with that of the entire membrane extract of the native membrane. It was found that the annular shell surrounding the KcsA channel isolated from *E.coli* was enriched in anionic phospholipids (i.e. PG, CL) (Dörr et al. 2014). This lipid specificity is in line with the observed preferential interaction of KcsA with anionic lipids in model membranes (Marius et al. 2005; Marius et al. 2008). Less preference, if any, was observed for the hydrophobic tails, although matching of the hydrophobic bilayer thickness with that of the hydrophobic length of the membrane spanning domains of KcsA presumably can be expected to be energetically most favorable (Killian 1998). Similar headgroup preferences for anionic lipids were found for SecYEG, isolated from *E.coli* membranes (Prabudiansyah et al. 2015). By contrast, studies conducted on purified nanodiscs containing photosynthetic RCs of *Rhodobacter Sphaeroides* showed non-selective lipid solubilization and no preferential membrane protein—lipid interactions could be assigned (Swainsbury et al. 2014).

The question whether nanodiscs truly can be considered as a snapshot of the native environment became somewhat under dispute when Keller and coworkers (Cuevas Arenas et al. 2017) demonstrated fast lipid exchange rates between plain nanodiscs (i.e. nanodiscs with lipids only) bounded by SMA 3:1 and constituted by di-14:0 PC lipids. However, as shown in **Chapter V**, nanodiscs bounded by SMA 3:1 molecules undergo faster lipid exchange than those bounded by more hydrophilic SMA 2:1 molecules. Data shown in **Chapter V** supports the idea of fast lipid translocation between plain nanodiscs in solution and reports that lipid exchange rates are slowed down when the nanodiscs are bounded by SMA molecules containing high Mw polymers and when the number of nanodiscs in solution decreases, this last suggesting a Brownian dependence of the process. Another thing to keep in mind here is that all the studies where fast lipid exchange rates have been detected are subjected to a common variable: the use of nanodiscs constituted by short phosphatidylcholine (di-14:0 PC) lipids, which might be easier to extract from nanodiscs than longer lipids. Furthermore, it is possible that the presence of membrane proteins in "native nanodiscs" may slow down the lipid exchange rates between nanodiscs or even prevent lipids from translocating to a neighboring nanodisc. Thus it is not yet clear whether nanodiscs obtained from biological membranes reflect a true snapshot of the native membrane. Nevertheless, the term native nanodiscs remains valid for SMA-bounded nanodiscs isolated from biological membranes, because these nanodiscs do not contain any other lipids than those that were present in the native membrane.

Limitations of SMA to solubilize membrane proteins of different size

Several studies commented on the possible limitations of SMA to solubilize large proteins or protein complexes (Lee et al. 2016; Lee and Pollock 2016). However, these were speculations, not based on experimental evidence. Recently, this question was experimentally addressed by Swainsbury and coworkers who confirmed that SMA copolymers solubilized the reaction centers (RCs) of *Rhodobacter sphaeroides* membranes to a different extent depending on their oligomeric state and hence on their size (Swainsbury et al. 2017). The percentage of recovery reported for nanodiscs containing monomeric RCs was found to be approximately ~50 % higher than those containing multimeric RC's. These results indicate that the solubilization efficiency of SMA is affected by the lipid profile and by the size of the proteins.

Biophysical properties of the nanodiscs and of the enclosed lipids

The overall picture

Small angle neutron scattering studies on di-14:0 PC nanodiscs bounded by SMA 2:1 showed that these particles have a discoidal shape with an average diameter of ~10 nm and a hydrophobic bilayer thickness of ~2.6 nm, in line with the reported hydrophobic thickness of di-14:0 PC bilayers in the fluid phase (Nagle and Tristram-Nagle, 2000). Furthermore, the core shell model of SMA-nanodiscs, predicts a single polymer annulus of approximately ~0.9 nm thick (Jamshad et al. 2015). However, it is not clear yet what the exact number is of SMA belts that encircle the nanodiscs. This is due to the high heterogeneity of commercially available SMA mixtures and the lack of knowledge on whether certain SMA species may be enriched in the nanodiscs, thus inhibiting stoichiometric calculations.

Nanodiscs containing membrane spanning proteins or plain nanodiscs: is there a difference in size?

The size distribution of nanodiscs containing membrane proteins is rather homogeneous regardless of the size of the membrane spanning protein. A detailed list is provided by Dörr and coworkers, reporting an overall size distribution of d~10—24 nm with no direct correlation between the size of the nanodisc and the size of the enclosed proteins (Dörr et al. 2016). As an example, Swainsbury and coworkers, reported an average particle size of d~14 nm for nanodiscs containing membrane proteins consisting of 11 TM (transmembrane) helices plus hydrophobic chromophores (Swainsbury et al. 2014). Bigger proteins, such as the respiratory complex IV of *Saccharomyces cerevisiae* consisting of 26 TM helices were found to be enclosed in smaller nanodiscs of d ~12 nm. It is believed that plain nanodiscs are somewhat smaller than protein-containing nanodiscs. For example, in **Chapter II** it is shown that plain nanodiscs obtained from a broad variety of vesicle preparations of different lipid composition have an overall size of d~6—9 nm. However, other studies conducted on plain phosphatidylcholine nanodiscs revealed a somewhat bigger particle size distribution of d~9—12 nm (Scheidelaar et al. 2015) or d~9—18 nm (**Chapter III**). In conclusion, the average size of the nanodiscs may be affected by the presence of spanning proteins, but there is no solid data that supports it.

Effect of SMA concentration and of SMA composition on the morphology and on the size of nanodiscs

As shown in **Chapter III**, by using electron microscopy (EM), we demonstrated that the morphological integrity of plain di-16:0 PC nanodiscs is most preserved in nanodiscs bounded by SMA polymers with the lowest styrene content (i.e. SMA 2:1>SMA 3:1>SMA 4:1) (**Chapter III**). Nanodiscs bounded by the most hydrophobic polymer variant, SMA 4:1, revealed the highest degree of polydispersity and furthermore, a strong tendency to aggregate. These effects were particularly pronounced when "soluble particles" (technically not nanodiscs) were obtained at a high SMA-to-lipid mass ratio of 3.0. Previous studies by Keller and coworkers (Vargas et al. 2015; Grethen et al. 2017) and by Zhang et al. (Zhang et al. 2015) demonstrated that the average size distribution of nanodiscs decreases concomitantly for increasing SMA concentrations. However, these studies were based on dynamic light scattering analyses (DLS) and hence, the size results may be biased by the scattering contribution of the SMA polymer in solution. As shown in **Chapter V**, SMA molecules in the scattering peak of the SMA in solution at D_H~6 nm. Recent studies by Ramamoorthy and coworkers (Ramadugu et al. 2017; Ravula et al. 2017b; Ravula et al. 2017a) introduced a new line of chemically modified SMA 1:1 polymers (so-called SMA-EA). Here, the maleic anhydride ring was opened via an aminolysis reaction using ethanolamine, resulting in the formation of a carboxylic acid and an ethanolamide. The main striking feature of SMA-EA polymers lies in their ability of yielding nanodiscs of d ~20—60 nm. These so-called "macro-nanodiscs" are prepared by using a SMA-EA-to-lipid molar ratio of 1, while nanodiscs obtained at a higher SMA-EA-to-lipid molar ratio of 3 were found to be ~10 nm in diameter. Macrodiscs have the ability of aligning spontaneously to a magnetic field, serving as a powerful tool to perform solid-state NMR studies. Macro-scaled nanodiscs were also reported by Fiori and coworkers (Fiori et al. 2017) of ~32 nm in diameter when bounded by synthetic cysteamine-PC labeled SMA preparations constituted of ~ 430 alternating monomers (~43 kDa). Even though nanodiscs bounded by OH-hydrolyzed SMA enable protein purification, their small size may become a limiting factor to purify big protein complexes. For this reason, SMA-EA and cysteamine-PC SMA preparations are promising alternatives to conventional SMA polymers as a tool for membrane protein research.

SMA belt, ordering or disordering effect?

It has been shown that SMA molecules behave as amphipathic "belts" encircling lipids whereby styrene units intercalate between the acyl chains of adjacent lipids. As a result of this interaction, the

organization of the enclosed lipids is somewhat affected leading to contradictory results. For example, EPR studies using spin-labeled stearic acid in di-14: 0 PC nanodiscs bounded by SMA 3:1 molecules indicated an increase in the acyl chain order of the lipids below and above the T_m, as compared to that in vesicular self-assemblies (Orwick-Rydmark et al. 2012). Similarly, laurdan GP (generalized polarization) studies reported a more ordered environment in SMA-nanodiscs than in vesicles at T> T_m (Tanaka et al. 2015, **Chapter III**). On the other hand, differential scanning calorimetry and TEMPO spin-labeled measurements on similar self-assemblies showed that the lipids participated in a less cooperative way during their melting (gel-to-fluid phase transition) together with a downshift in T_m (**Chapter III**, **Chapter V**, Orwick-Rydmark et al. 2012; Jamshad et al. 2015; Grethen et al. 2017). Based on these results, it was suggested that SMA increases the acyl chain order of the enclosed lipids, but does not affect the terminal region of the lipids and hence does not perturb the center of the bilayer. Interestingly, the T_m of the lipids enclosed in MSP-nanodiscs (i.e. nanodiscs bounded by a Membrane Scaffolding Protein, which has a fixed length) was found to be slightly higher than that in vesicle preparations and this was interpreted as an ordering effect of the amphipathic protein belt on the enclosed lipids (Shaw et al. 2004; Denisov et al. 2005). However, SMA polymers behave rather differently to MSP, since they consist of a polymer that behaves as a flexible belt (data shown in **Chapter IV**), adapting to a molecular expansion of the enclosed material.

Composition and length of SMA affect the thermotropic properties of the enclosed lipids

As shown in **Chapter III**, the thermotropic properties of the lipids enclosed in nanodiscs are found to be most affected when these are bounded by SMA molecules with the highest amount of styrene. As an example, di-14:0 PC nanodiscs bounded by SMA 3:1 polymers displayed a T_m value of ~16 ˚C (Orwick-Rydmark et al. 2012), while that corresponding to identical self-assemblies but bounded by SMA 2:1 was established at ~22 ˚C (Jamshad et al. 2015). This apparent discrepancy in T_m was investigated in depth by using different SMA variants of increasing hydrophobicity and by using a broad range of saturated phosphatidylcholines. As shown in **Chapter III**, the T_m value of saturated PC lipids decreases concomitantly as the styrene content of the SMA belt increases, regardless of the acyl chain composition (C15—C18) . These results were supported by laurdan GP studies, yielding similar downshifts in T_m. Differences in T_m values were ascribed to the heterogeneous distribution of the styrene monomers of SMA in the polymer growing chain, being highest for hydrophobic SMA 4:1 and thus leading to a more inhomogeneous partitioning of SMA into the membrane (Scheidelaar et al. 2016). Remarkably, increasing concentrations of SMA led to a further downshift in T_m. A similar trend between SMA

concentration and T_m was reported by Keller and coworkers (Grethen et al. 2017; Oluwole et al. 2017). Thus, a general recommendation would be the use of the minimum amount of SMA required to ensure solubilization within a desired time period.

By using different length SMA fractions described in **Chapter V**, we found a lower cooperativity of the gel-to-fluid phase transition of the lipids enclosed in nanodiscs bounded by short SMA polymers than of those bounded by long SMA polymers. This was indicated by a huge broadening of the gel-to-fluid transition thermogram and may be ascribed to an increase in the lipid surface area covered by short SMA polymers. In summary, the data presented here suggest that the native lipid organization in nanodiscs is best preserved when membrane solubilization is conducted with long SMA polymers that preferably contain a low styrene-to-maleic acid ratio.

Conclusion

SMA polymers have been successfully used in the purification of membrane proteins from biomembranes into nanodiscs, enabling their study by a wide range of biophysical techniques. There are strong indications that membrane proteins preserve their native annular environment, serving as an optimal tool to study native protein—lipid interactions. Furthermore, nanodiscs mimic rather efficiently the architecture of membranes, holding a lipid bilayer configuration and retaining to a high extent the thermotropic properties of the enclosed lipids. In contrast to other nanodisc self-assemblies (e.g. MSP), SMA polymers behave as a rather flexible belt, and hence will most likely allow conformational changes by membrane proteins embedded in them. It has been shown that both the composition and length of SMA play a decisive role in membrane solubilization and in nanodisc structural stability. Both are ensured to a high extent by conducting the solubilization with SMA of low styrene content and of limited size. Finally, it should be mentioned that the full potential of SMA-mediated membrane solubilization may be much larger than has been thought so far, since new polymer modifications yield macroscopic nanodiscs that enable solid-state NMR analyses and furthermore, are resistant to drastic changes in pH and to the presence of high concentrations of a diverse range of cations (e.g. transition metals, alkaline earth metals). Future challenges will be to understand the detailed molecular mechanism of solubilization and thus to understand for example why low M_n polymers exhibit highest membrane solubilization efficiency, why lipids encircled by high M_n polymers are the most stable, or how the

composition of the target membrane affects membrane solubilizing properties and properties of the resulting nanodiscs. Furthermore, as discussed in **Chapter III**, it still remains unclear to what extent the distribution of monomer units in the polymer chain affects the membrane solubilization properties and the biophysical properties of the lipids they enclose. This latter can be investigated by using well-defined periodic SMA polymers.

References

Cuevas Arenas R, Klingler J, Vargas C, Keller S (2016) Influence of lipid bilayer properties on nanodisc formation mediated by styrene/maleic acid copolymers. Nanoscale 8:15016–15026.

Cuevas Arenas R, Danielczak B, Martel A, Porcar L, Breyton C, Ebel C, Keller S (2017) Fast Collisional Lipid Transfer Among Polymer-Bounded Nanodiscs. Sci Rep 7:45875.

Denisov IG, McLean MA, Shaw AW, Grinkova YV, Sligar SG (2005) Thermotropic phase transition in soluble nanoscale lipid bilayers. J Phys Chem B 109:15580–15588.

Dörr JM, Koorengevel MC, Schäfer M, Prokofyev AV, Scheidelaar S, van der Cruijsen EAW, Dafforn TR, Baldus M, Killian JA (2014) Detergent-free isolation, characterization, and functional reconstitution of a tetrameric K+ channel: the power of native nanodiscs. Proc Natl Acad Sci U S A 111:18607–18612.

Dörr JM, Scheidelaar S, Koorengevel MC, Dominguez JJ, Schäfer M, van Walree CA, Killian JA (2016) The styrene-maleic acid copolymer: A versatile tool in membrane research. Eur Biophys J 45:3–21.

Dörr JM, van Coevorden-Hameete MH, Hoogenraad CC, Killian JA (2017) Solubilization of human cells by the styrene-maleic acid copolymer: Insights from fluorescence microscopy. Biochim Biophys Acta 1859:2155–2160.

Fiori MC, Jiang Y, Altenberg GA, Liang H (2017) Polymer-encased nanodiscs with improved buffer compatibility. Sci Rep 7:7432.

Grethen A, Oluwole AO, Danielczak B, Vargas C, Keller S (2017) Thermodynamics of nanodisc formation mediated by styrene/maleic acid (2:1) copolymer. Sci Rep 7:11517.

Jamshad M, Grimard V, Idini I, Knowles TJ, Dowle MR, Schofield N, Sridhar P, Lin Y, Finka R, Wheatley M, Thomas ORT, Palmer RE, Overduin M, Govaerts C, Ruysschaert J-M, Edler KJ, Dafforn TR (2015) Structural analysis of a nanoparticle containing a lipid bilayer used for detergent-free extraction of membrane proteins. Nano Research 8:774–789.

Killian J (1998) Hydrophobic mismatch between proteins and lipids in membranes. Biochimica et Biophysica Acta (BBA) - Reviews on Biomembranes 1376:401–416.

Lee SC, Pollock NL (2016) Membrane proteins: is the future disc shaped? Biochem Soc Trans 44:1011–1018.

Lee SC, Knowles TJ, Postis VLG, Jamshad M, Parslow RA, Lin Y-P, Goldman A, Sridhar P, Overduin M, Muench SP, Dafforn TR (2016) A method for detergent-free isolation of membrane proteins in their local lipid environment. Nat Protoc 11:1149–1162.

Marius P, Alvis SJ, East JM, Lee AG (2005) The interfacial lipid binding site on the potassium channel KcsA is specific for anionic phospholipids. Biophys J 89:4081–4089.

Marius P, Zagnoni M, Sandison ME, East JM, Morgan H, Lee AG (2008) Binding of anionic lipids to at least three nonannular sites on the potassium channel KcsA is required for channel opening. Biophys J 94:1689–1698. doi: 10.1529/biophysj.107.117507

Morrison KA, Akram A, Mathews A, Khan ZA, Patel JH, Zhou C, Hardy DJ, Moore-Kelly C, Patel R, Odiba V, Knowles TJ, Javed M-U-H, Chmel NP, Dafforn TR, Rothnie AJ (2016) Membrane protein extraction and purification using styrene-maleic acid (SMA) copolymer: effect of variations in polymer structure. Biochem J 473:4349–4360.

Nagle JF, Tristram-Nagle S (2000) Structure of lipid bilayers. Biochim Biophys Acta 1469:159–195

Oluwole AO, Danielczak B, Meister A, Babalola JO, Vargas C, Keller S (2017) Solubilization of Membrane Proteins into Functional Lipid-Bilayer Nanodiscs Using a Diisobutylene/Maleic Acid Copolymer. Angew Chem Int Ed Engl 56:1919–1924.

Orwick-Rydmark M, Lovett JE, Graziadei A, Lindholm L, Hicks MR, Watts A (2012) Detergent-free incorporation of a seven-transmembrane receptor protein into nanosized bilayer Lipodisq particles for functional and biophysical studies. Nano Lett 12:4687–4692.

Prabudiansyah I, Kusters I, Caforio A, Driessen AJM (2015) Characterization of the annular lipid shell of the Sec translocon. Biochim Biophys Acta 1848:2050–2056.

Ramadugu VSK, Di Mauro GM, Ravula T, Ramamoorthy A (2017) Polymer nanodiscs and macro-nanodiscs of a varying lipid composition. Chem Commun (Camb) 53:10824–10826.

Ravula T, Ramadugu SK, Di Mauro G, Ramamoorthy A (2017a) Bioinspired, Size-Tunable Self-Assembly of Polymer-Lipid Bilayer Nanodiscs. Angew Chem Int Ed Engl 56:11466–11470.

Ravula T, Hardin NZ, Ramadugu SK, Ramamoorthy A (2017b) pH Tunable and Divalent Metal Ion Tolerant Polymer Lipid Nanodiscs. Langmuir 33:10655–10662.

Scheidelaar S, Koorengevel MC, Pardo JD, Meeldijk JD, Breukink E, Killian JA (2015) Molecular model for the solubilization of membranes into nanodisks by styrene maleic Acid copolymers. Biophys J 108:279–290.

Scheidelaar S, Koorengevel MC, van Walree CA, Dominguez JJ, Dörr JM, Killian JA (2016) Effect of Polymer Composition and pH on Membrane Solubilization by Styrene-Maleic Acid Copolymers. Biophys J 111:1974–1986.

Shaw AW, McLean MA, Sligar SG (2004) Phospholipid phase transitions in homogeneous nanometer scale bilayer discs. FEBS Lett 556:260–264

Swainsbury DJK, Scheidelaar S, van Grondelle R, Killian JA, Jones MR (2014) Bacterial reaction centers purified with styrene maleic acid copolymer retain native membrane functional properties and display enhanced stability. Angew Chem Int Ed Engl 53:11803–11807.

Swainsbury DJK, Scheidelaar S, Foster N, van Grondelle R, Killian JA, Jones MR (2017) The effectiveness of styrene-maleic acid (SMA) copolymers for solubilisation of integral membrane proteins from SMA-accessible and SMA-resistant membranes. Biochim Biophys Acta 1859:2133–2143.

Tanaka M, Hosotani A, Tachibana Y, Nakano M, Iwasaki K, Kawakami T, Mukai T (2015) Preparation and Characterization of Reconstituted Lipid-Synthetic Polymer Discoidal Particles. Langmuir 31:12719–12726.

Vargas C, Arenas RC, Frotscher E, Keller S (2015) Nanoparticle self-assembly in mixtures of phospholipids with styrene/maleic acid copolymers or fluorinated surfactants. Nanoscale 7:20685–20696.

Zhang R, Sahu ID, Liu L, Osatuke A, Comer RG, Dabney-Smith C, Lorigan GA (2015) Characterizing the structure of lipodisq nanoparticles for membrane protein spectroscopic studies. Biochim Biophys Acta 1848:329–333.

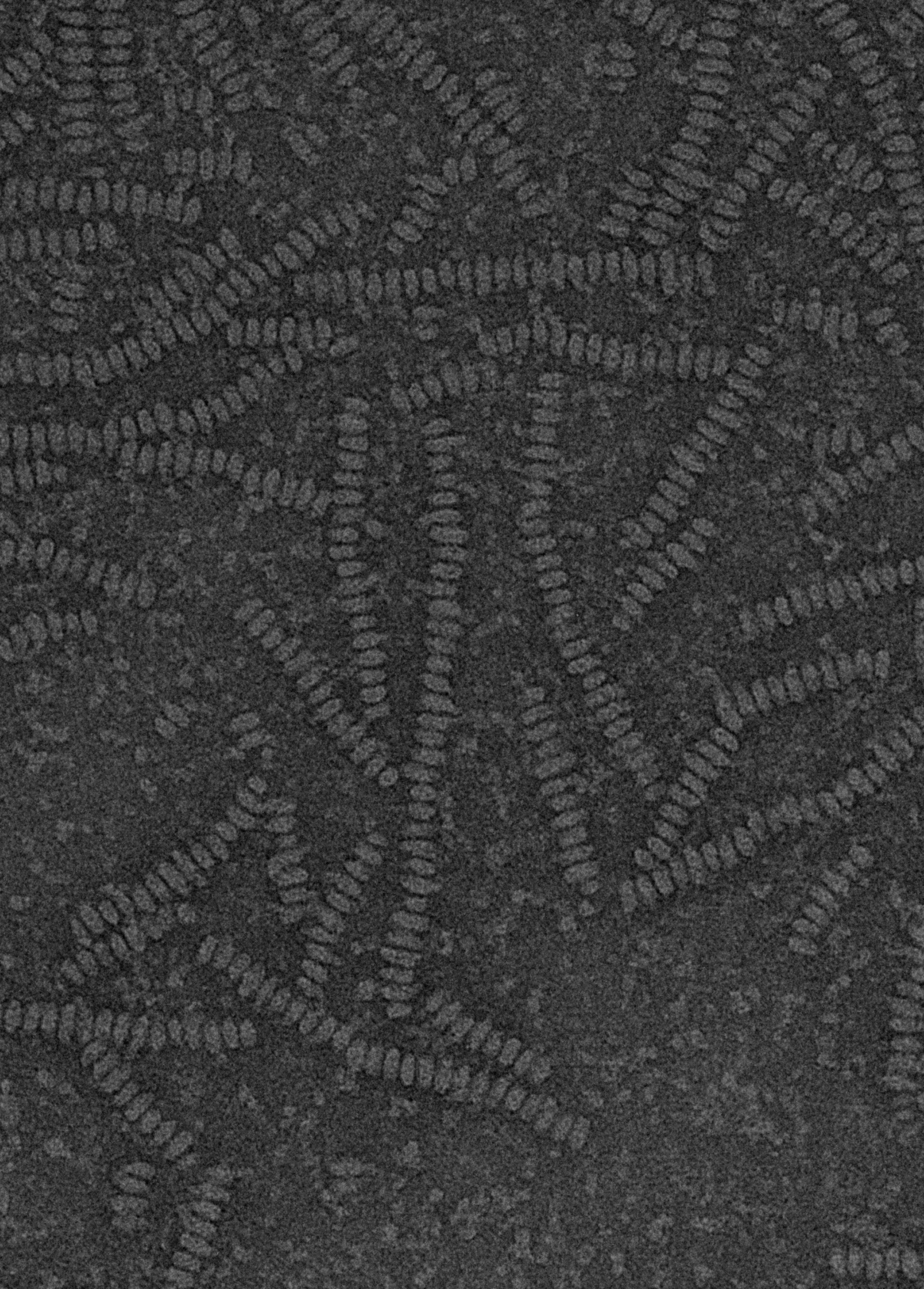

Appendix

Layman's Summary
Nederlandse Samenvatting
Resumen en Español
Curriculum vitae
List of Publications
Acknowledgements

Layman´s Summary

My research of the last four years has been focused on lipid membranes. What is a lipid membrane? In brief we could say that membranes are the envelope of cells. Membranes play a key role in vital processes of prokaryotic and eukaryotic organisms. For example, through this semipermeable barrier, cells take in essential nutrients for their survival and secrete damaging agents (e.g. toxins) to the extracellular space. In order to understand this thesis we must zoom in first on the composition of membranes. Membranes mainly consist of lipids and proteins. Lipids are tiny molecules that consist of a hydrophobic (doesn't like water) and a hydrophilic part. When lipids are incorporated into an aqueous media they will form a so-called lipid bilayer, with the hydrophilic groups looking towards the outside of the cell on one side and to the inner part of the cell on the other side, while the hydrophobic regions will be located in the center of the structure, thus being completely shielded from the water region. The most energetically favorable "shape" of this lipid bilayer will consist of sphere, and this is known as a vesicle.

The second component of membranes is membrane proteins. In brief, proteins are the result of the polymerization of amino acids. Up to now, twenty amino acids have been found in proteins, thus you may have an idea of the wide range of different combinations of amino acids available. Each protein has a specific task that contributes to the survival of the cell. A important fact about membrane proteins is that they literally need lipids. When membrane proteins are extracted from their native lipid surrounding, they tend to misfold, precipitate or aggregate and therefore are unable to conduct their biological function.

In order to conduct research studies on membrane proteins, first they must be extracted from the biological membrane they are embedded in. The most common way to achieve membrane protein purification is by using detergents. In brief, detergents will "break down" the membrane and will co-solubilize membrane proteins and lipids into micelles. However, the number of lipids co-solubilized is far away from being that in biological membranes, and furthermore, micelles consist of a poor mimic of the architecture of membranes, thus membrane proteins tend to destabilize in detergent-rich environments. As you can imagine, researchers have been struggling how to solve this problem for many years. Here, is where I will introduce the main actor of thesis: the styrene-maleic acid copolymer.

In the last ten years researchers have demonstrated the solubilizing properties of styrene and maleic acid polymers. However, they behave in a rather different way as detergents. Instead of solubilizing the membrane components into micelles, they "cut" an intact disc-shaped fragment from the

membrane. These so-called nanodiscs, represent a snapshot of the membrane, thus enable the co-purification of membrane proteins and of their native lipid environment. By using a cooking metaphor we could say that biological membranes consist of a fully spread pastry dough and SMA is a confectionery tool that cuts circular patches from the dough.

Nowadays SMA has become a very popular tool and is used by membrane researchers around the globe. A vast amount of research articles provided insight into the mechanism of solubilization and into the thermodynamics involved in the addition of SMA to a membrane suspension. However, when I started my PhD four years ago the method was not (yet) so well characterized. Today, I feel proud to say that I contributed to the development of the field, and my contribution will be briefly discussed as bellow.

In **Chapter II** we aimed to demonstrate whether SMA polymer has a preference solubilizing specific lipid species. Why is this so important? I already explained that membrane proteins need lipids to assure their stability and biological function. However, each membrane protein is surrounded by specific lipid molecules and fluctuations in their lipid environment may result in loss of activity/stability. In order to obtain fully functional/stable proteins in nanodiscs, we must be sure that all the lipids are equally well solubilized by SMA, thus the nanodiscs obtained would reflect a snapshot of the native membrane. By using a wide range of bioanalytical tools, we found that SMA was fully promiscuous and all the lipids were equally well solubilized as long as they were found in a fluid phase. On the other hand, lipids adopting highly ordered structures (e.g. gel phase, liquid-ordered phase) were remarkably more difficult to solubilize by SMA, paving the way for a novel method to purify ordered lipid domains from biological membranes.

In **Chapter III** we focused on the organization of lipids encircled in nanodiscs bounded by different SMA variants. This was approached by investigating the lipid thermotropic properties. Similar to matter, lipids undergo physical state transitions as function of temperature. For example, water at low temperatures adopts crystal structures (i.e. ice) and thaws at increasing temperatures adoption a more disordered phase (i.e. liquid). Similarly, lipids at low temperatures adopt highly ordered domains (i.e. gel phase) and adopt disordered structures at high temperatures (i.e. liquid crystalline). This transition takes place at a specific temperature (T_m) for each lipid molecule and has a specific heat exchange assigned to it (ΔH_{cal}). By simply comparing these two parameters of lipids in nanodiscs and to those in vesicles we are able to demonstrate which system is less perturbed by the presence of the SMA polymer. Results showed SMA polymers with low styrene content had a much milder effect on the stability of the enclosed lipids. These results were combined with EM imaging, where it was shown that nanodiscs bounded by SMA with low styrene content were the most stable and

retained to the highest extent their circular morphological integrity. In brief, the native organization of lipids in nanodiscs is better preserved when these are encircled by SMA polymers with low styrene content.

In **Chapter IV** we showed that the SMA belt surrounding the nanodisc behaves in a rather flexible way. This was explored with azobenzene photoswitches. Azobenzene is a molecule that undergoes trans-cis isomerization when exposed to light at 365 nm, leading to an increase of its geometric volume. Summarizing, we promote the swelling of molecules embedded inside nanodiscs. If the SMA molecules hold the nanodiscs tightly, the incorporated azobenzene molecules would not be able to isomerize since the nanodisc will not be able to accommodate an increase in the volume of the enclosed material. We observed that azobenzene molecules isomerized to the highest extent and rather fast inside the nanodiscs, regardless of the styrene content of the polymer belt. This data suggests that nanodiscs are dynamic particles that are able to "breathe". This finding is very important, since some membrane proteins (e.g. channels, pores) undergo conformational changes when conducting their biological function, and these may imply an increase in the volume occupied by the membrane protein.

In **Chapter V**, we developed a method to "fragment" commercial SMA blends into better length-defined SMA molecules. This was accomplished by differential solubility in hexane/acetone mixtures. Results showed that low Mn (short) SMA molecules insert to the highest extent in lipid monolayers and solubilize most efficiently lipid vesicles. Furthermore, we observed a rather linear tendency of the extent of polymer insertion and membrane solubilization with the polymer length. These results suggest that short SMA molecules are optimal to achieve membrane solubilization. However, stability analyses showed that nanodiscs bounded by low M_n SMA molecules are the most unstable, leading to a poor retention of the native thermotropic properties and to fast lipid exchange rates between nanodiscs. Summarizing, we provide insight into the effect of length on the mechanism of membrane solubilization and on the structural stability of the resulting nanodiscs.

Overall, this thesis does not contain a proof of concept study neither a fundamental discovery that will save mankind, but contains solid and systematic studies that contribute to optimize a well-established procedure. Nowadays, most research groups seem to be aiming for rapid publications in journals with an as high impact factor as possible, rather than on providing insight into what is (partly) discovered. Luckily, I form part of those whose research quality is measured by the opinion of my colleagues and not by the impact factor of a journal.

Nederlandse Samenvatting

De afgelopen vier jaar lag de focus van mijn onderzoek op membranen bestaande uit lipiden. Wat zijn deze membranen eigenlijk? Kort gezegd zijn membranen de buitenste begrenzing van de cel. Membranen spelen een belangrijke rol in cruciale processen van prokaryote en eukaryote organismen. Cellen moeten hun essentiele voedingsstoffen door dit semipermeabele membraan opnemen zodat ze overleven, en kunnen schadelijke stoffen (bijv. toxines) in de extracellulaire ruimte uitscheiden.

Om te begrijpen waar dit proefschrift over gaat, moeten we eerst meer weten over de samenstelling van membranen. Membranen bestaan voornamelijk uit lipiden en eiwitten. Lipiden zijn kleine moleculen die bestaan uit een hydrofoob ("watervrezend") deel en een hydrofiel deel. Als lipiden in waterige media worden gebracht, vormen ze een 'lipide bilaag', waarin de hydrofiele delen aan de ene kant naar de buitenzijde van de cel gericht zijn en aan de andere kant naar de binnenzijde van de cel, en de hydrofobe delen zich in het midden bevinden, waardoor ze volledig zijn afgesloten van het waterige milieu. De meest gunstige vorm van deze lipide bilaag is energetisch gezien een bol, en dit noemen we een vesikel.

Het tweede onderdeel van membranen zijn de membraaneiwitten. Samengevat; eiwitten zijn het resultaat van de aaneenschakeling van aminozuren. Tot nu toe zijn er 20 verschillende aminozuren gevonden in eiwitten, dus dit geeft een idee over hoeveel verschillende combinaties van aminozuren er mogelijk zijn. Elk eiwit heeft een specifieke functie die bijdraagt aan het overleven van de cel. Een belangrijk detail van membraaneiwitten is dat ze lipiden nodig hebben om hun vorm en functie te behouden. Als membraaneiwitten uit hun natuurlijke lipidenomgeving onttrokken worden, hebben ze de neiging om verkeerd te vouwen, te precipiteren of om aan elkaar te klonteren, waardoor ze hun biologische functie verliezen.

Om membraaneiwitten te kunnen onderzoeken, moeten ze eerst ontrokken worden van het biologische membraan waarin ze zijn ingebouwd. De meest gebruikelijke manier om membraaneiwitten te zuiveren is door detergent te gebruiken. Detergent breekt de membranen af en lost de membraaneiwitten samen met de lipiden op in micellen. Het probleem is echter dat het aantal lipiden wat samen met de membraaneiwitten oplost, lang niet het aantal lipiden benadert dat normaal in een biologisch membraan voorkomt. Bovendien hebben micellen een structuur die erg afwijkt van de structuur van membranen. Zoals je je misschien kunt voorstellen, hebben wetenschappers al jaren moeite met het oplossen van deze problemen. Daarom introduceer ik hier

de hoofdrolspeler van mijn proefschrift: het styreen-maleïnezuur copolymeer (SMA). In de laatste tien jaar hebben onderzoekers het oplossend vermogen van styreen-maleïnezuur polymeren gedemonstreerd. Opvallend is dat deze polymeren zich anders gedragen dan detergent. In plaats van dat de opgeloste membraancomponenten micellen vormen, worden er intacte schijf-vormige fragmenten uit het membraan 'geknipt'. Deze zogenoemde 'nanodiscs' laten een momentopname van het membraan zien, en maken het mogelijk om membraaneiwitten samen met hun natuurlijke omgeving van lipiden te zuiveren. Als we een culinaire metafoor gebruiken, zou je kunnen zeggen dat de biologische membranen een platgerold deeg zijn, en SMA een koekvorm is die cirkels uit dit deeg snijdt.

Tegenwoordig is SMA een populaire tool die wereldwijd wordt gebruikt door onderzoekers van membranen. Een grote hoeveelheid wetenschappelijke artikelen heeft inzicht verschaft in de manier waarop SMA membranen oplost, en in de thermodynamica van de toevoeging van SMA aan een membraansuspensie. Toen ik mijn PhD vier jaar geleden begon, waren deze processen echter nog niet zo duidelijk in kaart gebracht. Vandaag de dag kan ik met trots zeggen dat ik heb bijgedragen aan de ontwikkeling van dit onderzoeksveld, en mijn bijdrage zal hieronder, in het kort, besproken worden.

In **Hoofdstuk 2** was het doel om te verduidelijken of SMA voorkeur heeft voor het oplossen van bepaalde lipiden. Waarom is dit zo belangrijk? Ik heb al uitgelegd dat membraaneiwitten lipiden nodig hebben om vorm en biologische functie te behouden. Elk membraaneiwit is omgeven door specifieke lipiden, en fluctuaties in deze lipidenomgeving kan het verlies van activiteit en/of stabiliteit als gevolg hebben. Om volledig functionele en stabiele eiwitten in de nanodiscs te behouden, moeten we er zeker van zijn dat alle lipiden even goed opgelost kunnen worden door SMA, zodat de nanodiscs een momentopname nabootsen van het oorspronkelijke membraan. Door het gebruik van een brede selectie aan bioanalytische methoden, hebben we gevonden dat SMA geen onderscheid maakt en alle lipiden even goed oplost, zolang ze zich in een vloeibare fase bevinden. Aan de andere kant bleek dat lipiden die een strak geordende structuur aannamen (bijv. in een gel fase, een vloeibare-geordende fase), opvallend genoeg moeilijker op te lossen waren door SMA, wat de weg vrijmaakt voor de ontwikkeling van een nieuwe methode om lipid-domeinen op te zuiveren uit biologische membranen.

In **Hoofdstuk 3** hebben we ons gericht op de organisatie van de lipiden die zich in de nanodiscs bevinden, en bij elkaar gehouden worden door verschillende varianten van het SMA polymeer. Dit is gedaan door de thermotropische eigenschappen van de lipiden te onderzoeken. Zoals in alle materie,

gaan lipiden door overgangen van hun fysieke toestand, afhankelijk van de temperatuur. Zo heeft water op lage temperaturen bijvoorbeeld een kristalstructuur (ijs), en als het dooit bij toenemende temperatuur ontstaat er een meer ontregelde staat van de watermoleculen (een vloeibare fase). Ook lipiden hebben bij lage temperatuur een strak geordende structuur (de gel fase), en nemen een meer ontregelde staat aan bij hogere temperaturen (bijvoorbeeld vloeibaar kristalijn). Deze overgang vindt plaats bij een specifieke temperatuur (Tm) voor elk lipide molecuul, en heeft een specifieke warmteuitwisseling die daaraan gekoppeld is (ΔHcal). Door simpelweg deze twee karakteristieken in nanodiscs en in vesikelen te vergelijken, konden we laten zien welk systeem minder verstoord werd door de aanwezigheid van het SMA polymeer. Resultaten lieten zien dat SMA polymeren met een laag styreen gehalte een veel milder effect hadden op de stabiliteit van de ingesloten lipiden. Deze resultaten hebben we gecombineerd met electronenmicroscopie, waarmee we hebben gezien dat de nanodiscs die door SMA met een laag styreen gehalte omgeven zijn, het meest stabiel waren en het beste hun circulaire morfologie behielden. Samengevat, de natuurlijke organisatie van lipiden in nanodiscs wordt beter behouden als deze omgeven worden door SMA polymeren met een laag styreen gehalte.

In **Hoofdstuk 4** hebben we laten zien dat de SMA 'riem' die de nanodiscs omgeeft zich vrij flexibel gedraagt. Dit hebben we onderzocht door middel van een azobenzeen "fotoschakelaar". Azobenzeen is een molecuul dat een trans-cis isomerizatie ondergaat als het blootgesteld wordt aan licht met een golflengte van 365 nm, wat leidt tot een toename van het geometrische volume. Dit betekent dat we het volume van de moleculen die ingebed zijn in de nanodiscs vergroten. Als de SMA moleculen de nanodiscs strak binden, zouden de ingebouwde azobenzeen moleculen niet in staat zijn om te isomerizeren omdat de nanodisc niet in staat is om uit te zetten. We hebben geobserveerd dat azobenzeen moleculen snel maximaal isomerizeerden in de nanodiscs, onafhankelijk van het styreen gehalte van de polymeer riem. Deze data suggereert dat nanodiscs dynamische structuren zijn die in staat zijn om te 'ademen'. Dit is een belangrijke bevinding, omdat sommige membraaneiwitten (bijvoorbeeld kanalen, poriën) ruimtelijke veranderingen ondergaan wanneer ze hun biologische functie uitoefenen, en dit zou een toename van het volume kunnen betekenen van het membraaneiwit in kwestie.

In **Hoofdstuk 5** hebben we een methode ontwikkeld om commerciële SMA in moleculen van specifieke lengtes te "fragmenteren". Dit is gedaan door gebruik te maken van de verschillende oplosbaarheid in een mix van hexaan/aceton. De resultaten lieten zien dat lage Mn (korte) SMA moleculen het meeste in lipide monolagen inserteren en het makkelijkst lipide vesikels oplossen.

Verder zagen we een vrij lineaire trend in de omvang van polymeer insertie en het efficiënt oplossen van een membraan, in relatie tot de polymeer lengte. Deze resultaten suggereren dat korte SMA moleculen het beste gebruikt kunnen worden om een membraan op te lossen. Daartegenover staat echter wel dat stabiliteitsanalyses lieten zien dat nanodiscs die door middel van lage Mn SMA moleculen gebonden werden, het meest onstabiel waren, wat leidt tot een matig behoud van de natuurlijke thermotropische eigenschappen, en tot snelle lipiden uitwisseling tussen nanodiscs. In dit hoofdstuk laten we het effect van de lengte van SMA zien op het oplossen van het membraan, en op de stabiliteit van de structuur van de nanodiscs.

Globaal gezien bevat dit proefschrift geen basisimplementatie voor gebruik in de praktijk en ook geen fundamentele ontdekking die de mensheid zal redden, maar het bevat solide en systematisch uitgevoerde studies die bijdragen aan de optimalisering van een gevestigde methode. Tegenwoordig lijken de meeste onderzoeksgroepen zich meer te richten op snelle publicaties in wetenschappelijke tijdschriften met een zo hoog mogelijke impact factor dan op het verschaffen van meer inzicht in dingen die al (deels) ontdekt zijn. Gelukkig maak ik deel uit van hen wiens onderzoekskwaliteit wordt gemeten aan de mening van mijn collega's, en niet aan de impact factor van een journal.

Resumen en Español

Durante los últimos cuatro años mi investigación se ha centrado en las membranas lipídicas. ¿Qué es una membrana lipídica? Se podría decir que las membranas son el envoltorio de las células. Las membranas lipídicas tienen un rol decisivo en la mayoría de los procesos vitales de células eucariotas y procariotas. Por ejemplo, las células consumen nutrientes que entran a través de su membrana semipermeable, y desechan agentes nocivos (e.g. toxinas) al espacio extracelular.

Para llegar a entender esta tesis primero debemos explicar brevemente la composición de las membranas celulares. Básicamente éstas están compuestas por lípidos y proteínas. Los lípidos son unas moléculas pequeñas constituidos por una parte hidrofóbica (fobia al agua) y por una parte hidrofílica (afinidad por el agua). De esta forma, al entrar en contacto con agua, los lípidos adoptan la estructura de bicapa lipídica, donde las regiones hidrofílicas están orientadas hacia el agua mientras que las regiones hidrofóbicas componen el centro de la estructura, escudándose del agua. La estructura de bicapa lipídica adopta la forma geométrica de una esfera (conocida como vesícula) siendo ésta la más favorable energéticamente.

El segundo componente más importante de las membranas es las proteínas de membrana. Las proteínas son el resultado de la polimerización de aminoácidos. Hoy en día, se han hallado veintidós aminoácidos distintos en proteínas. Resulta evidente el gran número de combinaciones de amino ácidos posibles, dando lugar a una gran variedad de proteínas. Cada proteína lleva a cabo una función específica y contribuye al mantenimiento y supervivencia celular. La mayoría de las proteínas de membrana siguen un mismo patrón: todas dependen de su entorno lipídicos. Es decir, las proteínas necesitan los lípidos encargados de rodearlas en las células. Tal es el grado de dependencia que en el momento son extraídas de su entorno lipídico tienden a precipitar, oligomerizar o a plegarse de una forma incorrecta. En cuyo caso, son incapaces de llevar a cabo (o se entorpece en gran medida) su función biológica.

Para poder investigar proteínas de membranas, primero éstas deben ser extraídas de la membrana celular donde se encuentran (i.e. proceso de purificación). La forma más común para extraerlas es mediante el uso de detergentes. Resumiendo, los detergentes “rompen” la membrana celular en muchos trozos llamados micelas. Las micelas están compuestas por moléculas de detergentes, proteínas y por lípidos. Sin embargo, el número de lípidos cosolubilizados en la micela junto con las proteínas dista mucho de parecerse a la cantidad presente en el entorno lipídico de la proteína en la membrana celular. Además, las micelas no retienen la estructura de bicapa lipídica de una membrana celular y por lo tanto las proteínas solubilizadas en micelas tienden a desestabilizarse en

auto-ensamblajes ricos en detergentes. Resulta evidente que los investigadores han intentado solucionar este problema durante muchos años. En este punto es cuando introduciré el objeto de estudio de esta tesis: el copolímero de estireno y ácido maleico.

Durante los últimos diez años se ha evidenciado el poder "solubilizante" de los polímeros de estireno y ácido maleico (SMA). Estos se comportan de una forma diferente a detergentes comunes. En vez de disolver la membrana celular en micelas, el polímero SMA "corta" trozos intactos en forma de disco de la membrana celular. Estos trozos reciben el nombre de "nanodiscos" y representar una "captura de pantalla" de la membrana celular, donde las proteínas de membrana se hallan rodeadas de su entorno lipídico. Usando una metáfora culinaria, se podría decir que la membrana celular representa un molde de masa extendido sobre una superficie y el polímero SMA consiste en una herramienta de corte que extrae trozos circulares de masa.

Hoy en día, los polímeros SMA son utilizados con frecuencia por la comunidad científica. Un gran número de estudios han contribuido a entender el mecanismo por el cual el polímero SMA penetra en la membrana celular, rompiéndola acto seguido en forma de nanodiscos y en la termodinámica involucrada en todo el proceso. Sin embargo, cuando yo empecé el doctorado, poco se conocía sobre el proceso de disolver membranas con polímeros SMA. Hoy en día me siento orgulloso de haber contribuido a entender y a optimizar este proceso. Mis contribuciones serán detalladas a continuación:

En el **Capítulo II** hemos demostrado que el polímero SMA no muestra ninguna preferencia por ciertas especies de lípidos. Anteriormente he explicado la importancia del entorno lipídico para garantizar la estabilidad de las proteínas de membrana. El entorno lipídico varía de una proteína de membrana a otra y éste debe hallarse de forma íntegra en los nanodiscos para obtener proteínas plenamente estables y funcionales. De esta forma, los nanodiscos representarían una "captura de pantalla" de la membrana celular. Mediante el uso de un gran rango de técnicas bioanalíticas conseguimos demostrar el polímero SMA es totalmente promiscuo y por lo tanto, no muestra ninguna preferencia por especificas especies de lípidos siempre y cuando éstos se encuentren en estado fluido. Al contrario, cuando los lípidos adoptan estructuras ordenadas (i.e. fase gel o líquida-ordenada), éstos se muestras mucho más reticentes a ser solubilizados por el polímero SMA.

En el **Capítulo III** nos centramos en la organización de los lípidos en nanodiscos cuando éstos se hallan rodeados por distintas variantes de polímeros SMA. Esto se ha investigado a través de las propiedades termotrópicas de los lípidos. Los lípidos, parecido a la materia, experimentan cambios de estado en función de la temperatura. Por ejemplo, el agua adopta estructuras cristalinas ordenadas a bajas temperaturas (i.e. hielo) mientras que se funde a altas temperaturas (i.e. líquido).

Los lípidos, generalmente adoptan estructuras ordenadas a bajas temperaturas (i.e. gel o líquido-ordenado) mientras que a altas temperaturas adoptan estructuras desordenadas (i.e. fluida). Esta transición tiene lugar a una cierta temperatura (T_m) que es específica para cada tipo de lípido y además tiene una cantidad de energía (calor) asociada a ella (ΔH_{cal}). Mediante la comparación de estos dos parámetros obtenidos de lípidos en nanodiscos y en vesículas (i.e. esferas de bicapa lipídica) podemos deducir que sistema se encuentra menos alterado por la presencia de un polímero SMA u otro. Los resultados demuestran que los polímeros SMA con bajo contenido en estireno afectan en un menor grado la estabilidad de los lípidos en nanodiscos. Las imagines obtenidas de los nanodiscos mediante el uso de microscopia electrónica, demuestran que los nanodiscos envueltos por polímeros SMA con bajo contenido en estireno retienen mejor la integridad morfológica circular que aquellos envueltos por polímeros con alto contenido en estireno. Resumiendo, la organización de los lípidos en nanodiscos se asemeja más a la observada en vesículas cuando los nanodiscos se encuentran envueltos por polímero SMA con bajo contenido e estireno.

En el **Capítulo IV** se llega a la conclusión de que el polímero SMA que envuelve el nanodisco se comporta de una forma relativamente flexible. Esto se demuestra a través del uso de foto-interruptores de azobenceno. El azobenceno es una molécula que experimenta isomerización trans-cis cuando es expuesta a luz a 365 nm. Como resultado de la isomerización trans-cis, la molécula de azobenceno sufre un aumento en su volumen geométrico total, por lo tanto, se podría decir que “se hincha”. En el supuesto caso que los polímeros SMA rodearan el nanodisco de una forma relativamente apretada, la isomerización del azobenceno estaría impedida debido a la dificultad de acomodar un aumento del volumen del material lipídico encerrado en el nanodisco. En este capítulo observamos que las moléculas de azobenceno se isomerizan relativamente rápido y alcanzan máximos valores de isomerización observables, independientemente del tipo de polímero SMA (bajo contenido o alto contenido en estireno). Este descubrimiento es muy importante, ya que sugiere que el material encerrado en los nanodiscos “respira” y por lo tanto sugiere que las proteínas atrapadas en ellos gozan de un grado de libertad de movimiento. De esta forma se permite que las proteínas lleven a cabo sus funciones biológicas con una mayor libertad ya que éstas pueden dar lugar a cambios conformacionales.

En el **Capítulo V** desarrollamos un método para “fragmentar” mezclas comerciales de polímeros SMA en polímeros de longitud definida. La fragmentación se lleva a cabo a través de solubilidad diferencial de los polímeros que constituyen la mezcla comercial en mezclas de hexano/acetona. Una vez fraccionada la mezcla comercial de polímeros SMA, investigamos su eficiencia solubilizadora en presencia de vesículas. Los resultados demuestran que los polímeros SMA de menor tamaño son los más eficientes a la hora de insertarse en la superficie de la vesícula y en su posterior solubilización.

Sin embargo, los nanodiscos envueltos por polímeros SMA de menor longitud resultan ser los menos estables, atendiendo a las propiedades termotrópicas de los lípidos (ver arriba). Adicionalmente, observamos que lípidos “migran” de un nanodisco a otro a través del impacto entre nanodiscos, siendo esta migración más eficiente entre nanodiscos envueltos por polímeros SMA de menor longitud.

En resumen, esta tesis no contiene ningún estudio de prueba de concepto ni un descubrimiento trascendental que vaya a salvar a la humanidad. Sin embargo, esta tesis contiene estudios sólidos y sistemáticos que contribuyen a entender en mayor medida un método bien asentado en la comunidad científica. Muchos grupos de investigación hoy en día se centran en publicar artículos rápidos en revistas de alto factor de impacto sin preocuparse de los detalles, en vez de contribuir a lo que ya ha sido en parte descubierto. Afortunadamente, pertenezco a un grupo de científicos cuya investigación se mide por la opinión de mis colegas y no por el factor de impacto de una revista.

Curriculum vitae

I was born on November 20th 1988 in Valencia, Spain. I obtained my secondary education in the American school of Valencia, based in Puçol, Valencia. Next, I followed a BsC and MsC program (i.e. Licenciatura) in Chemistry in the University of Valencia. Later I was awarded an Erasmus grant and moved to Leiden. Here, I followed a one year internship in the department of soft matter chemistry in the University of Leiden under the supervision of prof. dr. Alexander Kros. I graduated in 2013 with a thesis on the "Coiled-coil driven membrane fusion: zipper vs. non-zipper-like peptide orientation". Later in November 2013, I was selected as PhD candidate on the department of membrane biochemistry and biophysics in the University of Utrecht, under the supervision of prof. dr. Antoinette Killian. My PhD has been focused on the interaction between styrene and maleic acid copolymers with lipid self-assemblies. During my PhD I had the chance of presenting my work in international (i.e. American biophysical society meetings) and national conferences (i.e. FOM Dutch biophysics, CHAINS). To the date, I have published 6 peer-reviewed articles and I am currently busy with the submission of two more.

List of publications

"Coiled-coil driven membrane fusion: zipper-like vs. non-zipper-like peptide orientation". F.Versluis, **J.J.Domínguez**, J. Voskuhl, A.Kros. *Faraday Discussions, 166, 349-359, 2013.*

"Molecular model for the solubilization of membranes into nanodisks by styrene maleic Acid copolymers". S.Scheidelaar, M.C.Koorengevel, **J.J.Domínguez**, J.Meeldijk, E. Breukink,J.A. Killian.*Biophysical Journal 108. 279-290, 2015.*

"*The styrene-maleic acid copolymer: a versatile tool in membrane research".* J.M.Dörr, S.Scheidelaar, M.C.Koorengevel, **J.J.Domínguez**, M.Schäffer,C.A.van Walree, J.A.Killian. *European Biophysical Journal, 45, 3-21, 2015.*

"Effect of Polymer Composition and pH on Membrane Solubilization by Styrene-Maleic Acid Copolymers". S.Scheidelaar, M.C.Koorengevel, **J.J.Domínguez**, J.M.Dörr, C.A.van Walree, J.A.Killian. *Biophysical Journal. 111(9), 1974-1986, 2016.*

"Solubilization of lipids and lipid phase by the styrene—maleic acid copolymer". **J.J.Domínguez**, J.M.Dörr, A.Iyer, M.C.Koorengevel, V.Subramaniam, J.A.Killian. *European Biophysical Journal, 46, 91-101, 2017.*

"Thermotropic properties of phosphatidylcholine nanodiscs bounded by styrene—maleic acid copolymers" **J.J.Dominguez**, J,M.Dörr, T.Oud-Braham, M.C.Koorengevel, M.van Steenbergen, J.A.Killian. *Chemistry and physics of lipids, 208 ,58-64, 2017.*

"Membrane solubilization by SMA copolymers: delineating the role of polymer length" **J.J.Domínguez,** M.C.Koorengevel, H. Jahn, N.Uwugiaren, J.Weijers, M.van Steenbergen,J.A.Killian. *In preparation.*

"*Styrene-maleic acid wrapped nanodiscs allows expansion of enclosed lipid material"* **J.J.Domínguez,** Cornelis A. van Walree, M.R.Egmond,J.A.Killian. *In preparation.*

Acknowledgements-Agradecimientos

I am very thankful to Prof. Dr. Antoinette Killian for giving me the opportunity of conducting a PhD program at the department of Membrane Biochemistry and Biophysics (MBB) in Utrecht University and for the tutoring and the guidance through these four years. I am grateful to Prof. Dr. Alexander Kros, Dr. Frank Versluis and Dr. Jens Voskuhl for the scientific guidance provided during my Masters internship in Leiden University and for introducing me in academia. Chapter III could not have been started without the collaboration of Mies Steenbergen with DSC measurements. I am very grateful to Guy Schoehn, Daphna Fenel and Hans Meeldijk for their collaboration with EM imaging (Chapter II, Chapter III and Chapter V). Dr. Patricia Marqués and Dr. Grzegorz Pawlik, thank you both for being a fundamental support during the first year of my PhD. Dr. Inge van't Veer, Dr. Sabine Oppedijk, Dr. Yao Liu and Dr. Jonas M. Dörr, thank you for being good friends. I am thankful to Dr. Michal Heger, Dr. Samuel Furse, Dr. Remko van Vught, Dr. Stefan Scheidelaar, Dr. Joost Ballering, Lisette Nijland, Xue Bao, Xiaoqi Wang, Adrian Kopf, Yang Xu, Manikam Sadasivam, Caroline Rutten and Linda Kumeling for being excellent colleagues. Ruud Cox and Martijn Koorengevel, thank you for the general scientific input and for the technical support throughout this whole thesis. I am grateful to Dr. Eefjan Breukink and to Dr. Anton De Kroon for useful scientific discussions. Prof. Dr. Maarten Egmond and Dr. Kees van Walree are acknowledged for their collaboration with kinetic studies and with the synthesis of products (Chapter IV). Filip Pamula, Naomi Uwugiaren, Yuri Damen, Jeroen Weijers, Marta Jorge, Giulia Garrone, Rosella Scardaci, Mahel Manis, Adolph Bierhuizen and Judith Niessen are acknowledged for being excellent students and colleagues. Mike Renne and Margriet Hokken, thank you for being amazing friends and for the corrections on the Nederlandse Samenvatting, I owe you both so much.

Agradezco a mis padres su apoyo incondicional, no solo durante los últimos cuatro años, sino durante toda mi vida. Agradezco a Marta el simple hecho de haberla conocido y de que ahora suponga la piedra angular de mi vida. Estoy agradecido con el Dr. Jordi Amat, Dr. Guillem Paniagua, Dr. Oskar González y el Dr. Victorio Sáez por ser mis más ilustres amigos (e ignorantes). Estoy agradecido con la Dra. Elena Pérez, Marta Vigil, Nadia Ramírez, David Vicente, Albert Amigó, Mónica Ochoa, Valeriano Díaz, Pablo Galán, Mónica Romera, Anna de la fuente, Ekin Karakurt, Luana Testa, Shorouk Fahmy, Amedeo Bellunato, Lia Lima, Estefania Ibáñez, Sander van Stigt, Erjen Jantzen, Gemma Riera, Bart Limburg y Velten Horn por hacerme sentir como en casa pese a estar a más de 1800 km de Valencia. Estoy agradecido al Prof. Dr. Félix Goñi por formar parte del comité de mi defensa doctoral. Estoy agradecido a Josep Vicent Frechina, Daniel Whitehair, Eugenia Bayarri, Marc Boyer, Cristina Jofre y Paula Jover por ser fundamentales en mi formación y por tener una paciencia infinita, sois unos profesores excelentes.